# Formulation and manufacture of Lipid Nanoparticles using the Micropore AXF crossflow systems.

MPhil Thesis

Liam O'Connor

Kkb22240

liam.o-connor@strath.ac.uk

Strathclyde Institute of Pharmacy and Biomedical Sciences (SIPBS)

Feb 2024

Word count: 26,446

Key words: Lipid nanoparticles; mRNA; $DilC_{18}$; Particle diameter; PDI; encapsulation efficiency.

**Declaration of Authenticity**

*'This thesis is the result of the author's original research. It has been composed by the author and has not been previously submitted for examination which has led to the award of a degree.'*



*Signed: Liam O'Connor*

*Date: 15th February 2024*

**Abstract**

Since its discovery in 1961, the therapeutic utilisation of messenger RNA (mRNA) to combat viral infection and genetic predispositions became a strong focal point for the field of molecular biology. Unlike DNA, mRNA's transient single strand structure alleviated concerns associated with long-circulation times and consequential off-target toxicity whilst simultaneously harbouring a reduced risk of genetic recombination. Although promising, challenges facing effective mRNA delivery to the cell cytosol hindered its therapeutic potential. Both exogenous mRNA's intrinsic immunostimulatory activity and susceptibility to host endonucleases inhibited mRNA's translational activity and potency. The result led to the exploration of two avenues to mitigate these pitfalls: nucleoside modification of mRNA to protect against innate immune clearance mechanisms and optimisation of lipid nanoparticles (LNPs) to enable successful delivery and uptake to the cell cytosol. Expedited by the SARS-CoV2 response, both played critical roles in the rapid development and success of Pfizer-BioNTech's Comirnaty and Moderna's Spikevax response. Despite the success of this LNP- based vaccine roll out, bottlenecks in the manufacture of LNPs highlighted the necessity for a scale-independent, uniform design, capable of formulating LNPs at benchtop to manufacturing throughputs. As such, varying microfluidic-based synthesis methods are being explored, one of which is the AXF crossflow technology developed by Micropore Technologies.

This project aims to develop a thorough understanding of the effect of the process parameters and fluid mixing dynamics within the range of Micropore's crossflow devices to support the fast and easy scale-up of LNP production processes and to enable local vaccine manufacture within developing countries. This will be achieved by evaluating the impact of operating speed, lipid concentration, choice of ionizable lipid on LNP critical quality attributes (CQAs) using Micropore AXF-Mini crossflow device. Succeeding this, LNP efficacy *in vitro* and methods scaling to an *in vivo* dosage concentration will be evaluated.

# Chapter 1: Introduction

1.1 Introduction of LNPs, mRNA and their use in vaccine development.

Liposomes, an early predecessor of Lipid nanoparticles (LNPs) (Tenchov *et al*., 2021), were first described in the early 1960's when Bangham discovered that egg lecithin, when combined with water, formed small amphiphilic nanospheres (Wagner & Vorauer-Uhl, 2011). Initially utilised as cell membrane models, it quickly became apparent that liposomes would be an ideal delivery candidate for small drug molecules (Gregoriadis, 2016; Wagner & Vorauer-Uhl, 2011), leading to the development and introduction of the first liposome-mediated therapeutic nano-drug approved by the FDA, Doxil®, in 1995 (Barenholz, 2012; Gregoriadis, 2016; Carla B. Roces *et al*., 2020; Wagner & Vorauer-Uhl, 2011). Coinciding with this, messenger RNA (mRNA) was first discovered in 1961 as a key component of the central dogma (Hou *et al*., 2021). Further elucidation into the function of mRNA quickly highlighted its potential as a therapeutic and vaccine candidate (Hou *et al*., 2021). It proved advantageous against previous DNA constructs due to its lack of interaction with the genome, preventing potential risk of detrimental genomic integrations (Chaudhary *et al*., 2021). In addition to this, mRNA's ability to encode multiple pathogenic antigens within the one transcript and its natural transient state (Chaudhary *et al*., 2021), provided a more potent immunostimulant that could metabolically degrade within a few days, avoiding any potential toxicity issues (Schlake *et al*., 2012). However, despite being advantageous, mRNA's natural transient state and single-strand structure made it highly susceptible to endogenous ribonucleases and translational inhibitors (Schlake *et al.*, 2012). As such, researchers explored the development of liposome mediated encapsulation and delivery of mRNA (Tenchov *et al.*, 2021; Thi *et al.*, 2021). The term 'Lipid nanoparticle' (LNP) was introduced in the late 1980's (Tenchov *et al*., 2021). LNPs provide a more stable, biocompatible delivery system (compared to non-replicating viral vectors) protecting against enzymatic degradation and allowing for targeted delivery to the cytosol (Chaudhary *et al*., 2021). Following the successful demonstration of liposome-mediated drug delivery in 1978 (Hou *et al*., 2021), it was proposed, due to the complex structure and polarity distribution of mRNA, a more intricate cationic lipid formulation could improve mRNA affinity and encapsulation efficiency (Hou *et al*., 2021; Swetha *et al*., 2023). As of 2023, LNPs are typically synthesised with four standard components as shown in *Figure 1*. These components consist of a cationic or ionizable lipid for mRNA binding; a helper lipid involved in aiding nanoparticle stability; cholesterol to introduce rigidity to the lipid membrane and

a PEGylated lipid as a propagator of steric hinderance involved in avoiding scavenger endothelial cells (Chaudhary *et al*., 2021; Evers *et al*., 2018; Swetha *et al*., 2023).

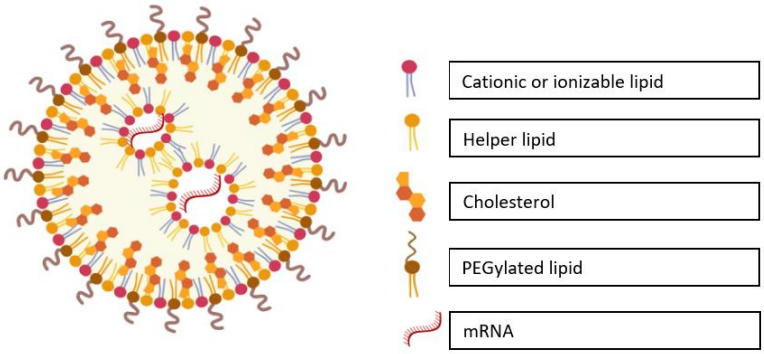


***Figure 1: Graphical display of a mRNA-LNP vaccine and the structural components implemented in colloidal formation. Illustrated through Bio-render.***

The cationic or ionizable lipid components are considered the most influential in the colloid formation of LNPs, distributing a positive charge complexing the phosphate backbone of mRNA. Cationic lipids, differential to ionizable, have a permanent positively charged head group, commonly due to a tertiary or quaternary amine (Yung *et al*., 2016). Whilst beneficial in maintaining mRNA affinity during the continually changing production process of LNPs, cationic LNP formulations can be problematic when introduced *in vivo,* demonstrating higher toxicity by interacting with the anionic sialylated glycoproteins of red blood cells (Chaudhary *et al*., 2021; Yung *et al*., 2016). This, in turn, can lead to off-target effects and impinged efficacy of therapeutics. As a result, many vaccine candidates have since opted for the inclusion of an ionizable lipid component. These lipids are neutral at physiological pH (pH~7.4) but become protonated when introduced to a low pH environment (<pH 6.0)(Evers *et al*., 2018; Hou *et al*., 2021). Contrary to cationic alternatives, this pH-mediated polarity is conducive to successfully delivering mRNA products. A neutral pH during bloodstream dissemination aids in the evasion of anionic biomolecules whilst vacuolar acidification of LNP-endosomes upon cell uptake of ionizable LNPs aids in membrane destabilisation and release of mRNA into the cell cytosol (Hu *et al*., 2015; Swetha *et al*., 2023; Thi *et al*., 2021). Consequently, many vaccine development and biopharma companies have employed these lipid-mediated delivery mechanisms in their prospective vaccine candidates (Thi *et al*., 2021).

## 1.2 Current LNP-mediated drug delivery landscape and MHRA/FDA approved vaccines.

Since the discovery mRNA and other nucleic acid-based constructs such as: small interfering RNA (siRNA) – non-coding RNA's designed to silence or alter gene expression; small activating RNA (saRNA) – an RNA construct designed to upregulate gene expression; microRNA (miRNA) – another RNA construct that targets mRNA transcripts typically modulating protein translation, oligo-nucleotide therapeutic intervention has become a key focal point in research and by extension, so has their delivery. Hallmark advancements such as the release of Onpattro, the first MHRA/FDA- approved LNP-siRNA therapeutic targeting hereditary transthyretin-mediated amyloidosis and the production of SARS-CoV2 vaccines from Moderna and Pfizer/BioNTech accelerated research interest and LNP adoption (Jürgens *et al.*, 2023; C. B. Roces *et al*., 2020). A recent survey conducted by E, D. Namiot (2023) found that between 2002 and 2021 a total of 486 clinical trials using nanoparticles were identified. Of those approved since 2016, 22% and 21% were liposomal and lipid-based products respectively (Namiot *et al*., 2023). In addition, the study found that between 2002 and 2016, liposomal/lipid-based nanoparticles contributed to 30% of nanoparticles in clinical trials, with the majority type in development being protein nanoparticles (51%) (Namiot *et al*., 2023). However, between the years of 2016 and 2021 this landscape changed with liposomal/lipid-based nanoparticles contributing to 52% of the total nanoparticles used in clinical trials and protein nanoparticle usage decreasing to 26% (Namiot *et al*., 2023). As of December 2021, there are currently 40 nucleic acid-LNP based therapeutics within the clinical pipeline. The current market value of LNP-based genomic medicines is approximately $51 billion with expectations of revenue decline following the reduction of SARS-CoV2 vaccination. However, market value is predicted to rebound to an estimated $48 billion by 2036 considering therapeutics in clinical trials (Verma, 2023).

Table 1: Summary of oligonucleotide/LNP-based therapeutics within the clinical pipline as of 2021

| | **Marketed/Filed** | **Phase III** | **Phase II** | **Phase I** |
|---|---|---|---|---|
| Gene addition and replacement **(8)** | N/A | N/A | Reqorsa<br>mRNA-4157<br>mRNA-3927 | mRNA-2752<br>MRT5005<br>mRNA-6231<br>MEDI1191 |

| | | | | |
|---|---|---|---|---|
| | | | mRNA-3705 | |
| Gene expression control **(5)** | Onpattro | N/A | ND-L02-s0201 | ALN-VSP<br>NBF-006<br>INT-1B3 |
| Gene editing **(2)** | N/A | N/A | NTLA-2002 | NTLA-2001 |
| DNA and RNA vaccines **(25)** | Comirnaty<br>SpikeVax | ARCT-154<br>ARCoV<br>CVnCoV<br>mRNA-1647 | ARCT-021<br>Covigenix<br>VAX-001<br>DS-5670<br>PTX-COVID19-B<br>mRNA-1893 | BNT161<br>CV7202<br>ChulaCov19 mRNA Vaccine<br>CoV2 SAM vaccine<br>mRNA MRK-1172<br>mRNA MRK-1777<br>mRNA-1010<br>mRNA-1283<br>mRNA-1345<br>mRNA-1388<br>mRNA-1443<br>mRNA-1653<br>mRNA-1851<br>mRNA-5671 |

## 1.3 Development of microfluidics

Whilst a new generation of promising LNP therapeutics progress through the clinical pipeline, one of the primary considerations and challenges facing their progression is having a suitable production method (Roces *et al*., 2019; Shepherd *et al*., 2021). Conventional methods explored for manufacturing LNPs involve techniques such as lipid film hydration, in which lipid formulations are dissolved in an organic solvent and vacuum-dried to form thin lipid films. When these films are rehydrated in a nucleic acid-containing buffer, they form spontaneous nanoparticles (Shah *et al*., 2020) This top-down approach, whilst effective, is less conducive to a manufacturing environment. The stochastic nature associated with LNP formation can create more polydisperse populations requiring further downstream size manipulation methods such as particle extrusion (Forbes *et al*., 2019). Consequently, large scale manufacture of LNPs in this manner can be a long, multi-step process, ultimately

resulting in larger production costs and potential intra-batch variability (Carla B. Roces *et al*., 2020; Shah *et al*., 2020). One method that aims to address these pitfalls is the development of microfluidic mixing. First proposed in 2004, the process involves combining a lipid mixture eluted in organic solvent with an aqueous buffer, containing the desired nucleic acid, in a mixing vessel (Webb *et al*., 2020). The turbulent mixing and change in polarity lead to the nanoprecipitation and self-assembly of nucleic acid containing LNPs. As such, a wide range of microfluidic mixing vessels, often existing in a microchip format, have been explored to optimise a monodisperse, robust LNP production method (Kimura *et a*l., 2018; Maeki *et al*., 2022). All of these adopt various fluid mixing dynamics. The most commonly utilised: Staggered Herringbone (SHB) - a chaotic mixing structure pioneered by Precision Nanosystems (PNI), designed for rapid mixing under low Total Flow Rates (TFR) <20mL/min; Bifurcating mixer – a toroidal structure implementing dean vortices better suited to higher TFR conditions, employed on the PNI Ignite system; Microfluidic Hydrodynamic Focusing (MHF) – a mixing approach in which two aqueous streams are introduced into a central organic stream and T-Junctions – a synthesis method in which an organic phase is introduced to an aqueous stream perpendicularly, resulting in a turbulent output flow (Ali *et al*., 2021; Evers *et al*., 2018; Jürgens *et al*., 2023; Kimura *et al*., 2018; Maeki *et al.*, 2022). Despite the individual merits of these fluid mixing structures, the necessity for a scale-independent, uniform design, capable of formulating LNPs at benchtop to manufacturing throughputs, remains imperative to the translational success of LNPs within the clinic (C. B. Roces *et al*., 2020; Shepherd *et al*., 2021). As such, varying mixing alternatives aiming to achieve these criteria are being explored, including the AXF crossflow technology developed by Micropore Technologies. Aiming to capitalise on the pitfalls of microfluidics, Micropore Technologies developed a crossflow membrane technology. Lipid formulations are forced through a micron filter perpendicular to the flow of an aqueous buffer containing mRNA/small drug molecules. This results in the formation of theoretically monodispersed LNPs under low shear conditions, which is particularly pertinent given the fragility of mRNA (Hou *et al*., 2021). Bypassing the scalability bottlenecks of microchip microfluidic mixing, Micropore Technologies have developed three mixing vessels: AXF™mini/Pathfinder – 1-200mL production volumes; AXF™one – 6-200L/hr production volumes; AXF™n – up to 1500L/hr production volumes. These cover the throughput requirements for every stage of the drug/vaccine development pipeline whilst maintaining a consistent mixing architecture required for robust LNP reproducibility.

## 1.4 Aims and Objectives

This project aimed to develop a thorough understanding of the effect of the process parameters and fluid mixing dynamics within the range of Micropore's crossflow devices to support the fast and easy scale-up of LNP and other nanoparticle production processes, helping to increase access to these emerging technologies and to enable local vaccine manufacture within developing countries. This was explored by evaluating the impact of operating speed, lipid concentration, choice of ionizable lipid on LNP critical quality attributes (CQAs) using Micropore AXF-Mini crossflow device. Once elucidated, LNP efficacy *in vitro* and methods scaling to an *in vivo* dosage concentration was evaluated to ensure therapeutic retention following synthesis.

# Chapter 2: Materials and Methods

## 2. Materials and Methods

### 2.1 Materials

>99.8% Ethanol (Fisher Scientific, Loughborough, UK); Distearoylphosphatidylcholine (DSPC) (Lipoid, Ludwigshafen, Germany); Cholesterol (Merck Life Science, Hertfordshire, UK); 1,2-Dioleoyl-3-trimethylammonium propane (DOTAP) (Avanti Polar Lipids, Alabaster, AL, USA); 1,2-Dimyristoyl-sn-glycero-3-methoxypolyethylene glycol (DMG-PEG2000) (Avanti Polar Lipids, Alabaster, AL, USA); SM-102 (Broadpharm, San Diego, CA, USA); C-12 200 (Broadpharma San Diego, CA, USA); 1,2-distearoyl-*sn*-glycero-3-phosphoethanolamine-*N*-[methoxy(polyethylene glycol)-2000 (DMPE-PEG2000) (Avanti Polar Lipids, Alabaster, AL, USA); ALC-0315 (Avanti Polar Lipids, Alabaster, AL, USA); ALC-0159 (Avanti Polar Lipids, Alabaster, AL, USA); ultrapure DNA/RNAse – $H_2O$ (Scientific laboratory supplies (SLS), Hessle, UK); poly A (Merck Life Science, Hertfordshire, UK); Firefly Luciferase (Fluc) mRNA (Stratech, Cambridgeshire, UK); deionised – $H_2O$ (SLS, Hessle, UK); 2-propanol (Fisher Scientific, Loughborough, UK); 15mL falcon tubes (VWR, Radnor, PA, USA); 1.5mL Eppendorf tubes (VWR, Radnor, PA, USA); 50mL Falcon tubes (VWR, Radnor, PA, USA); Amicon ultra centrifugal filters 100K (Merck Life Science, Hertfordshire, UK); Megafuge 40 Centrifuge (ThermoFisher Scientific, New York, USA); Dialysis tubing cellulose membrane 25mm (Merck Life Science, Hertfordshire, UK); Sodium citrate dihydrate (Merck Life Science, Hertfordshire, UK); Citric acid (Merck Life Science, Hertfordshire, UK); 200mL beaker (VWR, Radnor, PA, USA); 400 mL beaker (VWR, Radnor, PA, USA); magnetic stirrer (VWR, Radnor, PA, USA); 50mL BD Luer-lock syringe (Fisher Scientific, Loughborough, UK); 10mL Luer-lock syringe (Fisher Scientific, Loughborough, UK); AL-1000 syringe driver (World precision instruments, Sarasota, FL, USA); AL-1010 syringe driver (World precision instruments, Sarasota, FL, USA); Micropore AXF-Mini (Micropore Technologies, Redcar, UK); BD Blunt needle (Fisher Scientific, Loughborough, UK); weigh boat (Fisher Scientific, Loughborough, UK); PBS tablets (Oxoid, Basingstoke, UK); 1,1'-dioctadecyl-3,3,3',3'-tetramethylindocarbocyanine perchlorate ($DilC_{18}$) (Invitrogen, Massachusetts, USA); Zen0040 low volume cuvette (VWR, Radnor, PA, USA); Malvern zetasizer cuvette (Malvern Instruments, Worcestershire, UK); Quant-IT ribogreen kit (Invitrogen, Massachusetts, USA); Malvern zeta-sizer ultra-series (Malvern Instruments, Worcestershire, UK); F96 Microwell Black plates (Invitrogen, Massachusetts, USA); F96 Microwell white, clear

bottom plates (Invitrogen, Massachusetts, USA); F96 Microwell black, clear bottom plates (Invitrogen, Massachusetts, USA); F96 Microwell clear, round bottom plates (Invitrogen, Massachusetts, USA); Glomax Explorer (Promega Corporation®, Madison, WI, USA); One-glo luciferase assay system (Promega Corporation®, Madison, WI, USA); POLARstar® Fluorescence microplate reader (Omega, Oertenberg, Germany); Alamar blue reagent (Invitrogen, Massachusetts, USA); Minimal Essential Medium (MEM) (Gibco, ThermoFisher Scientific, New York, USA); fetal bovine serum (FBS) (Gibco, ThermoFisher Scientific, New York, USA); sodium pyruvate (Gibco, ThermoFisher Scientific, New York, USA); penicillin/streptomycin (Gibco, ThermoFisher Scientific, New York, USA); 10X NorthernMax MOPS Buffer (Invitrogen, Massachusetts, USA); Agarose powder (Invitrogen, Massachusetts, USA); 9kb RNA Millenium hyperladder (Invitrogen, Massachusetts, USA); SYBR Green II gel stain (Invitrogen, Massachusetts, USA); Formaldehyde loading dye (Invitrogen, Massachusetts, USA); Sub-Cell GT Cell Gel electrophoresis tank (Bio-Rad, Hercules, CA, USA); EZ Gel doc imager (Bio-Rad, Hercules, CA, USA).

## 2.2 Methods

### 2.2.1: Formulation and stock preparation of organic and aqueous phase

Prior to formulation preparation, all lipid stocks were prepared at a concentration of 20 mg/mL and eluted >99.8 % ethanol. Stocks were then stored at -20°C until DOTAP, SM-102, ALC-0315 and C-12 200 lipid mixtures were prepared for LNP production. Four formulations of lipid mixtures were prepared at the following molar ratios: Distearoylphosphatidylcholine (DSPC) (10): Cholesterol (38.5): 1,2-Dioleoyl-3-trimethylammonium propane (DOTAP) (50): DMG-PEG2000 (1.5); Distearoylphosphatidylcholine (DSPC) (10): Cholesterol (38.5): SM-102 (50): DMG-PEG2000 (1.5); Distearoylphosphatidylcholine (DSPC) (9.4): Cholesterol (42.7): ALC-0315 (46.3): ALC-0159 (1.6); Distearoylphosphatidylcholine (DSPC) (16): Cholesterol (46.5): C-12 200 (35): DMPE-PEG2000 (2.5). In the case where lipid yield and LNP uptake was being assessed, the lipophilic fluorophore, 1,1'-dioctadecyl-3,3,3',3'-tetramethylindocarbocyanine perchlorate ($DiIC_{18}$) was added into the lipid phase before microfluidics at 1 % and 0.25 % molar fraction. Before crossflow mixing, DOTAP, SM-102 and ALC-0315 lipid mixtures were prepared at an initial starting concentration of 1.8 mg/mL, 1.9 mg/mL and 1.9 mg/mL respectively. In the case of C-12 200, lipid mixtures were prepared at an initial lipid concentration of 11.6 mg/mL

and diluted down to 2.3 mg/mL utilising >99 % ethanol. All lipid mixtures were allowed to reach room temperature before injection into the Micropore AXF Mini. Poly A-containing aqueous phase was prepared in 50 mM Citrate buffer pH6 for DOTAP LNPs due to the cationic nature of these lipids and 50 mM Citrate buffer pH4 for ionizable SM-102 and ALC-0315 LNP production. In the case of C-12 200 LNP production, Poly A - containing aqueous phase was prepared in 50 mM sodium acetate buffer pH4. Poly A- buffer mixtures were prepared at a poly A starting concentration of 0.0268 mg/mL prior to production of both DOTAP and SM-102 LNPs. For ALC-0315 and C-12 200, Poly A- buffer mixtures were prepared at a poly A starting concentration of 0.0248 mg/mL and 0.0938 mg/mL respectively. In the case of Firefly Luciferase (Fluc) mRNA, mRNA-Citrate buffer mixtures were prepared at a mRNA starting concentration of 0.0283 mg/mL prior to production of SM-102 LNPs.

2.2.2: Crossflow manufacture of Lipid Nanoparticles (LNPs) on Micropore AXF-Mini

All LNPs were produced at an aqueous: organic Flow Rate Ratio (FRR) of 3:1 and an ionizable/cationic amine to nucleic acid phosphate (n/p) ratio of 6. Lipid and aqueous mixtures were loaded into BD syringes and fitted into 2 independent world precision instruments (WPI) AL-1010 syringe drivers. In the case where Total Flow Rates (TFR's) below 30 mL/min were tested, 10 mL BD syringes were utilised, unless scaling to TFR's exceeded this, then 50 mL syringes were utilised for consistency. Syringes were connected to the Micropore AXF Mini via 1/16" OD PFA tubing and Total Flow Rates were set. DOTAP- Dil$C_{18}$ formulations were mixed at a TFR range of 20-60 mL/min and SM-102 formulations at a TFR range of 10-60 mL/min. For all formulations, organic and aqueous phases were injected into the AXF Mini simultaneously and 1 mL of LNPs were collected in 15 mL falcon tubes for downstream sizing, uniformity measuring, purification, zeta potential, encapsulation efficiency and nucleic acid recovery measurements.

2.2.3: Characterisation of LNP particle size and polydispersity index (PDI) through Dynamic Light Scattering (DLS)

Succeeding crossflow mixing mediated LNP production, aliquots of LNPs were collected and diluted in 50 mM Citrate buffer to a 0.1 mg/mL lipid concentration. The particle sizes and PDI were then measured by DLS using a Malvern zeta-sizer ultra-series (Malvern Instruments Ltd., Worcestershire, UK) utilising a 632.8 nm 10 mW He-Ne laser with a detection angle set at 173°. LNPs were measured using a 1.47 refractive index and a 1.28 cP viscosity with the dispersant set at citrate buffer.

Zetasizer Software v.7.11 (Malvern Instruments Ltd., Worcestershire, UK.) was used for the acquisition of data.

2.2.4: Dialysis and Spin column purification of LNPs

Once LNP particle diameter and PDI had been determined, 1 mL of newly synthesized LNPs were loaded into 14,000 Da dialysis membrane, immersed in 1X Phosphate Buffered Saline (PBS) pH 7.4 and allowed to spin for 1 hr in the case of cationic formulations and 4 hrs for ionizable formulations to allow for buffer exchange. In the case of ionizable formulations purified through spin column, 1 mL of LNPs were mixed with 39 mL of 1X PBS and centrifuged at 2000 RCF at 4°C through 100,000 K Millipore Amicon Ultra 15 mL spin column, until LNPs had been centrifuged down to 1 mL. Following purification, aliquots of LNPs were collected and subsequent aliquots were diluted in 1X PBS to a 0.1 mg/mL final lipid concentration. Particle diameters, PDI and zeta potential were measured by DLS using a Malvern zeta-sizer ultra-series (Malvern Instruments Ltd., Worcestershire, UK) utilising a 632.8 nm 10 mW He-Ne laser with a detection angle set at 173°. LNPs were measured using a 1.34 refractive index and a 1.02 cP viscosity with the dispersant set at PBS. Zetasizer Software v.7.11 (Malvern Instruments Ltd., Worcestershire, UK) was used for the acquisition of data. LNPs were then stored at 4°C until further downstream characterisation.

2.2.5: Dil$C_{18}$ fluorescence assay

Quantification of lipid content during the manufacture of LNPs was undertaken to determine the lipid loss/LNP dilution during crossflow production and purification after a low poly A recovery was observed in previous SM-102 samples. The addition of a lipophilic fluorophore, 1,1'-dioctadecyl-3,3,3',3'-tetramethylindocarbocyanine perchlorate (Dil$C_{18}$) was added into the lipid phase before microfluidics at a 0.1 molar ratio (Forbes *et al*., 2019) for initial experiments and subsequently reduced to molar ratio 0.025 due to an over-saturation of fluorescence emission. 400 µL aliquots of samples were removed before microfluidics, post-microfluidics and post-purification to better understand lipid concentration at each stage of the LNP production process. Lipid content of each aliquot was then quantified against a DOTAP- Dil$C_{18}$lipid phase dilution series ranging from 2400 – 0 µg/mL. To account for a spectral shift of Dil$C_{18}$ fluorescence when incorporated into the lipid membrane, subsequent experiments incorporated a LNP dilution series, synthesised on Precision Nanosystems Nanoassemblr, ranging 800 – 0 µg/mL to quantify lipid content of LNPs post-microfluidics. The optic settings were set at 544 - 590 nm excitation/emission and gain

1000 (POLARstar® Omega, BMG Labtech, Ortenberg, Germany). The recovery concentrations were then calculated from both the $DilC_{18}$- lipid phase and $DilC_{18}$- LNP standard curve.

2.2.6: Ribogreen assay

After purification, aliquots were removed from LNP samples and diluted down to achieve an encapsulated poly A concentration of 3 µg/mL. A Quant-iT Ribogreen RNA assay was then undertaken. Samples were quantified against a 1000 ng/mL and 200 ng/mL poly A curve to quantify fluorescent emissions between nucleic acid cargo. Encapsulation efficiency (EE) was calculated by the difference in fluorescent emission in triton-X treated samples, causing lysis, against the untreated samples. Mass balance (MB) recovery of poly A cargo in LNP samples was then calculated using the 1000 ng/mL poly A standard curve. The percentage recovery was calculated against a theoretical 100% yield of 750 ng/mL poly A. The samples were analysed at 475 - 525 nm excitation/emission on GloMax Explorer (Promega Corporation®, Madison, WI, USA). This same protocol was also utilised for calculating the encapsulation and nucleic acid recovery of LNP – Firefly Luciferase (Fluc) mRNA samples. Samples were quantified against a 1000 ng/mL and 200ng/mL Fluc mRNA curve. Samples were tested in technical duplicates and results of biological replicates were presented individually as a means to demonstrate inter-day and intra-sample variability.

2.2.7: PPL command script construction

AL-1010 syringe drivers were set to a baud rate of 19,200 and pump address' were defined. Pump programming Language (PPL) command scripts were generated utilising SyringepumpproV1 Standard PPL creator. PPL scripts were generated for individual pumps and communicated to dispense an initial wastage volume of 2 mL and 5 x 1 mL aliquots at a TFR of 30 mL/min. Following initial optimisation and introduction of a new Ultra-Low Volume (ULV) insert, PPL scripts were generated and communicated to dispense an initial wastage volume of 800 µL and a 1 mL sample volume at a desired TFR (30 mL/min).

2.2.8: Evaluating HEK293 cell viability following LNP treatment.

Human Embryonic Kidney (HEK) 293 cells were seeded on a clear round bottom 96 well plate at a cell density of $1x10^4$ and supplemented with Minimal Essential Media (MEM) supplemented with FBS, Penicillin/streptomycin and Amphotericin B. Plates were then incubated for 72 hrs at 37°C, 5 % $CO_2$ to allow wells to reach ~80 %

confluency. Following incubation, MEM media was removed, and MEM media supplemented with LNPs at a 2, 1, 0.5 and 0.25 µg/mL nucleic acid concentration, was added in triplicate to HEK293 cells incubated for a further 24 hrs at 37°C, 5 % $CO_2$. Control cells with untreated MEM media and 1% triton-X were additionally utilised. After incubation, plates were supplemented with 10 µL of Alamar blue reagent and plates were incubated at 37°C, 5 % $CO_2$ for a further 6 hrs to allow for dye metabolism. Fluorescence was then measured using a GloMax Explorer (Promega Corporation®, Madison, WI, USA) at Ex/Em of 520/580-640 nm, and cell viability was calculated relative to untreated cell fluorescence emission.

2.2.9: Evaluating LNP uptake into HEK293 cells.

HEK293 cells were seeded on a black clear bottom 96 well plate at a cell density of $1x10^4$ and supplemented with Minimal Essential Media (MEM) supplemented with FBS, Penicillin/streptomycin and Amphotericin B. Plates were then incubated for 72 hrs at 37°C, 5 % $CO_2$ to allow wells to reach ~80 % confluency. Following incubation, MEM media was removed, and MEM media supplemented with $DilC_{18}$ – containing LNPs at 2, 1, 0.5 and 0.25 µg/mL nucleic acid concentration, was added in triplicate to HEK293 cells. $DilC_{18}$ fluorescence was measured at point of dosage and then incubated for a further 24 hrs at 37°C, 5 % $CO_2$. Control cells with untreated MEM media was additionally utilised. Succeeding incubation, excess media was removed, and 1 % triton-X PBS was added to all wells and plates were incubated at 37°C, 5% $CO_2$ for 20 mins to allow for cell lysis. Fluorescence was then measured using a GloMax Explorer (Promega Corporation®, Madison, WI, USA) at Ex/Em of 520/580-640 nm, and LNP uptake was then calculated relative to the point of dosage fluorescence emission.

2.2.10: Evaluating expression of Fluc mRNA payload in HEK293 cells through LNP delivery.

HEK293 cells were seeded on a white clear bottom 96 well plate at a cell density of $1x10^4$ and supplemented with Minimal Essential Media (MEM) supplemented with FBS, Penicillin/streptomycin and Amphotericin B. Plates were then incubated for 72 hrs at 37°C, 5 % $CO_2$ to allow wells to reach ~80 % confluency. Following incubation, MEM media was removed, and MEM media supplemented with LNPs at 2, 1, 0.5 and 0.25 µg/mL nucleic acid concentration, was added in triplicate to HEK293 cells and incubated for a further 24 hrs at 37°C, 5 % $CO_2$. Control cells with untreated MEM media was additionally utilised. Succeeding incubation, 100 µL of One- glo luciferin

substrate was added to all wells and bioluminescence was then measured using a GloMax Explorer (Promega Corporation®, Madison, WI, USA). Fluc mRNA expression was then measured relative to untreated cells.

2.2.11: Evaluating Fluc mRNA integrity following LNP encapsulation and cell treatment.

Following cell treatments, aliquots of Fluc mRNA-LNP samples were diluted down to 10 µg/mL, mRNA was then extracted through an ethanol/ 3 M sodium acetate (pH5.2) extraction. Samples were mixed and centrifuged at 14,000 RPM for 20 mins. Supernatant was removed, ethanol/ 3 M sodium acetate (pH5.2) was added and the process was then repeated. mRNA pellets were then resuspended in 35 µL of RNAse-free $H_2O$ and stored at 4°C until gel electrophoresis preparation. In short, 0.5 g of agarose powder was added to 1X NothernMax MOPS buffer and heated until dissolved. Once cooled to approximately 55°C, 5 µL of SYBR Green II gel stain was added to the mixture, poured into a gel cast and allowed to set. Once dried, agarose gel was immersed in 300 mL of 1x NorthernMax MOPS buffer. Samples and a 9kb RNA millennium hyperladder were mixed with formaldehyde loading dye (3:1 v/v) and heated for 10 mins at 70°C to allow for denaturation of nucleic acid secondary structures. In addition to samples a positive control utilising naked Fluc mRNA, and a no template control (NTC) were also formaldehyde-heat treated. Succeeding treatment, 400 ng of sample was loaded on to the agarose gel and run at 90 V for 1 hr. The agarose gel was then removed and visualised under UV light using a Bio-Rad EZ gel doc imager.

2.2.12: Investigating the effects of purification volume on LNP CQAs

To further contextualise experiments aiming at scaling LNP concentrations to reach an *in vivo* dosage concentration, the dilution effect on LNP CQAs was evaluated. SM-102 poly A LNPs were synthesized as previously described utilising the Micropore AXF-Mini. 4 mL of SM-102 LNPs were produced, 1 mL was dialysed as previously described and three 1 mL aliquots were the diluted in 9 mL, 19 mL and 39 mL of PBS and centrifuged at 2000 RCF at 4°C, returning to an end volume of 1 mL. SM-102 LNPs were then evaluated to assess the impact dilution volume played on LNP CQAs.

2.2.13: Evaluation of LNP concentration scaling methods.

Following in-depth analysis of SM-102 LNP transfection capability and *in vitro* performance, of two methods to reach a greater than 0.1 mg/mL nucleic acid dosage,

a suitable dosage for *in vivo* investigation, were evaluated. In short, 8 mL SM-102 LNPs, at a poly A concentration of 0.02 mg/mL, were synthesised at a TFR of 30mL/min utilising the Micropore AXF-Mini as previously described. LNPs were subsequently aliquoted, and 1 mL was purified through dialysis, as previously described. Further 1.5 mL, 2.5 mL and 3.5 mL aliquots of the remaining sample was then purified through spin column purification, as previously described with exception that all aliquots were centrifuged to an end volume of 500 µL, resulting in 3 aliquots with a theoretical poly A concentration of 0.06 mg/mL, 0.1 mg/mL and 0.14 mg/mL. In addition to concentrating SM-102 LNPs through spin column, LNP concentration was increased at the manufacturing stage. SM-102 LNPs were synthesised utilising the same TFR and FRR conditions on the Micropore AXF-Mini as previously with the exception that LNPs were manufactured at 0.02 mg/mL, 0.05 mg/mL and 0.1 mg/mL poly A concentration and further purified through dialysis. All LNPs CQAs were then characterised as previously described and an effective scaling method was selected.

### 2.2.14: Statistical analysis

Samples were tested and presented as a mean value n=3 ± standard deviation (SD) unless stated otherwise. Statistical analysis was tested utilising one or two – way analysis of variance (ANOVA) with a Tukey's post ad-hoc to compare the mean values of samples. The ANOVA method utilised (one or two – way) for each experiment is clarified in the discussion section and appendix. Analysis was undertaken through GraphPad Prism 10 with $P > 0.05$ (ns), $P < 0.05$ (*), $P < 0.01$ (**), $P < 0.001$ (***) and $P < 0.0001$ (****) as seen in Appendix 7.

# Chapter 3: Results

## 3. Results

### 3.1 Investigation into the effect of mixing speed on DOTAP LNP Critical Quality attributes (CQAs)

To investigate the effect of mixing speed on the CQAs of LNPs, DOTAP LNPs were manufactured at a mixing speed range of 10-60mL/min through AXF crossflow production and further characterised through DLS and ribogreen assessment. The results in *Figure 2* show the size and PDI of LNPs before and after purification. LNPs presented a stable, reproducible inter-day particle size that reduced as the TFR of mixing was increased. LNPs manufactured at a TFR10, 20 and 30mL/min produced particles at 125 nm ± 7 nm, 104 nm ± 4 nm and 92 nm ± 3nm respectively as seen in *Figure 2*. Despite varying mixing speeds all particle PDIs presented a value of <0.2 (0.17 ± 0.03, 0.16 ± 0.03 and 0.15 ± 0.03) which in turn was consistent following dialysis purification (*Figure 2*). Regarding their zeta potential, the LNPs were near neutral (average zeta potential ranging from 4 – 8 mV, *Figure 2*). However, when the manufacturing speed was further increased to TFR 40, 50 and 60mL/min produced particles at 108 nm ± 7 nm, 103 nm ± 4 nm and 100 nm ± 3nm respectively (*Figure 2*). Notwithstanding the PDIs of LNP's remained low (<0.2) with neutral average zeta potential before and after purification (*Figure 2*).

Following LNP size, PDI and zeta potential characterisation, samples were diluted to 3 µg/mL and assessed for encapsulation efficiency and poly A recovery through a ribogreen assay. All samples tested, with the exception of DOTAP TFR 40 mL/min n2, presented >99 % encapsulation efficiency when fluorescence difference was measure between triton-X treated vs non-triton-X treated samples. Additionally, DOTAP LNPs had a poly A retention ranging 48 – 68 % across LNPs manufactured at all speeds tested (*Table 2*). Following initial analysis of DOTAP LNPs, a notable size increase was observed in particle diameter between LNPs synthesised at mixing speeds of 30mL/min and 40mL/min as seen in *Figure 2*. Due to inconsistency with previous findings, mixing speeds 30-60 mL/min was reassessed as shown in *Figure 3*. LNPs manufactured at a TFR30, 40, 50 and 60 mL/min produced particles at 106 nm ± 2 nm, 102 nm ± 4 nm, 100 nm ± 9 nm and 95 nm ± 4 nm respectively. Despite varying mixing speeds all particle PDIs presented a value of <0.2 (0.15 ± 0.03, 0.15 ± 0.01, 0.14 ± 0.02 and 0.16 ± 0.02) which in turn was consistent following dialysis purification. Particles presented a near neutral average zeta potential ranging from 1.4 – -2.2 mV. Following reassessment of DOTAP LNP's, sample encapsulation

efficiency and poly A recovery was evaluated through a ribogreen assay (*Table 3*). All samples presented >99 % encapsulation efficiency when fluorescence difference was measure between triton-X treated vs non-triton-X treated samples. Additionally, DOTAP LNPs had a poly A retention ranging 53- 69 % across LNPs manufactured at all speeds tested.

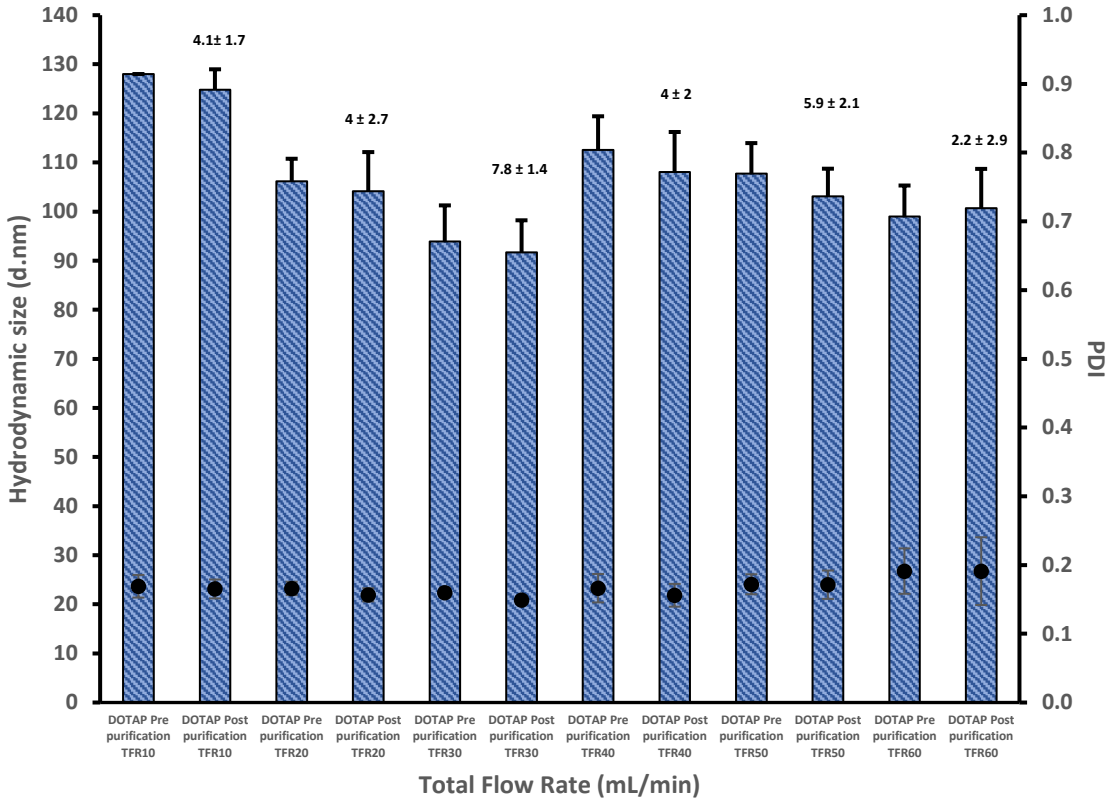


***Figure 2: DOTAP LNPs particle diameter and PDI before and after dialysis purification (n=3).*** *This figure displays the hydrodynamic size of DOTAP:DSPC:Chol:DMG-PEG2000 (50:10:38.5:1.5) poly A containing – LNPs synthesized at varying TFR's and PDI of particle population prior to and succeeding 1 hr dialysis purification. The particle sizes and PDI were measured by DLS using a Malvern zeta-sizer ultra-series utilising a 632.8 nm 10 mW He-Ne laser with a detection angle set at 173°. LNPs were measured using a 1.47 refractive index and a 1.28cP viscosity with the dispersant set at citrate buffer prior to dialysis and LNPs were then measured using a 1.34 refractive index and a 1.02 cP viscosity with the dispersant set at PBS after dialysis. Zeta potential (mV) was additionally measured succeeding LNP purification and is displayed above bar chart measurements. Zetasizer Software v.7.11 (Malvern Instruments Ltd.) was used for the acquisition of data. Statistical analysis of data was undertaken through a one or two- way ANOVA with a Tukey's post ad-hoc on GraphPad Prism 10 software, shown in Appendix 7A. Results represent mean ± SD, n = 3.*

Table 2: Nucleic acid loading within DOTAP LNPs synthesised at TFRs of 10-60mL/min

| *Sample* | | *Encapsulation Efficiency (%) – PolyA* | *Nucleic acid recovery (%) – PolyA* |
|---|---|---|---|
| **DOTAP TFR 10mL/min** | **Day 1** | 100 ± 0 | 56 ± 2 |
| | **Day 2** | 100 ± 0 | 54 ± 5 |
| | **Day 3** | 100 ± 0 | 52 ± 2 |
| **DOTAP TFR 20mL/min** | **Day 1** | 100 ± 0 | 62 ± 6 |
| | **Day 2** | 100 ± 0 | 49 ± 2 |
| | **Day 3** | 100 ± 0 | 51 ± 2 |
| **DOTAP TFR 30mL/min** | **Day 1** | 100 ± 0 | 47 ± 0 |
| | **Day 2** | 100 ± 0 | 61 ± 8 |
| | **Day 3** | 100 ± 0 | 57 ± 3 |
| **DOTAP TFR 40mL/min** | **Day 1** | 100 ± 0 | 62 ± 2 |
| | **Day 2** | 81 ± 13 | 60 ± 2 |
| | **Day 3** | 100 ± 1 | 62 ± 0 |
| **DOTAP TFR 50mL/min** | **Day 1** | 100 ± 0 | 54 ± 9 |
| | **Day 2** | 100 ± 0 | 71 ± 1 |
| | **Day 3** | 100 ± 1 | 68 ± 0 |
| **DOTAP TFR 60mL/min** | **Day 1** | 100 ± 0 | 58 ± 5 |
| | **Day 2** | 100 ± 0 | 65 ± 1 |
| | **Day 3** | 100 ± 0 | 62 ± 1 |

***Table 2: Ribogreen analysis of DOTAP LNPs manufactured TFR 10 - 60 mL/min.*** *This table displays the calculated encapsulation efficiency and nucleic acid recovery (Mass Balance) of DOTAP LNPs utilising 1000 ng/mL and 200 ng/mL poly A standard curves. Encapsulation efficiency was calculated by the difference in fluorescent emission in triton-X treated samples, causing lysis, against the untreated samples. Mass balance recovery of poly A cargo in LNP samples were then calculated using the 1000 ng/mL poly A standard curve and percentage recovery was calculated against a theoretical 100% yield of 750 ng/mL of polyA. The samples were analysed at 475 - 525 nm excitation/emission on GloMax Explorer. Statistical analysis of data was undertaken through a one or two- way ANOVA with a Tukey's post ad-hoc on GraphPad Prism 10 software, shown in Appendix 7B.*

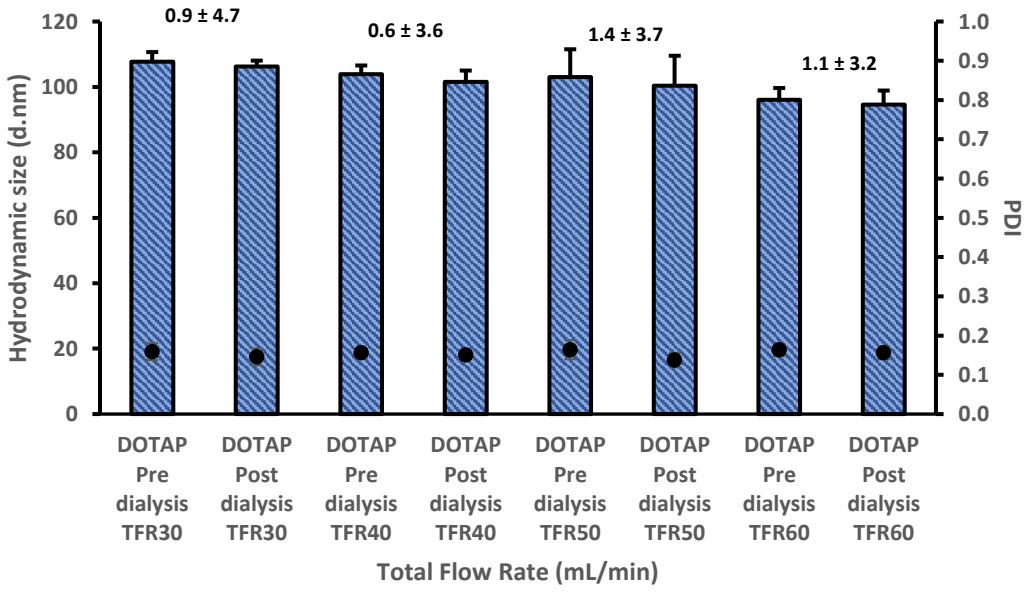

***Figure 3: DOTAP LNPs particle diameter and PDI before and after dialysis purification (n=3).*** *This figure displays the hydrodynamic size of DOTAP:DSPC:Chol:DMG-PEG2000 (50:10:38.5:1.5) poly A containing – LNPs synthesized at varying TFR's and PDI of particle population prior to and succeeding 1 hr dialysis purification. The particle sizes and PDI were measured by DLS using a Malvern zeta-sizer ultra-series utilising a 632.8 nm 10 mW He-Ne laser with a detection angle set at 173°. LNPs were measured using a 1.47 refractive index and a 1.28 cP viscosity with the dispersant set at citrate buffer prior to dialysis and LNPs were then measured using a 1.34 refractive index and a 1.02 cP viscosity with the dispersant set at PBS after dialysis. Zeta potential (mV) was additionally measured succeeding LNP purification and is displayed above bar chart measurements. Zetasizer Software v.7.11 (Malvern Instruments Ltd.) was used for the acquisition of data. Statistical analysis of data was undertaken through a one or two- way ANOVA with a Tukey's post ad-hoc on GraphPad Prism 10 software, shown in Appendix 7C. Results represent mean ± SD, n = 3.*

Table 3: Nucleic acid loading within DOTAP LNPs synthesised at TFRs of 30-60mL/min

| ***Sample*** | | ***Encapsulation Efficiency (%) – PolyA*** | ***Nucleic acid recovery (%) – PolyA*** |
|---|---|---|---|
| **DOTAP TFR 30mL/min** | **Day 1** | 100 ± 0 | 55 ± 1 |
| | **Day 2** | 100 ± 0 | 68 ± 0 |
| | **Day 3** | 100 ± 0 | 53 ± 5 |
| **DOTAP TFR 40mL/min** | **Day 1** | 100 ± 0 | 55 ± 4 |
| | **Day 2** | 100 ± 0 | 69 ± 0 |
| | **Day 3** | 100 ± 0 | 64 ± 12 |
| **DOTAP TFR 50mL/min** | **Day 1** | 100 ± 0 | 59 ± 0 |
| | **Day 2** | 99 ± 1 | 60 ± 1 |
| | **Day 3** | 100 ± 0 | 67 ± 2 |
| **DOTAP TFR 60mL/min** | **Day 1** | 100 ± 0 | 59 ± 0 |
| | **Day 2** | 100 ± 0 | 67 ± 4 |
| | **Day 3** | 100 ± 0 | 68 ± 1 |

***Table 3: Ribogreen analysis of DOTAP LNPs.*** *This table displays the calculated encapsulation efficiency and nucleic acid recovery (Mass Balance) of DOTAP LNPs utilising 1000 ng/mL and 200 ng/mL poly A standard curves. Encapsulation efficiency was calculated by the difference in fluorescent emission in triton-X treated samples, causing lysis, against the untreated samples. Mass balance recovery of poly A cargo in LNP samples were then calculated using the 1000 ng/mL poly A standard curve and percentage recovery was calculated against a theoretical 100 % yield of 750 ng/mL of poly A. The samples were analysed at 475 - 525 nm excitation/emission on GloMax Explorer. Statistical analysis of data was undertaken through a one or two- way ANOVA with a Tukey's post ad-hoc on GraphPad Prism 10 software, shown in Appendix 7D.*

3.2 Evaluation of the effect of dialysis and spin column purification on SM-102 LNP CQAs

Following the data gathered from DOTAP LNPs, the next step was to evaluate the manufacturing process with ionisable lipids therefore SM-102 LNPs were prepared under one of the selected TFRs, of 30mL/min. SM-102 LNPs presented a stable reproducible inter-day particle size that proved comparable to corresponding DOTAP LNPs manufactured at the same TFR (± 11 nm) as shown in *Figure 4A*. SM-102 LNPs manufactured at 30mL/min produced particles at 96 nm ± 5 nm and a PDI of 0.12 ± 0.01 prior to purification. Following dialysis purification, SM-102 LNPs presented minimal deviation from initial size and PDI measurements with average zeta potential of 10.6 mV ± 4. Subsequently, SM-102 formulations displayed ~15 nm increase in particle diameter after spin column purification. In conjunction with this observation, the PDI of the corresponding sample decreased to 0.1 ± 0.01. In addition to this, sample purified through spin column displayed a lower zeta potential than its corresponding dialysed sample of -3 mV ± 2. Following LNP size, PDI and zeta potential characterisation, samples were diluted to 3 µg/mL and assessed for encapsulation efficiency and poly A recovery through a ribogreen assay. All samples tested, with the exception of SM-102 TFR 30 mL/min dialysis n1, presented >99 % encapsulation efficiency when fluorescence difference was measure between triton-X treated vs non-triton-X treated samples. Additionally, SM-102 LNPs had a poly A retention ranging 54 – 63 % across LNPs manufactured at all speeds tested.

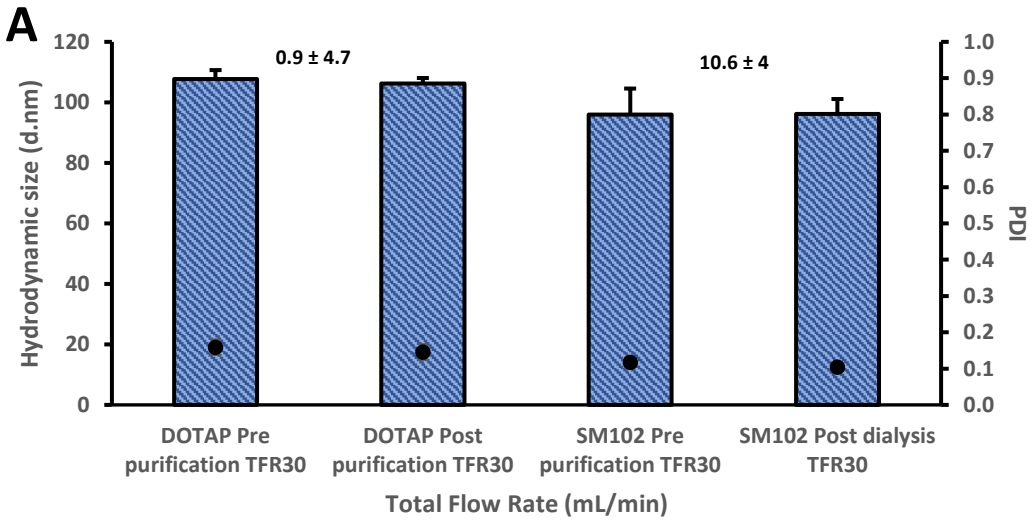

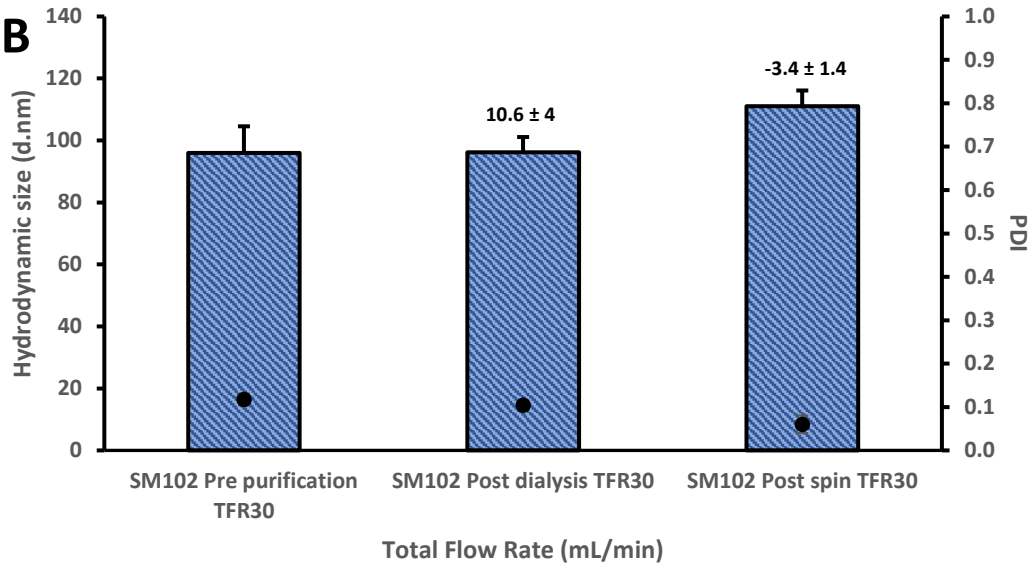


***Figure 4: SM-102 LNPs particle diameter and PDI before and after dialysis/spin purification (n=3). (A) DOTAP and SM-102 LNPs particle diameters, PDI and Zeta potential of formulations manufactured at the same TFR.*** *This figure displays the hydrodynamic size of DOTAP:DSPC:Chol:DMG-PEG2000(50:10:38.5:1.5) poly A containing – LNPs synthesized at a TFR of 30 mL/min and PDI of particle population prior to and succeeding 1 hr dialysis purification.* ***(B) SM-102 LNPs particle diameters, PDI and Zeta potential of formulations manufactured at the same TFR and purified through dialysis and spin column.*** *This figure displays the hydrodynamic size of SM-102:DSPC:Chol:DMG-PEG2000(50:10:38.5:1.5) poly A containing – LNPs synthesized at a TFR of 30 mL/min and PDI of particle population prior to and succeeding 1hr dialysis purification and spin column purification. The particle sizes and PDI were measured by DLS using a Malvern zeta-sizer ultra-series utilising a 632.8 nm 10 mW He-Ne laser with a detection angle set at 173°. LNPs were measured using a 1.47 refractive index and a 1.28 cP viscosity with the dispersant set at citrate buffer prior to dialysis and LNPs were then measured using a 1.34 refractive index and a 1.02 cP viscosity with the dispersant set at PBS after dialysis. Zeta potential (mV) was additionally measured succeeding LNP purification and is displayed above bar chart measurements. Zetasizer Software v.7.11 (Malvern Instruments Ltd.) was used for the acquisition of data. Statistical analysis of data was undertaken through a one or two- way ANOVA with a Tukey's post ad-hoc on GraphPad Prism 10 software, shown in Appendix 7E. Results represent mean ± SD, n = 3.*

Table 4: Ribogreen analysis of SM-102 LNPs purified through dialysis and spin column

| *Sample* | | *Encapsulation Efficiency (%) – PolyA* | *Nucleic acid recovery (%) – PolyA* |
|---|---|---|---|
| **SM-102 post dialysis TFR 30mL/min** | **Day 1** | 92 ± 0 | 63 ± 0 |
| | **Day 2** | 100 ± 0 | 54 ± 0 |
| | **Day 3** | 100 ± 0 | 58 ± 0 |
| **SM-102 post spin TFR 30mL/min** | **Day 1** | 99 ± 0 | 57 ± 2 |
| | **Day 2** | 99 ± 0 | 57 ± 0 |
| | **Day 3** | 99 ± 0 | 55 ± 1 |

***Table 4: Ribogreen analysis of SM-102 LNPs.*** *This table displays the calculated encapsulation efficiency and nucleic acid recovery (Mass Balance) of SM-102 LNPs utilising 1000 ng/mL and 200 ng/mL poly A standard curves. Encapsulation efficiency was calculated by the difference in fluorescent emission in triton-X treated samples, causing lysis, against the untreated samples. Mass balance recovery of poly A cargo in LNP samples were then calculated using the 1000 ng/mL poly A standard curve and percentage recovery was calculated against a theoretical 100 % yield of 750 ng/mL of poly A. The samples were analysed at 475 - 525 nm excitation/emission on GloMax Explorer. Statistical analysis of data was undertaken through a one or two- way ANOVA with a Tukey's post ad-hoc on GraphPad Prism 10 software.*

## 3.3 Investigating the recovery of lipids following purification through dialysis of DOTAP LNPs.

DOTAP LNPs were manufactured and characterised as previously described utilising AXF crossflow production, DLS particle characterisation and ribogreen analysis to assess encapsulation however with 1% $DilC_{18}$ was incorporated into lipid formulations. LNPs presented a stable reproducible inter-day particle size that reduced as the TFR of mixing was increased. LNPs manufactured at a TFR10, 30 and 60 mL/min produced particles at 134 nm $\pm$ 2 nm, 113 nm $\pm$ 3 nm and 93 nm $\pm$ 3 nm respectively as seen in *Figure 5*. Despite varying mixing speeds all particle PDIs presented a value of <0.2 following 1hr dialysis (0.18 $\pm$ 0.02, 0.17 $\pm$ 0.02 and 0.18 $\pm$ 0.03). Additionally, particles presented a near neutral average zeta potential ranging from -4.6 – -7.8 mV. As seen in *Table 5,* $DilC_{18}$ fluorescence analysis of DOTAP LNP's presented a decrease in emission signal ranging from 7-18 % compared to that of pre-dialysed samples. This reduction was then accounted for in the ribogreen assay and further LNP characterisation of samples through ribogreen analysis was tested. All DOTAP presented >99 % encapsulation efficiency when fluorescence difference was measure between triton-X treated vs non-triton-X treated samples. Additionally, DOTAP LNPs had a poly A retention ranging 88 – 100 % across all speeds tested, as shown in *Table 6*.

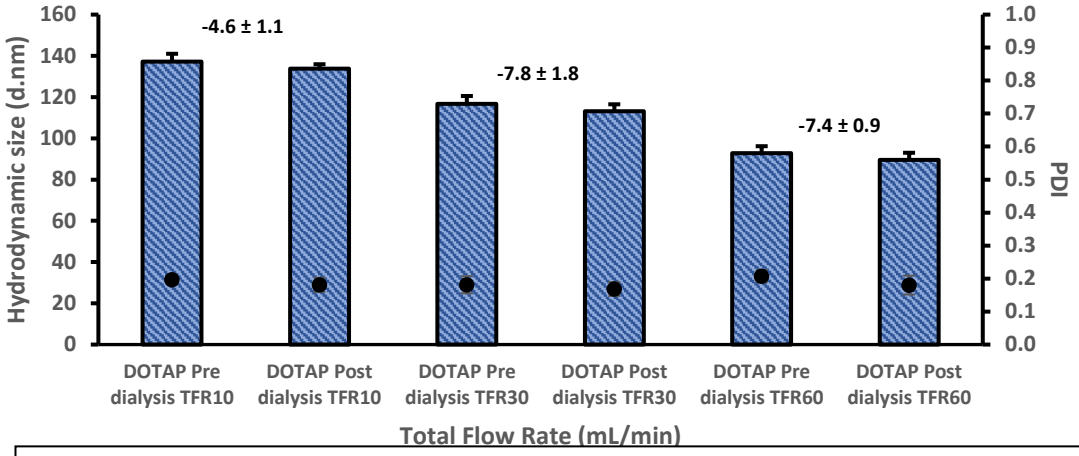


***Figure 5: DOTAP LNPs particle diameter and PDI before and after dialysis/spin purification (n=3).*** *This figure displays the hydrodynamic size of DOTAP:DSPC:Chol:DMG-PEG2000:DilC$_{18}$ (50:10:38.5:1.5:0.25) poly A containing – LNPs synthesized at varying TFR and PDI of particle population prior to and succeeding 1 hr dialysis purification. The particle sizes and PDI were measured by DLS using a Malvern zeta-sizer ultra-series utilising a 632.8 nm 10 mW He-Ne laser with a detection angle set at 173°. LNPs were measured using a 1.47 refractive index and a 1.28 cP viscosity with the dispersant set at citrate buffer prior to dialysis and LNPs were then measured using a 1.34 refractive index and a 1.02 cP viscosity with the dispersant set at PBS after dialysis. Zeta potential (mV) was additionally measured succeeding LNP purification and is displayed above bar chart measurements. Zetasizer Software v.7.11 (Malvern Instruments Ltd.) was used for the acquisition of data. Statistical analysis of data was undertaken through a one or two- way ANOVA with a Tukey's post ad-hoc on GraphPad Prism 10 software, shown in Appendix 7G. Results represent mean ± SD, n = 3.*

Table 5: Relative lipid recovery of DOTAP-DilC$_{18}$ LNPs following dialysis purification

***DilC recovery post-dialysis (%)***

| Sample | Day 1 | Day 2 | Day 3 |
|---|---|---|---|
| TFR 10 mL/min | 90 | 90 | 93 |
| TFR 30 mL/min | 86 | 87 | 87 |
| TFR 60 mL/min | 83 | 82 | 85 |

***Table 5: Relative Lipid recovery of DOTAP- DilC$_{18}$ LNP's succeeding dialysis purification, calculated from DilC$_{18}$ fluorescence emission at 590 nm (n=3).*** *This table displays the calculated lipid recovery percentage relative to pre-purified LNP sample from fluorescence emission of DOTAP:DSPC:Chol:DMG-PEG2000:DilC$_{18}$ (50:10:38.5:1.5:1) LNPs synthesised at varying TFR's where optic settings were set and measured at 544 - 590 nm excitation/emission and gain 1000 on the POLARstar® Omega.*

Table 6: Ribogreen analysis of DOTAP-DilC$_{18}$ LNPs synthesised at 10 mL/min to 60 mL/min

| *Sample* | | *Encapsulation Efficiency (%) – PolyA* | *Nucleic acid recovery (%) – PolyA* |
|---|---|---|---|
| **DOTAP TFR 10mL/min** | **Day 1** | 100 ± 0 | 92 ± 9 |
| | **Day 2** | 100 ± 0 | 88 ± 3 |
| | **Day 3** | 100 ± 0 | 95 ± 7 |
| **DOTAP TFR 30mL/min** | **Day 1** | 100 ± 0 | 99 ± 8 |
| | **Day 2** | 99 ± 0 | 98 ± 5 |
| | **Day 3** | 100 ± 0 | 98 ± 10 |
| **DOTAP TFR 60mL/min** | **Day 1** | 100 ± 0 | 96 ± 7 |
| | **Day 2** | 100 ± 0 | 100 ± 4 |
| | **Day 3** | 100 ± 0 | 100 ± 2 |

***Table 6: Ribogreen analysis of DOTAP- DilC$_{18}$ LNPs.*** *This table displays the calculated encapsulation efficiency and nucleic acid recovery (Mass Balance) of DOTAP-DilC$_{18}$ LNPs utilising 1000 ng/mL and 200 ng/mL poly A standard curves. Encapsulation efficiency was calculated by the difference in fluorescent emission in triton-X treated samples, causing lysis, against the untreated samples. Mass balance recovery of poly A cargo in LNP samples were then calculated using the 1000 ng/mL poly A standard curve and percentage recovery was calculated against a theoretical 100 % yield of 750 ng/mL of poly A. The samples were analysed at 475 - 525 nm excitation/emission on GloMax Explorer.*

## 3.4: DilC$_{18}$ assay optimisation

### 3.4.1: 1% DilC$_{18}$ DOTAP lipid phase standard curve characterisation

Following the reduced poly A recovery of previous SM-102 formulations, lipid concentration in LNP formulations was investigated to ensure a FRR of 3:1 was being achieved under current manufacturing parameters on the Micropore AXF-Mini. In order to quantify the lipid content, indicated by DilC$_{18}$ fluorescence emission, a DOTAP- DilC$_{18}$ lipid phase dilution series ranging 2400 – 0 µg/mL was plotted to establish suitability as a standard curve. Analysis of standard curves plots, shown in *Figure 6*, showed a linear regression $R^2$ value of <0.98 indicating linear regression was not achieved. A larger level of variance between the 2 variables assessed (fluorescence emission and lipid concentration) was observed and curves yielded $R^2$ values of 0.9064 and 0.9756 respectively. To be able to predict with a degree of accuracy and ensure lipid concentrations extrapolated are representative, an $R^2$ value of >0.98 is required, therefore curves were deemed unsuitable for lipid quantification and further optimisation was undertaken.

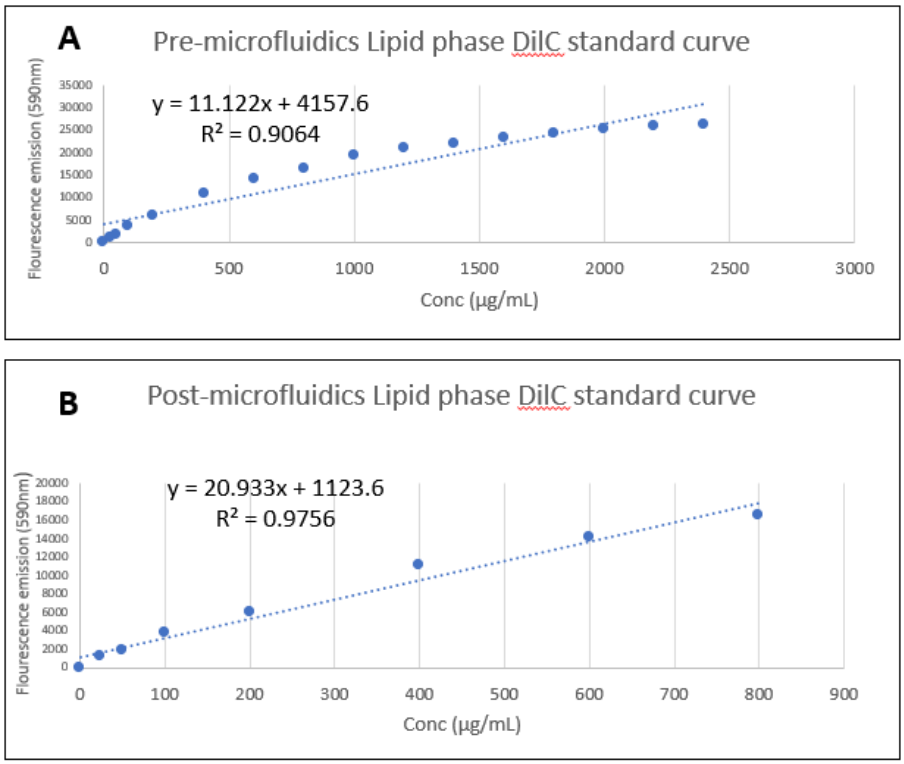


***Figure 6: 1 % DOTAP DilC$_{18}$ standard curve. (A) DOTAP- DilC$_{18}$ lipid phase dilution series ranging 2400 – 0 µg/mL. (B) DOTAP- DilC$_{18}$ lipid phase dilution series ranging 800 – 0 µg/mL.*** *This figure displays the fluorescence emission of a DOTAP:DSPC:Chol:DMG-PEG2000:DilC$_{18}$ (50:10:38.5:1.5:1) lipid phase dilution series with a starting total lipid concentration at 2400 µg/mL. Optic settings were set and measured at 544 - 590 nm excitation/emission and gain 1000 on the POLARstar® Omega.*

### 3.4.2: 0.25% $DilC_{18}$ DOTAP lipid phase standard curve characterisation

Succeeding initial DOTAP- $DilC_{18}$ (1 %) standard curves inadmissible of lipid quantification, a second dilution series reducing the molar ratio of $DilC_{18}$ to 0.25 % was loaded onto a 96 well plate in duplicate and measured on the POLARstar® Omega plate reader. Optic settings were set at 544 - 590 nm excitation/emission and gain 1000. As seen in *Figure 7*, both standard curves displayed a linear regression $R^2$ value of >0.98 and limit of detection (LOD) and limit of quantification (LOQ) suitable for quantification of lipid content through the LNP manufacturing and purification process.

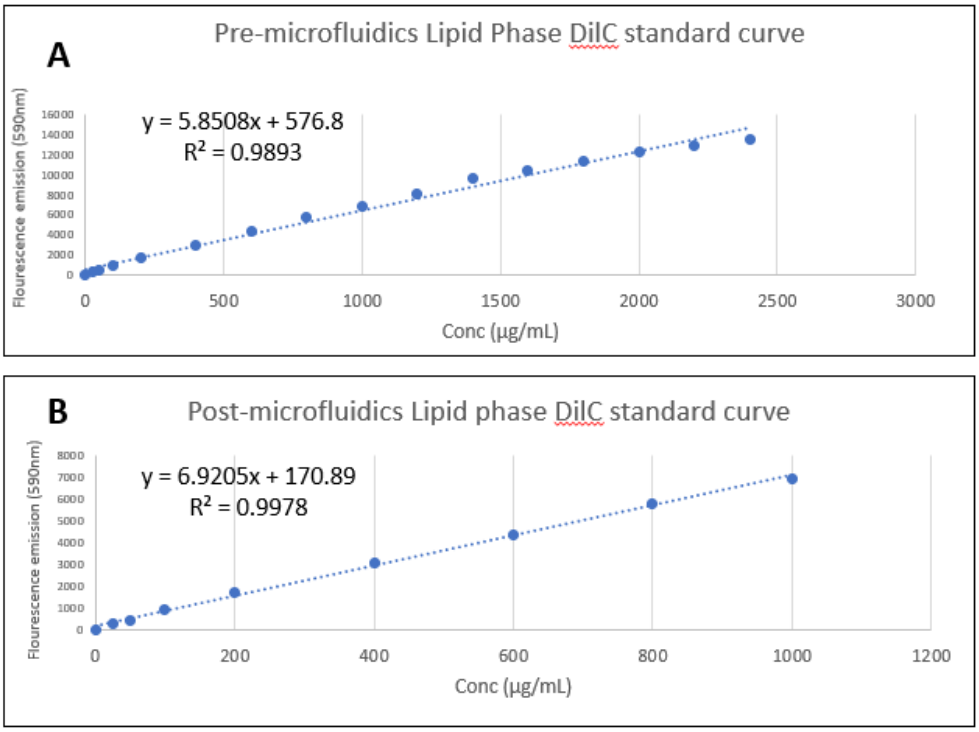


***Figure 7: 0.25 % DOTAP $DilC_{18}$ standard curve. (A) DOTAP- $DilC_{18}$ lipid phase dilution series ranging 2400 – 0 µg/mL. (B) DOTAP- $DilC_{18}$ lipid phase dilution series ranging 800 – 0 µg/mL.*** *This figure displays the fluorescence emission of a DOTAP:DSPC:Chol:DMG-PEG2000:$DilC_{18}$ (50:10:38.5:1.5:0.25) lipid phase dilution series with a starting total lipid concentration at 2400 µg/mL. Optic settings were set and measured at 544 - 590 nm excitation/emission and gain 1000 on the POLARstar® Omega.*

3.4.3: Evaluating the lipid recovery during DOTAP LNP production at a mixing speed of 60 mL/min

Following DOTAP- $DilC_{18}$ lipid phase standard curve optimisation, DOTAP- $DilC_{18}$ LNPs were manufactured and characterised as previously described. As shown in *Figure 8,* LNPs presented a stable reproducible particle size ~97 nm ± 6 nm and a PDI <0.2 (0.191 ± 0.03) suitable for RES evasion with minimal particle deviation occurring during dialysis-induced buffer exchange. Particles presented a near neutral average zeta potential (-3.3 ± 1.6). Following DOTAP LNP characterisation, lipid content of aliquots removed prior to microfluidics, post microfluidics and post purification were assessed for $DilC_{18}$ fluorescence to ensure lipid content was consistent with theoretical values and a FRR of 3:1 Aqueous: organic phase was maintained throughout the production process. Both standard curves displayed a linear regression $R^2$ value of >0.98 and limit of detection (LOD) and limit of quantification (LOQ) appropriate for quantification of lipid content as shown in *Figure 9*. Total lipid content was calculated using the equation of the line with the 2400 µg/mL standard curve being utilised for pre-microfluidic aliquots that have a theoretical value of 1844 µg/mL and the 1000 µg/mL curve being utilised for post microfluidic aliquots that have a theoretical value of 461 µg/mL. DOTAP- $DilC_{18}$ aliquots presented comparable lipid concentration to theoretical concentrations prior to microfluidics, however post microfluidic aliquots presented >10 % deviation from desired theoretical values. Following $DilC_{18}$ fluorescence measurements, LNP samples were diluted to 3 µg/mL and assessed for encapsulation efficiency and poly A recovery through a ribogreen assay. Triplicate LNP samples were tested twice under different dilutions considering: i) the percentage reduction of $DilC_{18}$ fluorescence following dialysis purification and ii) the absolute lipid concentrations calculated from standard curves. As shown in *Table 8*, All samples tested, presented 100 % encapsulation efficiency when fluorescence difference was measure between triton-X treated vs non-triton treated samples. Poly A recovery was markedly higher and comparable to previous findings in samples diluted accounting for percentage loss during dialysis providing a mass balance of 77 %. Samples diluted according to the absolute lipid concentration presented a lower average mass balance recovery of 43 %.

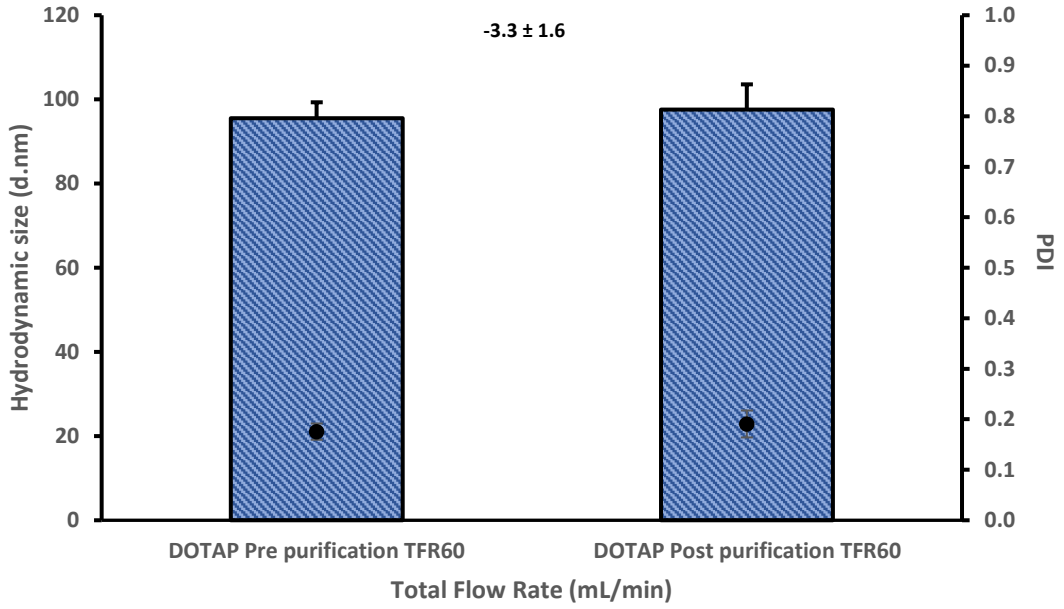


***Figure 8: 0.25 % DOTAP- DilC$_{18}$ LNPs particle diameter and PDI before and after dialysis purification (n=3).*** *This figure displays the hydrodynamic size of DOTAP:DSPC:Chol:DMG-PEG2000:DilC$_{18}$ (50:10:38.5:1.5:0.25) poly A containing - LNPs and PDI of particle population prior to and succeeding 1 hr dialysis purification. The particle sizes and PDI were measured by DLS using a Malvern zeta-sizer ultra-series utilising a 632.8 nm 10 mW He-Ne laser with a detection angle set at 173°. LNPs were measured using a 1.47 refractive index and a 1.28 cP viscosity with the dispersant set at citrate buffer prior to dialysis and LNPs were then measured using a 1.34 refractive index and a 1.02 cP viscosity with the dispersant set at PBS after dialysis. Zeta potential (mV) was additionally measured succeeding LNP purification and is displayed above bar chart measurements. Zetasizer Software v.7.11 (Malvern Instruments Ltd.) was used for the acquisition of data. Results represent mean ± SD, n = 3.*

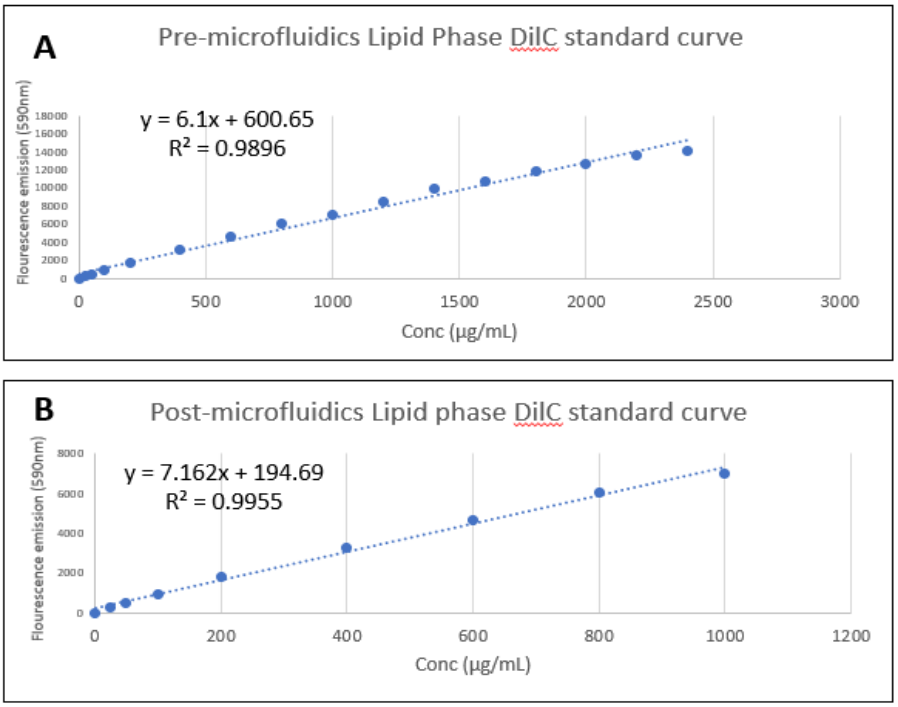


***Figure 9: 0.25 % DOTAP DilC$_{18}$ standard curve. (A)*** *DOTAP- DilC$_{18}$ lipid phase dilution series ranging 2400 – 0 µg/mL.* ***(B)*** *DOTAP- DilC$_{18}$ lipid phase dilution series ranging 1000 – 0 µg/mL. This figure displays the fluorescence emission of a DOTAP:DSPC:Chol:DMG-PEG2000:DilC$_{18}$ (50:10:38.5:1.5:0.25) lipid phase dilution series with a starting total lipid concentration at 2400 µg/mL. Optic settings were set and measured at 544 - 590 nm excitation/emission and gain 1000 on the POLARstar® Omega.*

Table 7: Lipid concentration at various stages of DOTAP-DilC$_{18}$ LNP manufacture

| Micropore | Desired Lipid concentration (µg/mL) | Lipid concentration (µg/mL) | | |
|---|---|---|---|---|
| | | n1 | n2 | n3 |
| Premixing | 1844 | 1895 | 1960 | 1978 |
| Post mixing | 461 | 660 | 1408 | 1209 |
| Post purification | 461 | 668 | 1054 | 861 |

***Table 7: Lipid concentration of 0.25% DOTAP- DilC$_{18}$ LNPs calculated from DilC$_{18}$ fluorescence emission at 590nm (n=3).*** *This table displays the calculated total lipid concentration from fluorescence emission of DOTAP:DSPC:Chol:DMG-PEG2000:DilC$_{18}$ (50:10:38.5:1.5:0.25) LNPs where optic settings were set and measured at 544 - 590 nm excitation/emission and gain 1000 on the POLARstar® Omega. Concentrations were calculated from DOTAP-DilC$_{18}$ lipid phase curves displayed in figure 9 and compared to desired theoretical lipid concentrations.*

Table 8: Ribogreen analysis of DOTAP-DilC$_{18}$ LNPs accounting for calculated lipid concentration variation

| ***Sample*** | | ***Encapsulation Efficiency (%) – PolyA*** | ***Nucleic acid recovery (%) – PolyA*** |
|---|---|---|---|
| **DOTAP TFR** | **Day 1** | 100 ± 0 | 80 ± 4 |
| **60mL/min** | **Day 2** | 100 ± 0 | 74 ± 10 |
| **(percentage loss)** | **Day 3** | 100 ± 0 | 76 ± 12 |
| **DOTAP TFR** | **Day 1** | 100 ± 0 | 56 ± 4 |
| **60mL/min** | **Day 2** | 100 ± 0 | 31 ± 5 |
| **(Absolute conc)** | **Day 3** | 100 ± 0 | 43 ± 1 |

***Table 8: Ribogreen analysis of DOTAP- DilC$_{18}$ LNPs.*** *This table displays the calculated encapsulation efficiency and nucleic acid recovery (Mass Balance) of DOTAP-DilC$_{18}$ LNPs utilising 1000 ng/mL and 200 ng/mL poly A standard curves. Encapsulation efficiency was calculated by the difference in fluorescent emission in triton-X treated samples, causing lysis, against the untreated samples. Mass balance recovery of poly A cargo in LNP samples were then calculated using the 1000 ng/mL poly A standard curve and percentage recovery was calculated against a theoretical 100 % yield of 750 ng/mL of poly A. The samples were analysed at 475 - 525 nm excitation/emission on GloMax Explorer.*

3.4.4: Evaluating the lipid recovery during DOTAP LNP production at a mixing speed of 20 mL/min.

Following initial DOTAP- $DilC_{18}$ lipid quantification testing, it was hypothesised that the lipophilic dye produced a greater excitation emission once incorporated into a lipophilic membrane as a consequence of the polarity change and therefore a secondary LNP-based standard curve would need to be utilised to quantify lipid content in newly formed LNPs. DOTAP- $DilC_{18}$ LNPs were manufactured utilising the same organic and aqueous phase on the Micropore AXF-Mini and PNI Nanoassemblr to ensure that differing particle size did not compromise $DilC_{18}$ fluorescence representation and that these two factors were irrespective of one another. Displayed in *Figure 10,* LNPs presented a stable reproducible particle size 101 nm $\pm$ 7 nm and a PDI <0.2 (0.177 $\pm$ 0.03) on the Micropore AXF-Mini and 60 nm SD $\pm$ 2 nm and a PDI >0.2 (0.214 $\pm$ 0.03) on the PNI Nanoassemblr. Particles presented a near neutral average zeta potential (-5.5 $\pm$ 4.4 & -2.3 $\pm$ 3.1). Following DOTAP LNP characterisation, lipid content of aliquots removed prior to microfluidics, post microfluidics and post purification were assessed for $DilC_{18}$ fluorescence to ensure lipid content was consistent with theoretical values and a FRR of 3:1 Aqueous: organic phase was maintained throughout the production process. Both standard curves displayed a linear regression $R^2$ value of >0.98 and limit of detection (LOD) and limit of quantification (LOQ) appropriate for quantification of lipid content (*Figure 11*). Total lipid content was calculated using the equation of the line with the 2400 µg/mL standard curve being utilised for pre-microfluidic aliquots that have a theoretical value of 1844 µg/mL and the 1000 µg/mL curve being utilised for post microfluidic aliquots that have a theoretical value of 461 µg/mL. DOTAP- $DilC_{18}$ aliquots presented comparable lipid concentration to theoretical concentrations prior to microfluidics and post microfluidics however post purification aliquots presented <10% deviation from desired theoretical values as shown in *Table 9*. Following $DilC_{18}$ fluorescence measurements, LNP samples were diluted to 3 µg/mL and assessed for encapsulation efficiency and poly A recovery through a ribogreen assay. Triplicate LNP samples were tested and diluted according to their post dialysis absolute lipid concentrations calculated from standard curves. Displayed in *Table 10*, all samples tested, presented 100% encapsulation efficiency when fluorescence difference was measure between triton-X treated vs non-triton treated samples. Poly A recovery was comparable to previous findings providing a mass balance of 69 % and 81 % for Micropore AXF-Mini and PNI Nanoassemblr-synthesised samples respectively.

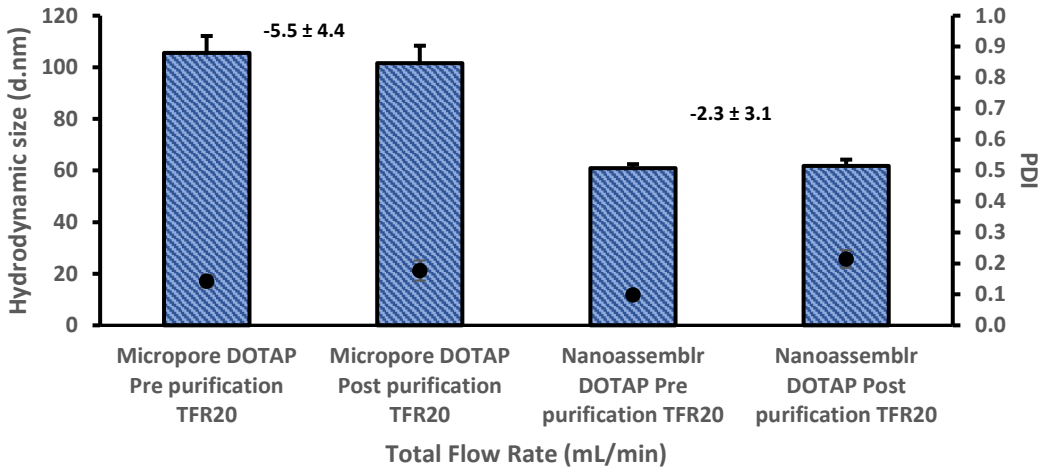


***Figure 10: Particle diameter and PDI before and after dialysis purification of 0.25 % DOTAP-DilC$_{18}$ LNP samples synthesised on the Micropore AXF-Mini and PNI Nanoassemblr (n=3).*** *This figure displays the hydrodynamic size of DOTAP:DSPC:Chol:DMG-PEG2000:DilC$_{18}$ (50:10:38.5:1.5:0.25) poly A containing - LNPs and PDI of particle population prior to and succeeding 1hr dialysis purification. The particle sizes and PDI were measured by DLS using a Malvern zeta-sizer ultra-series utilising a 632.8 nm 10 mW He-Ne laser with a detection angle set at 173°. LNPs were measured using a 1.47 refractive index and a 1.28 cP viscosity with the dispersant set at citrate buffer prior to dialysis and LNPs were then measured using a 1.34 refractive index and a 1.02 cP viscosity with the dispersant set at PBS after dialysis. Zeta potential (mV) was additionally measured succeeding LNP purification and is displayed above bar chart measurements. Zetasizer Software v.7.11 (Malvern Instruments Ltd.) was used for the acquisition of data. Statistical analysis of data was undertaken through a one or two- way ANOVA with a Tukey's post ad-hoc on GraphPad Prism 10 software, shown in Appendix 7H.*

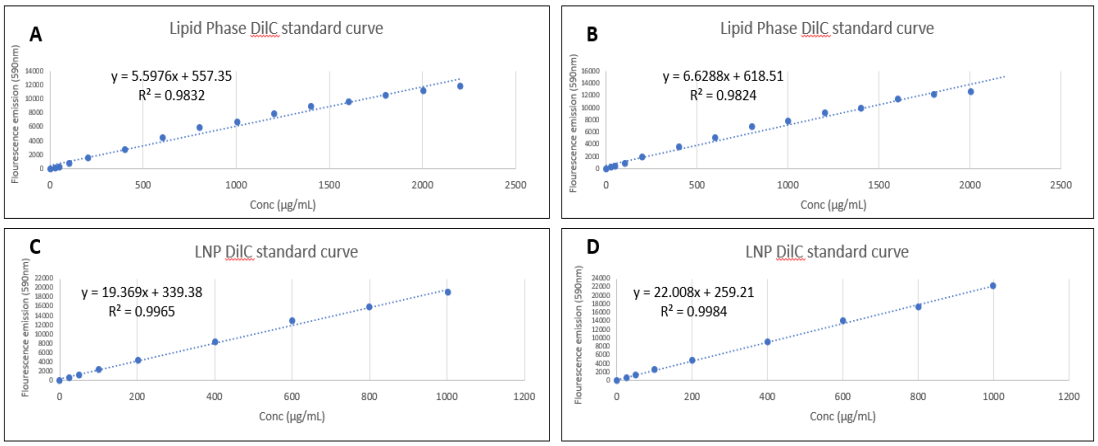


***Figure 11: 0.25 % DOTAP DilC$_{18}$ lipid phase and LNP standard curve. (A)*** *DOTAP- DilC$_{18}$ lipid phase dilution series ranging 2200 – 0 µg/mL.* ***(B)*** *DOTAP- DilC$_{18}$ lipid phase dilution series ranging 2000 – 0 µg/mL.* ***(C)*** *DOTAP- DilC$_{18}$ LNP dilution series ranging 1000 – 0 µg/mL.* ***(D)*** *DOTAP- DilC$_{18}$ LNP dilution series ranging 1000 – 0 µg/mL. This figure displays the fluorescence emission of a DOTAP:DSPC:Chol:DMG-PEG2000:DilC$_{18}$ (50:10:38.5:1.5:0.25) lipid phase dilution series with a starting total lipid concentration at 2200µg/mL and fluorescence emission of a DOTAP:DSPC:Chol:DMG-PEG2000:DilC$_{18}$ (50:10:38.5:1.5:0.25) LNP dilution series with a total lipid concentration of 1000 µg/mL. Optic settings were set and measured at 544 - 590 nm excitation/emission and gain 1000 on the POLARstar® Omega.*

Table 9: Lipid concentration at various stages of DOTAP-DilC$_{18}$ LNP manufacture utilising the Micropore AXF-Mini and PNI Nanoassemblr

| **Nanoassemblr** | **Desired Lipid concentration (µg/mL)** | **Lipid concentration (µg/mL)** | | |
|---|---|---|---|---|
| | | n1 | n2 | n3 |
| Premixing | 1844 | 1790 | 1845 | 1852 |
| Post mixing | 461 | 445 | 487 | 485 |
| Post purification | 461 | 279 | 301 | 364 |
| **Micropore** | **Desired Lipid concentration (µg/mL)** | **Lipid concentration (µg/mL)** | | |
| | | n1 | n2 | n3 |
| Premixing | 1844 | 1790 | 1845 | 1852 |
| Post mixing | 461 | 443 | 429 | 461 |
| Post purification | 461 | 361 | 370 | 378 |

***Table 9: Lipid concentration of 0.25 % DOTAP- DilC$_{18}$ LNPs calculated from DilC$_{18}$ fluorescence emission at 590nm (n=3).*** *This table displays the calculated total lipid concentration from fluorescence emission of DOTAP:DSPC:Chol:DMG-PEG2000:DilC$_{18}$ (50:10:38.5:1.5:0.25) LNPs where optic settings were set and measured at 544 - 590 nm excitation/emission and gain 1000 on the POLARstar® Omega. Concentrations were calculated from DOTAP- DilC$_{18}$ lipid phase curves displayed in figure 11 and compared to desired theoretical lipid concentrations.*

Table 10: Ribogreen analysis of DOTAP-DilC$_{18}$ LNPs synthesised at 20 mL/min on the Micropore AXF-Mini and PNI Nanoassemblr

| ***Sample*** | | ***Encapsulation Efficiency (%) – PolyA*** | ***Nucleic acid recovery (%) – PolyA*** |
|---|---|---|---|
| **Micropore DOTAP TFR 20mL/min** | **Day 1** | 100 ± 0 | 67 ± 2 |
| | **Day 2** | 100 ± 0 | 70 ± 3 |
| | **Day 3** | 100 ± 0 | 69 ± 0 |
| **Nanoassemblr DOTAP TFR 20mL/min** | **Day 1** | 100 ± 0 | 84 ± 4 |
| | **Day 2** | 100 ± 0 | 84 ± 6 |
| | **Day 3** | 100 ± 0 | 75 ± 0 |

***Table 10: Ribogreen analysis of DOTAP- DilC$_{18}$ LNPs.*** *This table displays the calculated encapsulation efficiency and nucleic acid recovery (Mass Balance) of DOTAP-DilC$_{18}$ LNPs utilising 1000 ng/mL and 200 ng/mL poly A standard curves. Encapsulation efficiency was calculated by the difference in fluorescent emission in triton-X treated samples, causing lysis, against the untreated samples. Mass balance recovery of poly A cargo in LNP samples were then calculated using the 1000 ng/mL poly A standard curve and percentage recovery was calculated against a theoretical 100 % yield of 750 ng/mL of poly A. The samples were analysed at 475 - 525 nm excitation/emission on GloMax Explorer.*

3.5: Evaluating the effect of varying Total Flow Rate (TFR mL/min) on SM-102 ionizable LNP formation and critical quality attributes (CQAs)

Evaluating if trends in manufacturing speeds were consistent across different lipid formulations, SM-102 LNPs were manufactured at 3 TFRs on the micropore AXF-mini and characterised through DLS and ribogreen assessment. Similar to DOTAP formulations, LNPs presented a stable reproducible particle size that reduced as the TFR of mixing was increased. LNPs manufactured at a TFR10, 30 and 60mL/min produced particles at 134 nm ± 7 nm, 106nm ± 4 nm and 89 nm ± 3 nm respectively. Despite varying mixing speeds all particle PDIs presented a value of <0.2 (0.133 ± 0.03, 0.13 ± 0.03 and 0.14 ± 0.03) which in turn improved to <0.1 following spin column purification. Particles presented a near neutral average zeta potential (-5 ± 0.6), shown in *Figure 12*. Following LNP size, PDI and zeta potential characterisation, samples were diluted to 3 µg/mL and assessed for encapsulation efficiency and poly A recovery through a ribogreen assay. All samples tested, presented >98 % encapsulation efficiency when fluorescence difference was measure between triton-X treated vs non-triton-X treated samples. Poly A cargo of SM-102 LNPs had a markedly increased retention than that of alternative DOTAP LNPs, presenting poly A recovery of >84 % across LNPs manufactured at all speeds tested (*Table 11*).

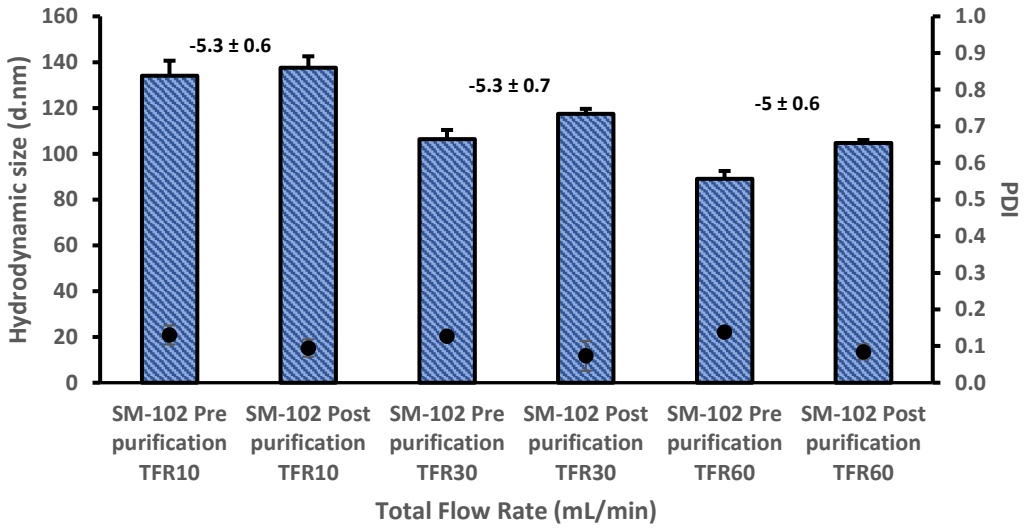

***Figure 12: Particle diameter and PDI before and after spin column purification of SM-102 LNP samples synthesised on the Micropore AXF-Mini at 10, 30 and 60 mL/min (n=3).*** *This figure displays the hydrodynamic size of SM-102:DSPC:Chol:DMG-PEG2000 (50:10:38.5:1.5) poly A containing - LNPs and PDI of particle population prior to and succeeding spin column purification. The particle sizes and PDI were measured by DLS using a Malvern zeta-sizer ultra-series utilising a 632.8 nm 10 mW He-Ne laser with a detection angle set at 173°. LNPs were measured using a 1.47 refractive index and a 1.28 cP viscosity with the dispersant set at citrate buffer prior to dialysis and LNPs were then measured using a 1.34 refractive index and a 1.02 cP viscosity with the dispersant set at PBS after dialysis. Zeta potential (mV) was additionally measured succeeding LNP purification and is displayed above bar chart measurements. Zetasizer Software v.7.11 (Malvern Instruments Ltd.) was used for the acquisition of data. Statistical analysis of data was undertaken through a one or two- way ANOVA with a Tukey's post ad-hoc on GraphPad Prism 10 software, shown in Appendix 7I.*

Table 11: Ribogreen analysis of SM-102 LNPs synthesised at TFRs 10- 60 mL/min

| ***Sample*** | | ***Encapsulation Efficiency (%) – PolyA*** | ***Nucleic acid recovery (%) – PolyA*** |
|---|---|---|---|
| **SM-102 TFR 10mL/min** | **Day 1** | 98 ± 0 | 87 ± 1 |
| | **Day 2** | 99 ± 0 | 94 ± 5 |
| | **Day 3** | 100 ± 0 | 84 ± 11 |
| **SM-102 TFR 30mL/min** | **Day 1** | 98 ± 0 | 90 ± 2 |
| | **Day 2** | 99 ± 0 | 90 ± 1 |
| | **Day 3** | 99 ± 0 | 101 ± 3 |
| **SM-102 TFR 60mL/min** | **Day 1** | 99 ± 0 | 97 ± 3 |
| | **Day 2** | 99 ± 0 | 107 ± 3 |
| | **Day 3** | 99 ± 0 | 111 ± 1 |

***Table 11: Ribogreen analysis of SM-102 LNPs.*** *This table displays the calculated encapsulation efficiency and nucleic acid recovery (Mass Balance) of SM-102 LNPs utilising 1000 ng/mL and 200 ng/mL poly A standard curves. Encapsulation efficiency was calculated by the difference in fluorescent emission in triton-X treated samples, causing lysis, against the untreated samples. Mass balance recovery of poly A cargo in LNP samples were then calculated using the 1000 ng/mL poly A standard curve and percentage recovery was calculated against a theoretical 100 % yield of 750 ng/mL of poly A. The samples were analysed at 475 - 525 nm excitation/emission on GloMax Explorer.*

### 3.6: Optimisation and evaluation of PPL-mediated automation of AL-1010 syringe drivers on DOTAP LNP formation and the effect of instrument priming of LNP CQAs

To valid the automation of AL-1010 syringe pumps, DOTAP LNPs were manufactured on the AXF-mini as previously described with the exception of the addition of an automated command script. The 1 mL aliquots of LNPs were then assessed through DLS and Ribogreen analysis to evaluate CQA consistency. LNPs presented a stable reproducible particle size across the five 1 mL aliquots collected. LNPs manufactured at a TFR30 mL/min produced particles at ranging from 88 – 99 nm and PDIs presented a value of <0.2 regardless of whether the AXF-Mini had been primed or non-primed with Aqueous and organic phase. Samples showed minimal deviation through dialysis purification and all particles presented a near neutral average zeta potential ranging from 0 – 1.8 mV, as seen in *Figure 13 and 14*. Following LNP size, PDI and zeta potential characterisation, samples were diluted to 3 µg/mL and assessed for encapsulation efficiency and poly A recovery through a ribogreen assay. All samples tested, presented 100 % encapsulation efficiency when fluorescence difference was measure between triton-X treated vs non-triton-X treated samples. Poly A cargo of DOTAP LNPs was comparable to previous findings providing a mass balance range 65-71 % (*Table 12*).

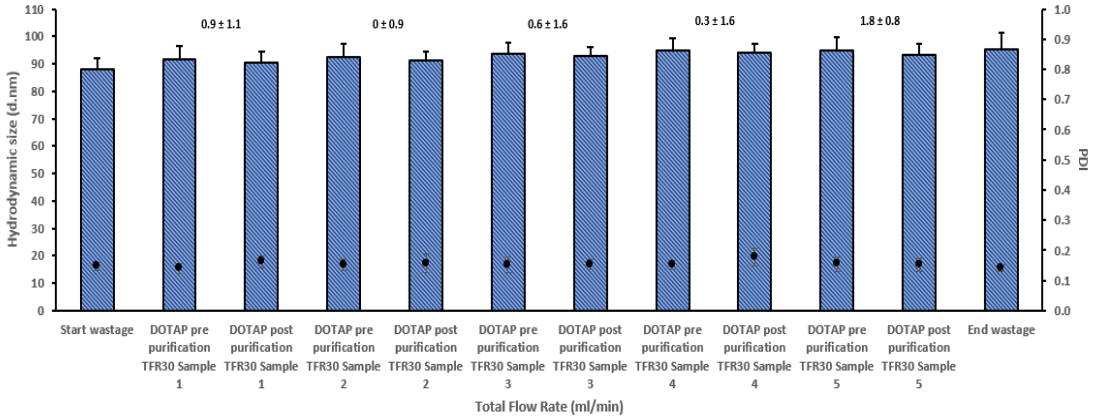


***Figure 13: Particle diameter and PDI before and after dialysis purification of DOTAP LNP samples synthesised on the Micropore AXF-Mini at 30mL/min through automated infusion with no prime (n=3).*** *This figure displays the hydrodynamic size of DOTAP:DSPC:Chol:DMG-PEG2000 (50:10:38.5:1.5) poly A containing - LNPs and PDI of particle population prior to and succeeding 1 hr dialysis purification. The particle sizes and PDI were measured by DLS using a Malvern zeta-sizer ultra-series utilising a 632.8 nm 10 mW He-Ne laser with a detection angle set at 173°. LNPs were measured using a 1.47 refractive index and a 1.28 cP viscosity with the dispersant set at citrate buffer prior to dialysis and LNPs were then measured using a 1.34 refractive index and a 1.02 cP viscosity with the dispersant set at PBS after dialysis. Zeta potential (mV) was additionally measured succeeding LNP purification and is displayed above bar chart measurements. Zetasizer Software v.7.11 (Malvern Instruments Ltd.) was used for the acquisition of data.*

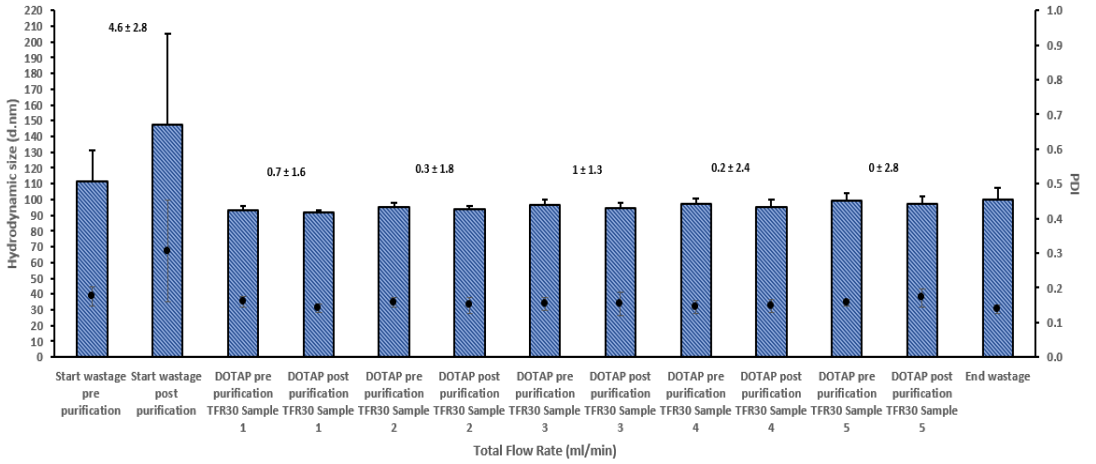


***Figure 14: Particle diameter and PDI before and after dialysis purification of DOTAP LNP samples synthesised on the Micropore AXF-Mini at 30mL/min through automated infusion primed (n=3).*** *This figure displays the hydrodynamic size of DOTAP:DSPC:Chol:DMG-PEG2000 (50:10:38.5:1.5) poly A containing - LNPs and PDI of particle population prior to and succeeding 1 hr dialysis purification. The particle sizes and PDI were measured by DLS using a Malvern zeta-sizer ultra-series utilising a 632.8 nm 10 mW He-Ne laser with a detection angle set at 173°. LNPs were measured using a 1.47 refractive index and a 1.28 cP viscosity with the dispersant set at citrate buffer prior to dialysis and LNPs were then measured using a 1.34 refractive index and a 1.02 cP viscosity with the dispersant set at PBS after dialysis. Zeta potential (mV) was additionally measured succeeding LNP purification and is displayed above bar chart measurements. Zetasizer Software v.7.11 (Malvern Instruments Ltd.) was used for the acquisition of data.*

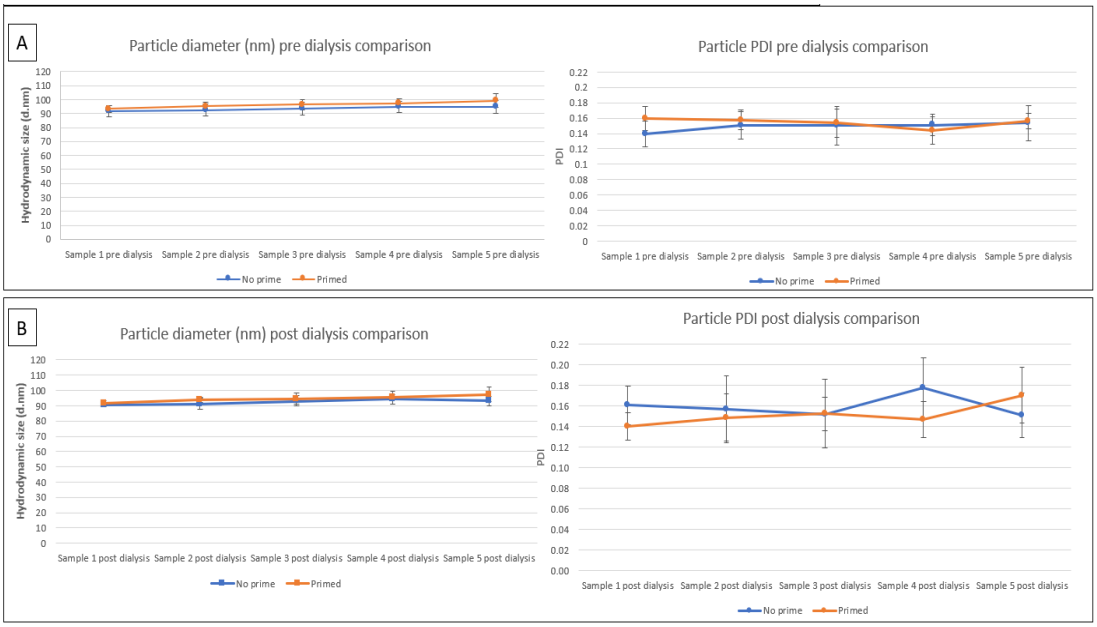


***Figure 15: Real-time particle diameter and PDI before and after dialysis purification of DOTAP LNP samples synthesised on the Micropore AXF-Mini at 30mL/min through automated infusion primed and non-primed (n=3).*** *This figure displays the hydrodynamic size of DOTAP:DSPC:Chol:DMG-PEG2000 (50:10:38.5:1.5) poly A containing - LNPs and PDI of particle population prior to and succeeding 1 hr dialysis purification. The particle sizes and PDI were measured by DLS using a Malvern zeta-sizer ultra-series utilising a 632.8 nm 10 mW He-Ne laser with a detection angle set at 173°. LNPs were measured using a 1.47 refractive index and a 1.28 cP viscosity with the dispersant set at citrate buffer prior to dialysis and LNPs were then measured using a 1.34 refractive index and a 1.02 cP viscosity with the dispersant set at PBS after dialysis. Zeta potential (mV) was additionally measured succeeding LNP purification and is displayed above bar chart measurements. Zetasizer Software v.7.11 (Malvern Instruments Ltd.) was used for the acquisition of data.*

Table 12: Ribogreen analysis of DOTAP LNPs synthesised at 30 mL/min following PPL- mediated automation

| ***Sample*** | | ***Encapsulation Efficiency (%) – PolyA*** | ***Nucleic acid recovery (%) – PolyA*** |
|---|---|---|---|
| **DOTAP TFR 30mL/min No prime** | **Sample 1** | 100 ± 0 | 67 ± 5 |
| | **Sample 2** | 100 ± 1 | 69 ± 4 |
| | **Sample 3** | 100 ± 0 | 71 ± 6 |
| | **Sample 4** | 100 ± 1 | 70 ± 5 |
| | **Sample 5** | 101 ± 1 | 65 ± 2 |
| **DOTAP TFR 30mL/min primed** | **Wastage** | 100 ± 1 | 52 ± 13 |
| | **Sample 1** | 100 ± 1 | 71 ± 2 |
| | **Sample 2** | 100 ± 1 | 72 ± 2 |
| | **Sample 3** | 100 ± 0 | 71 ± 3 |
| | **Sample 4** | 100 ± 1 | 69 ± 4 |
| | **Sample 5** | 100 ± 1 | 69 ± 4 |

***Table 12: Ribogreen analysis of DOTAP LNPs.*** *This table displays the calculated encapsulation efficiency and nucleic acid recovery (Mass Balance) of DOTAP LNPs utilising 1000 ng/mL and 200 ng/mL poly A standard curves. Encapsulation efficiency was calculated by the difference in fluorescent emission in triton-X treated samples, causing lysis, against the untreated samples. Mass balance recovery of poly A cargo in LNP samples were then calculated using the 1000 ng/mL poly A standard curve and percentage recovery was calculated against a theoretical 100 % yield of 750 ng/mL of poly A. The samples were analysed at 475 - 525 nm excitation/emission on GloMax Explorer.*

## 3.7: Evaluation of PPL-mediated automation of AL-1010 syringe drivers on SM-102 LNP formation and LNP CQAs

To avoid assumptions, following validation of syringe pump automation with DOTAP LNPs, SM-102 LNPs were manufactured using the newly optimised automated command script and characterised through DLS and ribogreen analysis to ensure consistency across differing formulations. LNPs synthesised at a TFR 30 mL/min presented a stable reproducible particle size 100 nm $\pm$ 7 nm. Additionally, particle PDI presented a value of <0.2 (0.133 $\pm$ 0.03) which was consistent following dialysis purification and a near neutral average zeta potential (7 $\pm$ 0.9), shown in *Figure 16*. Following LNP size, PDI and zeta potential characterisation, samples were diluted to a nucleic acid concentration of 3 µg/mL and assessed for encapsulation efficiency and poly A recovery through a ribogreen assay. All samples tested, presented >99 % encapsulation efficiency when fluorescence difference was measure between triton-X treated vs non-triton-X treated samples and a poly A recovery of >73 % across triplicates (*Table 13*).

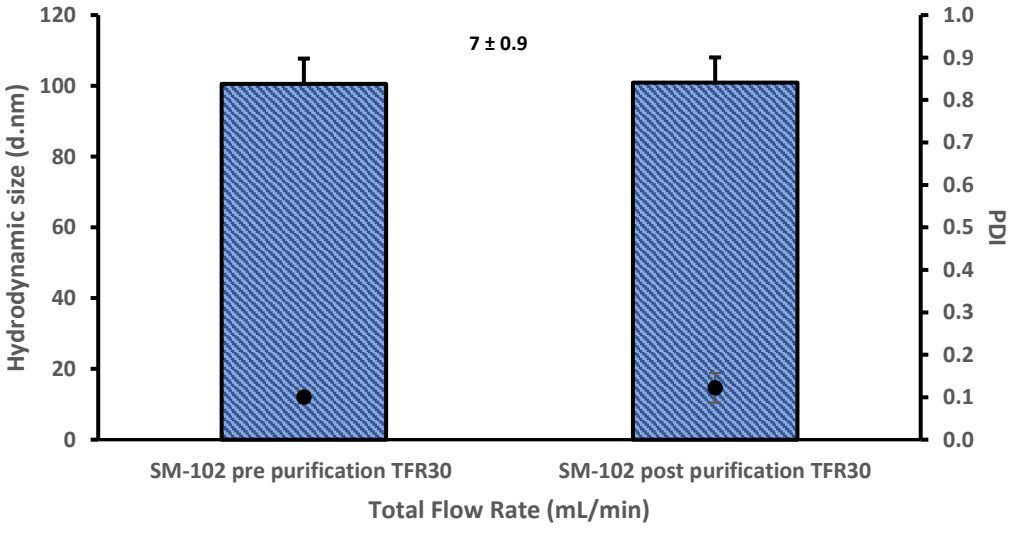

***Figure 16: Validation of SM-102 LNPs synthesised through PPL mediated syringe pump automation (n=3).*** *This figure displays the hydrodynamic size of SM-102:DSPC:Chol:DMG-PEG2000 (50:10:38.5:1.5) poly A containing - LNPs and PDI of particle population prior to and succeeding 1 hr dialysis purification. The particle sizes and PDI were measured by DLS using a Malvern zeta-sizer ultra-series utilising a 632.8 nm 10 mW He-Ne laser with a detection angle set at 173°. LNPs were measured using a 1.47 refractive index and a 1.28 cP viscosity with the dispersant set at citrate buffer prior to dialysis and LNPs were then measured using a 1.34 refractive index and a 1.02 cP viscosity with the dispersant set at PBS after dialysis. Zeta potential (mV) was additionally measured succeeding LNP purification and is displayed above bar chart measurements. Zetasizer Software v.7.11 (Malvern Instruments Ltd.) was used for the acquisition of data.*

Table 13: Ribogreen analysis of SM-102 LNPs synthesised at 30 mL/min following PPL- mediated automation

| ***Sample*** | | ***Encapsulation Efficiency (%) – PolyA*** | ***Nucleic acid recovery (%) – PolyA*** |
|---|---|---|---|
| **SM-102 TFR 30mL/min** | **Day 1** | 100 ± 0 | 76 ± 2 |
| | **Day 2** | 100 ± 0 | 73 ± 2 |
| | **Day 3** | 100 ± 0 | 79 ± 2 |

***Table 13: Ribogreen analysis of SM-102 LNPs.*** *This table displays the calculated encapsulation efficiency and nucleic acid recovery (Mass Balance) of SM-102 LNPs utilising 1000 ng/mL and 200 ng/mL poly A standard curves. Encapsulation efficiency was calculated by the difference in fluorescent emission in triton-X treated samples, causing lysis, against the untreated samples. Mass balance recovery of poly A cargo in LNP samples were then calculated using the 1000 ng/mL poly A standard curve and percentage recovery was calculated against a theoretical 100 % yield of 750 ng/mL of poly A. The samples were analysed at 475 - 525 nm excitation/emission on GloMax Explorer.*

## 3.8: Evaluation of DOTAP and SM-102 LNP cytotoxicity *in vitro*

Following establishment of PPL mediated automation of syringe drivers and reproducible synthesis of both cationic DOTAP and ionizable SM-102 LNP- poly A formulations, HEK293 cells were treated in triplicate at varying LNP concentrations to assess the potential impact of LNP treatment on cell metabolic function. Succeeding addition of Alamar blue reagent and fluorescence measurement at 520-640nm EX/EM, both DOTAP and SM-102- poly A treated HEK293 cells presented a cell viability, relative to untreated cell lines, of >96 % following treatment at 46, 23, 11.5 and 5.25 µg/mL lipid concentrations.

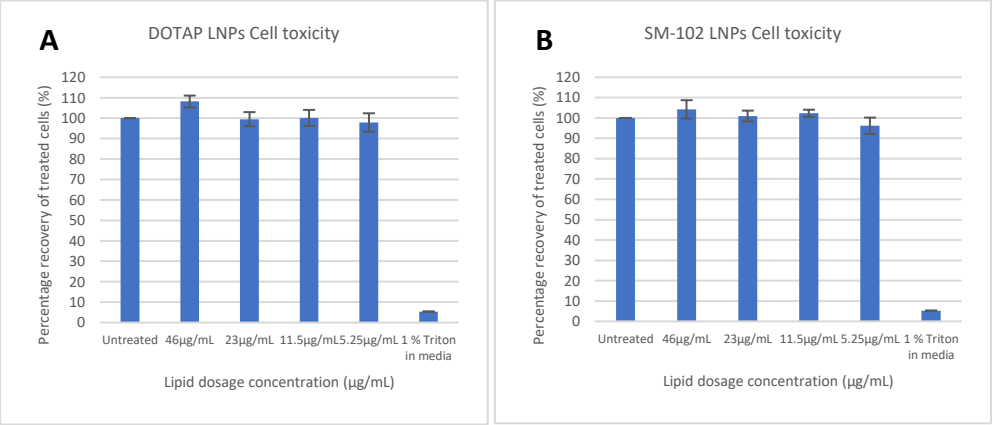


***Figure 17: Evaluation of HEK293 cell viability succeeding (A) DOTAP and (B) SM-102 – poly A LNP treatment and varying dosage concentrations (n=3).*** *This figure displays the metabolic activity of HEK293 cells 24 hrs after DOTAP and SM-102 LNP treatment through fluorometric measurement of an Alamar blue reagent. HEK293 cells seeded on a 96 well clear bottom plate at a cell density of $1x10^5$ were incubated at 37°C, 5 % $CO_2$ until confluent, following which, LNPs were diluted to desired concentration, utilising MEM media as diluent. Cells were treated and incubated for a further 24hrs. Control wells were utilised supplementing HEK293 cells with MEM media and 1 % Triton- X MEM media. Following 24 hr incubation, all wells were supplemented with 10% Alamar blue reagent and incubated for a further 6hrs to allow for dye metabolism. 96 well plates were then analysed at 520 - 640nm excitation/emission on GloMax Explorer. Fluorescence change was then normalised and measured relative to untreated cells and cell viability was calculated.*

3.9: Investigation into the effect of ULV insert on DOTAP LNP CQAs

Following evaluation and exploration of mixing speed and PPL mediated automation of syringe drivers, further investigation was undertaken to assess the effect of changing AXF-Mini 9.9 mm low volume insert with a 9.9 mm UltraLow Volume (ULV) insert on DOTAP LNPs synthesised under mixing speeds of 30 mL/min. DOTAP LNPs were manufactured as previously described and particle diameter, PDI and zeta potential was assessed. DOTAP LNPs manufactured utilising the 9.9 mm ULV insert presented a reproducible particle population of 75 nm $\pm$ 7 nm and PDI <0.2 (0.17 $\pm$ 0.01). The zeta potential of the particle population additionally stayed within a neutral range of -1.7 mV $\pm$ 0.9, shown in *Figure 18A*. Compared to LNPs synthesised under the same TFR conditions with the low volume insert, DOTAP LNPs exhibited a particle diameter reduction of approximately 20 nm with minimal deviation observed in particle PDI and zeta potential. Following initial LNP characterisation, samples were diluted to a nucleic acid concentration of 3 µg/mL and assessed for encapsulation efficien cy and poly A recovery through a ribogreen assay. All samples tested, presented >99% encapsulation efficiency when fluorescence difference was measure between triton-X treated vs non-triton-X treated samples. A Poly A recovery of ~ 65 % across triplicates was observed in samples synthesised utilising the 9.9 mm low volume insert whilst a > 10 % increase in poly A recover was observed in LNPs synthesised using the ULV insert (*Table 14*).

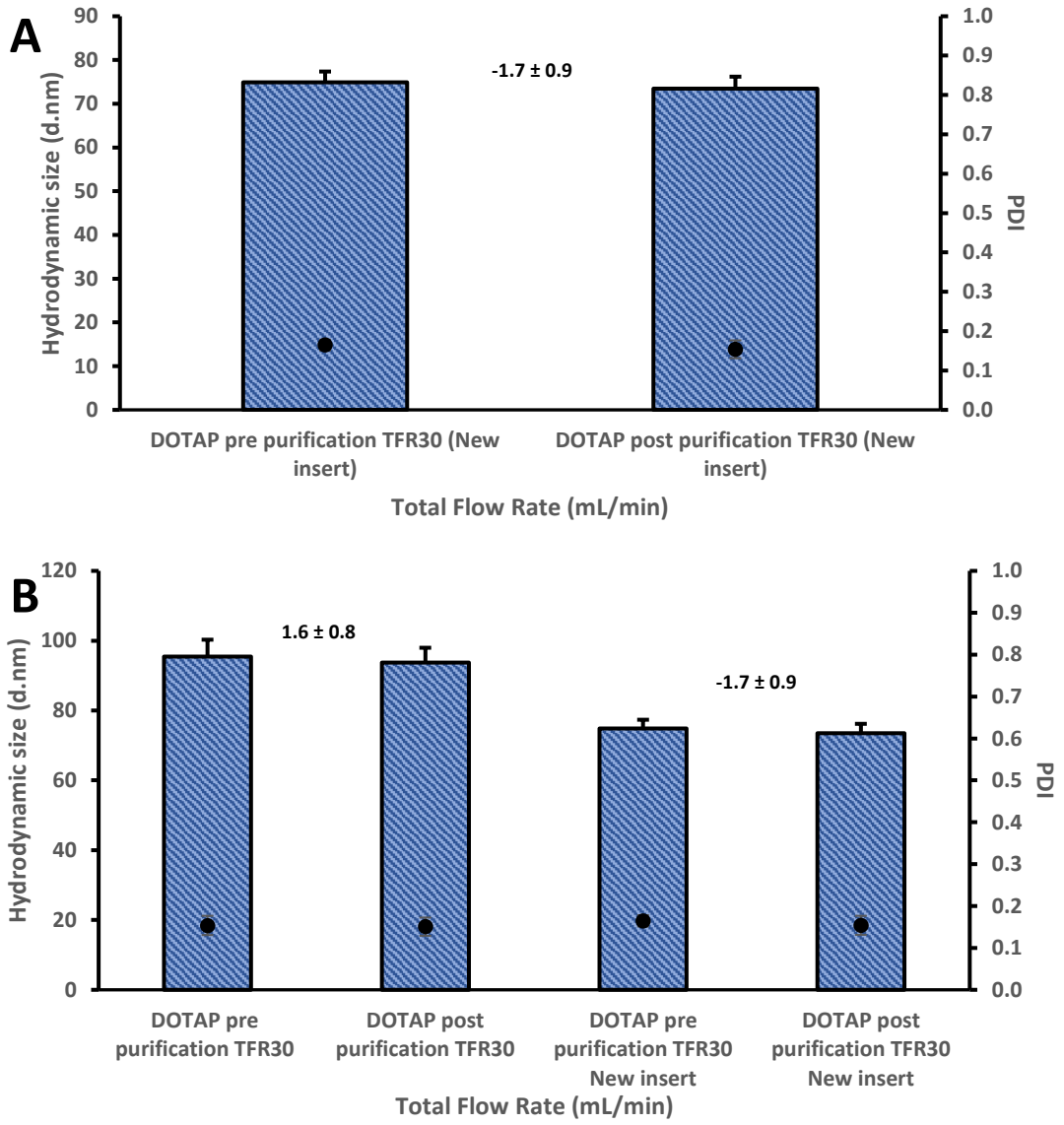


***Figure 18: Particle diameter and PDI before and after dialysis purification of DOTAP LNP samples synthesised on the Micropore AXF-Mini at 30 mL/min through automated infusion with ULV insert (n=3). (A) Particle size and PDI of DOTAP LNPs manufactured using new ULV insert. (B) Particle size and PDI comparison of DOTAP LNPs manufactured using LV insert and new ULV insert.*** *This figure displays the hydrodynamic size of DOTAP:DSPC:Chol:DMG-PEG2000 (50:10:38.5:1.5) poly A containing - LNPs and PDI of particle population prior to and succeeding 1 hr dialysis purification. The particle sizes and PDI were measured by DLS using a Malvern zeta-sizer ultra-series utilising a 632.8 nm 10 mW He-Ne laser with a detection angle set at 173°. LNPs were measured using a 1.47 refractive index and a 1.28 cP viscosity with the dispersant set at citrate buffer prior to dialysis and LNPs were then measured using a 1.34 refractive index and a 1.02 cP viscosity with the dispersant set at PBS after dialysis. Zeta potential (mV) was additionally measured succeeding LNP purification and is displayed above bar chart measurements. Zetasizer Software v.7.11 (Malvern Instruments Ltd.) was used for the acquisition of data. Statistical analysis of data was undertaken through a one or two- way ANOVA with a Tukey's post ad-hoc on GraphPad Prism 10 software, shown in Appendix 7J.*

Table 14: Ribogreen analysis of DOTAP LNPs synthesised at 30 mL/min utilising a LV insert and ULV insert

| *Sample* | | *Encapsulation Efficiency (%) – PolyA* | *Nucleic acid recovery (%) – PolyA* |
|---|---|---|---|
| **DOTAP TFR 30mL/min Low volume insert** | **Day 1** | 100 ± 1 | 65 ± 0 |
| | **Day 2** | 100 ± 1 | 65 ± 0 |
| | **Day 3** | 100 ± 1 | 66 ± 0 |
| **DOTAP TFR 30mL/min Ultra Low volume insert** | **Day 1** | 100 ± 0 | 75 ± 4 |
| | **Day 2** | 100 ± 0 | 79 ± 0 |
| | **Day 3** | 100 ± 0 | 75 ± 2 |

***Table 14: Ribogreen analysis of DOTAP LNPs manufactured using LV insert and new ULV insert.*** *This table displays the calculated encapsulation efficiency and nucleic acid recovery (Mass Balance) of DOTAP LNPs utilising 1000 ng/mL and 200 ng/mL poly A standard curves. Encapsulation efficiency was calculated by the difference in fluorescent emission in triton-X treated samples, causing lysis, against the untreated samples. Mass balance recovery of poly A cargo in LNP samples were then calculated using the 1000 ng/mL poly A standard curve and percentage recovery was calculated against a theoretical 100 % yield of 750 ng/mL of poly A. The samples were analysed at 475 - 525 nm excitation/emission on GloMax Explorer. Statistical analysis of data was undertaken through a one or two- way ANOVA with a Tukey's post ad-hoc on GraphPad Prism 10 software, shown in Appendix 7K.*

3.10: Process parameter validation utilising ALC-0315 and C-12 200 ionizable lipid-based formulations

Following validation of the 9.9 mm UltraLow Volume (ULV) insert and automated mixing conditions, SM-102, ALC-0315 and C-12 200 - poly A formulations were evaluated. All ionizable lipid formulations were prepared, LNPs were synthesised at a TFR30mL/min and LNPs were purified through spin column centrifugation. As shown in *Figure 19*, SM-102 LNPs manufactured utilising the 9.9 mm ULV insert presented a reproducible particle population of 98 nm $\pm$ 3 nm and PDI <0.2 (0.08 $\pm$ 0.02). The zeta potential of the particle population additionally stayed within a neutral range of -3.4 mV $\pm$ 0.7. ALC-0315 LNPs also presented a reproducible particle population of 95 nm $\pm$ 2 nm and PDI <0.2 (0.13 $\pm$ 0.02). The zeta potential of the particle population additionally stayed within a neutral range of -7.5 mV $\pm$ 1.9. Analysis of C-12 200 LNPs also presented a reproducible particle population of 73 nm $\pm$ 1 nm and PDI <0.2 (0.16 $\pm$ 0.01). The zeta potential of the particle population additionally stayed within a neutral range of -7.5 mV $\pm$ 2.2. Following initial LNP characterisation, samples were diluted to a nucleic acid concentration of 3 µg/mL and assessed for encapsulation efficiency and poly A recovery through a ribogreen assay. All SM-102 LNP samples tested, presented >99% encapsulation efficiency when fluorescence difference was measure between triton-X treated vs non-triton-X treated samples and Poly A recovery of ~100 % across triplicates samples. ALC-0315 LNPs presented both a lower encapsulation efficiency between triplicate samples of 93 % and nucleic acid recovery of ~84 %. In the case of C-12 200 samples, LNPs presented an average encapsulation efficiency of 99 % and poly A recovery of 96 % (*Table 15*).

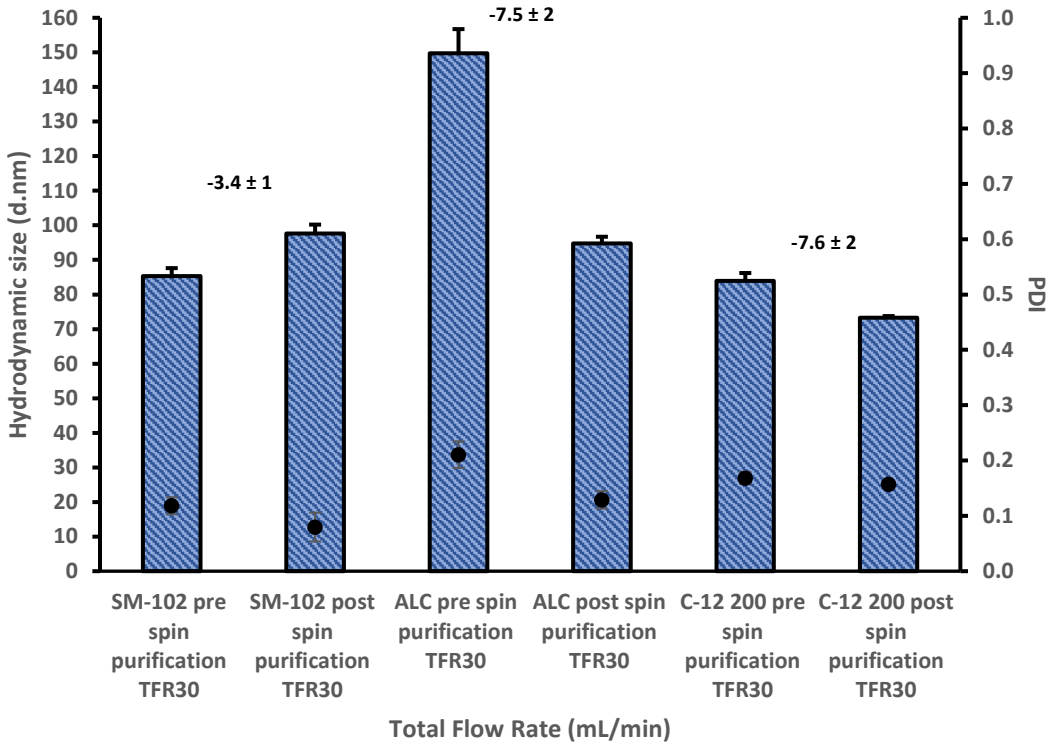


***Figure 19: Particle diameter and PDI before and after spin column purification of SM-102, ALC-0135 and C-12 200 LNP samples synthesised on the Micropore AXF-Mini at 30 mL/min (n=3).*** *This figure displays the hydrodynamic size of SM-102:DSPC:Chol:DMG-PEG2000 (50:10:38.5:1.5), ALC-0315:DSPC:Chol:ALC-0159 (46.3:9.4:42.7:1.6) and C-12 200:DSPC:Chol:DMPE-PEG2000 (35:16:46.5:2.5) poly A containing - LNPs and PDI of particle population prior to and succeeding spin column purification. The particle sizes and PDI were measured by DLS using a Malvern zeta-sizer ultra-series utilising a 632.8 nm 10 mW He-Ne laser with a detection angle set at 173°. LNPs were measured using a 1.47 refractive index and a 1.28 cP viscosity with the dispersant set at citrate buffer prior to purification and LNPs were then measured using a 1.34 refractive index and a 1.02 cP viscosity with the dispersant set at PBS after purification. Zeta potential (mV) was additionally measured succeeding LNP purification and is displayed above bar chart measurements. Zetasizer Software v.7.11 (Malvern Instruments Ltd.) was used for the acquisition of data. Statistical analysis of data was undertaken through a one or two- way ANOVA with a Tukey's post ad-hoc on GraphPad Prism 10 software, shown in Appendix 7L.*

Table 15: Ribogreen analysis of SM-102, ALC-0315 and C-12 200 LNPs synthesised at 30 mL/min

| *Sample* | | *Encapsulation Efficiency (%) – PolyA* | *Nucleic acid recovery (%) – PolyA* |
|---|---|---|---|
| **SM-102 TFR 30mL/min** | **Day 1** | 100 ± 0 | 100 ± 1 |
| | **Day 2** | 99 ± 1 | 102 ± 1 |
| | **Day 3** | 99 ± 0 | 102 ± 0 |
| **ALC-0315 TFR 30mL/min** | **Day 1** | 96 ± 1 | 82 ± 1 |
| | **Day 2** | 92 ± 0 | 86 ± 0 |
| | **Day 3** | 92 ± 1 | 85 ± 1 |
| **C-12 200 TFR 30mL/min** | **Day 1** | 99 ± 0 | 101 ± 1 |
| | **Day 2** | 98 ± 1 | 94 ± 1 |
| | **Day 3** | 99 ± 0 | 93 ± 1 |

***Table 15: Ribogreen analysis of SM-102, ALC-0315 and C-12 200 LNPs manufactured at a TFR30 mL/min utilizing ULV insert.*** *This table displays the calculated encapsulation efficiency and nucleic acid recovery (Mass Balance) of SM-102, ALC-0315 and C-12 200 LNPs utilising 1000 ng/mL and 200 ng/mL poly A standard curves. Encapsulation efficiency was calculated by the difference in fluorescent emission in triton-X treated samples, causing lysis, against the untreated samples. Mass balance recovery of poly A cargo in LNP samples were then calculated using the 1000 ng/mL poly A standard curve and percentage recovery was calculated against a theoretical 100 % yield of 750 ng/mL of poly A. The samples were analysed at 475 - 525 nm excitation/emission on GloMax Explorer. Statistical analysis of data was undertaken through a one or two- way ANOVA with a Tukey's post ad-hoc on GraphPad Prism 10 software, shown in Appendix 7M.*

3.11: Assessment of *in vitro* efficacy of SM-102 LNPs in HEK293 cells

Succeeding evaluation and exploration of mixing speed, PPL mediated automation of syringe drivers, the effect of changing AXF-Mini insert and validation of ALC-0315 and C-12 200 lipid formulations on synthesised under mixing speeds of 30 mL/min, SM-102 formulations were selected for downstream investigation of *in vitro* efficacy. SM-102 -poly A and SM-102-Fluc mRNA LNPs were manufactured as previously described and particle diameter, PDI and zeta potential was assessed. SM-102-poly A LNPs manufactured utilising the 9.9 mm ULV insert presented a reproducible particle population of 77 nm ± 2 nm and PDI <0.2 (0.13 ± 0.04). The zeta potential of the particle population additionally stayed within a neutral range of 0.1 mV ± 7, shown in *Figure 20*. Compared to LNPs synthesised under the same TFR conditions, SM-102-Fluc mRNA LNPs exhibited a particle diameter of 71 nm ± 2 nm and PDI <0.2 (0.17 ± 0.03). Additionally, the zeta potential of the particle population additionally stayed within a neutral range of -0.9 mV ± 8, shown in *Figure 20.* Following dialysis purification, both poly A and Fluc mRNA formulated LNPs increased particle diameter to 80 and 82 nm respectively, with minimal deviation to the PDI of each particle population. Following initial LNP characterisation, samples were diluted to a nucleic acid concentration of 3 µg/mL and assessed for encapsulation efficiency and nucleic acid recovery through a ribogreen assay. All samples tested, presented >97 % encapsulation efficiency when fluorescence difference was measure between triton-X treated vs non-triton-X treated samples. A Poly A recovery ranging 78 – 100 % was observed across triplicate samples whilst a Fluc mRNA recovery ranging 77 – 88 % was seen across triplicate samples (*Table 16*). Following DLS and ribogreen characterisation of SM-102 LNPs, LNP cytotoxicity was assessed as previously described. Succeeding fluorescence measurement at 520-640 nm EX/EM, SM-102 LNP treated HEK293 cells presented a cell viability, relative to untreated cell lines, of >98 % following treatment at 46, 23, 11.5 and 5.25 µg/mL lipid concentrations (*Figure 21A*). In addition to this, analysis of SM-102 uptake in HEK293 cells showed a dose dependent uptake, greater than 90 % at 23, 11.5 and 5.25 µg/mL lipid concentrations, with a limited uptake being observed in the highest lipid concentration 46 µg/mL at ~40 % (*Figure 21B*). Efficiency of Fluc mRNA translation was assessed, as shown in *Figure 21C*, a dose-dependent response relative to untreated cell lines was observed, with the greatest bioluminescence emission being observed in the 2 µg/mL mRNA dosage concentration. Following assessment of LNP *in vitro* performance, analysis of

Fluc mRNA through gel electrophoresis demonstrated mRNA integrity was maintained following SM-102 LNP encapsulation (*Figure 21D*).

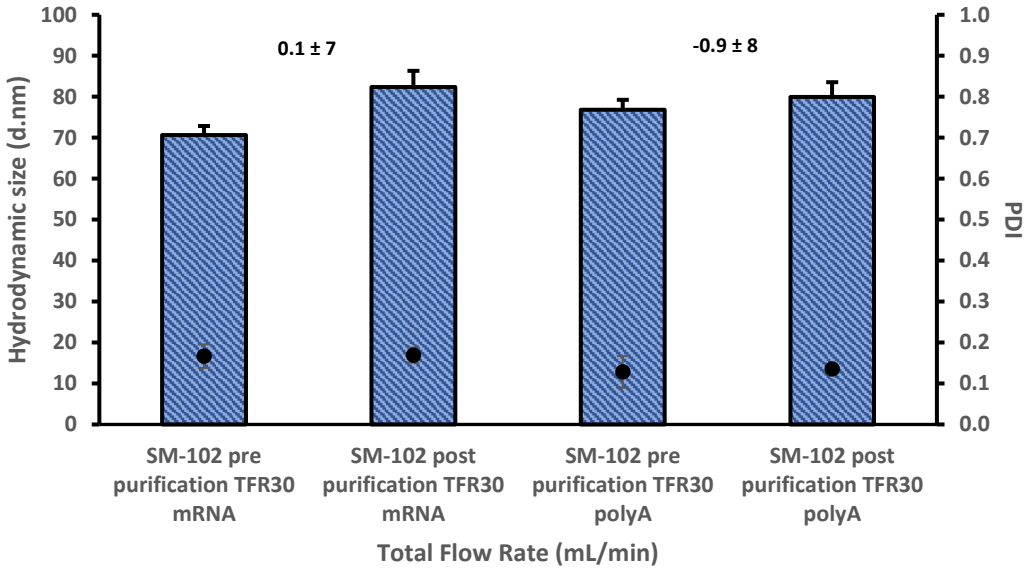


***Figure 20: Particle diameter and PDI before and after dialysis purification of SM-102 LNP samples synthesised on the Micropore AXF-Mini at 30 mL/min through automated infusion with ULV insert (n=3).*** *This figure displays the hydrodynamic size of SM-102:DSPC:Chol:DMG-PEG2000 (50:10:38.5:1.5) poly A and Fluc mRNA containing - LNPs and PDI of particle population prior to and succeeding 4 hr dialysis purification at 4°C. The particle sizes and PDI were measured by DLS using a Malvern zeta-sizer ultra-series utilising a 632.8 nm 10 mW He-Ne laser with a detection angle set at 173°. LNPs were measured using a 1.47 refractive index and a 1.28 cP viscosity with the dispersant set at citrate buffer prior to dialysis and LNPs were then measured using a 1.34 refractive index and a 1.02 cP viscosity with the dispersant set at PBS after dialysis. Zeta potential (mV) was additionally measured succeeding LNP purification and is displayed above bar chart measurements. Zetasizer Software v.7.11 (Malvern Instruments Ltd.) was used for the acquisition of data. Statistical analysis of data was undertaken through a one or two- way ANOVA with a Tukey's post ad-hoc on GraphPad Prism 10 software, shown in Appendix 7N.*

Table 16: Ribogreen analysis of SM-102 poly A and Fluc mRNA LNPs synthesised at 30 mL/min

| *Sample* | | *Encapsulation Efficiency (%) – PolyA* | *Nucleic acid recovery – PolyA* | *Encapsulation Efficiency (%) – mRNA* | *Nucleic acid recovery – mRNA* |
|---|---|---|---|---|---|
| **SM-102** | **Day 1** | 99 ± 0 | 78 ± 1 | 98 ± 0 | 77 ± 3 |
| **TFR** | **Day 2** | 100 ± 0 | 84 ± 3 | 97 ± 0 | 78 ± 1 |
| **30mL/min** | **Day 3** | 99 ± 0 | 103 ± 1 | 98 ± 0 | 88 ± 2 |

***Table 16: Ribogreen analysis of SM-102 LNPs.*** *This table displays the calculated encapsulation efficiency and nucleic acid recovery (Mass Balance) of SM-102 LNPs utilising both 1000 ng/mL and 200 ng/mL poly A and mRNA standard curves. Encapsulation efficiency was calculated by the difference in fluorescent emission in triton-X treated samples, causing lysis, against the untreated samples. Mass balance recovery of nucleic acid cargo in LNP samples were then calculated using both standard curves and percentage recovery was calculated against a theoretical 100% yield of 750 ng/mL of nucleic acid. The samples were analysed at 475 - 525 nm excitation/emission on GloMax Explorer. Statistical analysis of data was undertaken through a one or two- way ANOVA with a Tukey's post ad-hoc on GraphPad Prism 10 software, shown in Appendix 7O.*

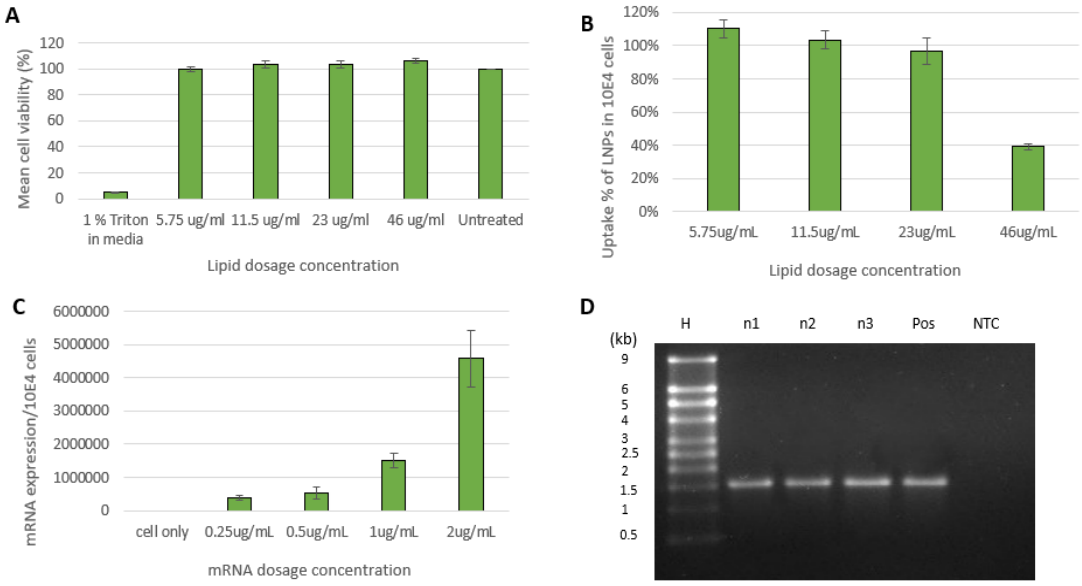


***Figure 21: In vitro efficacy of SM-102 LNPs in HEK293 cell lines (n=3). (A) Fluorescence emission of HEK293 cells treated at varying SM-102 concentrations and incubated or 24 hrs.*** *Dye metabolism was measured relative to untreated HEK293 cells and cell viability was measured (Ex/Em 520 nm/580/640 nm)**. (B) Measurement of SM-102 LNP uptake into HEK293 cells through DilC$_{18}$ fluorescence.*** *Cells were treated with varying concentrations of LNPs and DilC$_{18}$ fluorescence was measured at time of dosage and at a 24 hr time point at which point cell culture media was removed and cells were treated with 1 % triton-X PBS. Fluorescence measurements were undertaken, and uptake was calculated relative to initial dosage readings (Ex/Em 52 0nm/580/640 nm) **(C) Evaluation of Fluc mRNA expression succeeding SM-102 LNP treatment and 24 hr incubation.*** *Cells were treated with varying LNP concentrations and incubated for 24 hrs. Succeeding incubation, wells were supplemented with luciferin substrate and bioluminescence was measured. **(D) Investigation of mRNA integrity following LNP synthesis and cell treatments.*** *A denaturing gel electrophoresis was undertaken to evaluate the stability of Fluc mRNA following LNP synthesis on the micropore AXF-Mini. Gel electrophoresis was undertaken on 1 % agarose containing 5 µL of SYBR Green II dye and submerged in 1x MOPS Buffer. The gel was run for 1 hr at 90 V, and isolate band sizes were calculated using the corresponding RNA Millenium Marker Hyperladder (9 kb). H: RNA Millenium Marker Hyperladder, n1-3: sample, Pos: Positive Fluc mRNA control, NTC: No template control. Statistical analysis of data was undertaken through a one or two-way ANOVA with a Tukey's post ad-hoc on GraphPad Prism 10 software, shown in Appendix 7P.*

3.12: Evaluation of purification volume on SM-102 LNP CQAs

Following robust validation of SM-102 LNP efficacy *in vitro*, the impact of buffer volume during spin column purification was assessed. SM-102 - poly A formulations were evaluated and prepared through AXF-crossflow production, LNPs were synthesised at a TFR30 mL/min. As shown in *Figure 22*, SM-102 LNPs manufactured utilising the 9.9 mm ULV insert presented a reproducible particle population prior to purification of 83 nm ± 4 nm and PDI <0.2 (0.13 ± 0.01). Succeeding dialysis purification, LNPs displayed a particle size of 85 nm ± 4 nm and PDI <0.2 (0.13 ± 0.02). The zeta potential of the particle population additionally stayed within a neutral range of -1.3 mV ± 1.7. Following spin column purification, LNPs initially diluted in 9 mL of PBS presented an average particle size of 91 nm ± 2 nm and PDI <0.2 (0.10 ± 0.02) with zeta additionally staying within a neutral range of 2.2 mV ± 0.6. LNPs initially diluted in 19 mL of PBS presented an average particle size of 89 nm ± 1 nm and PDI <0.2 (0.12 ± 0.02). The zeta potential of the particle population remained within a neutral range of -0.4 mV ± 0.4. LNPs initially diluted in 39 mL of PBS presented an average particle size of 98 nm ± 3 nm and PDI <0.2 (0.08 ± 0.02). The zeta potential of the particle population additionally stayed within a neutral range of -3.4 mV SD ± 0.7. Following initial LNP characterisation, samples were diluted to a nucleic acid concentration of 3 µg/mL and assessed for encapsulation efficiency and poly A recovery through a ribogreen assay. All SM-102 LNP samples tested, presented >99 % encapsulation efficiency when fluorescence difference was measure between triton-X treated vs non-triton-X treated samples. A Poly A recovery of 100 % across triplicate samples purified through spin column was observed and 84 % across triplicate samples purified through dialysis (*Table 17*).

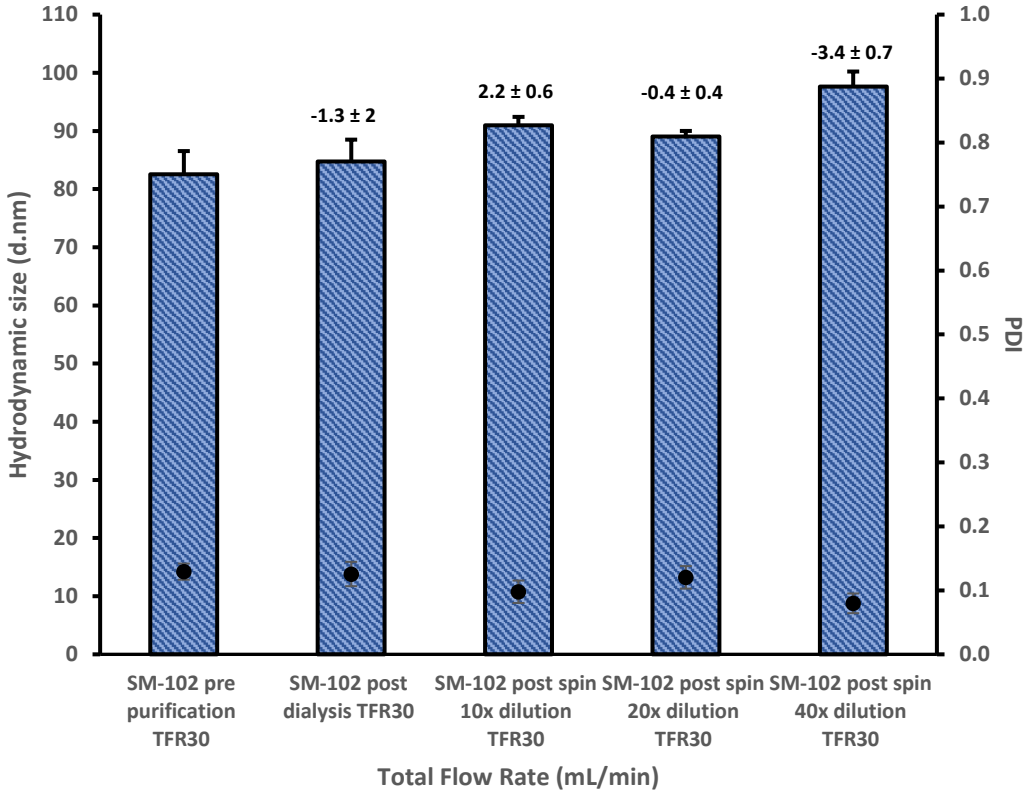


***Figure 22: Particle diameter and PDI before and after spin column purification, utilising varying dilution volumes, of SM-102 LNP samples synthesised on the Micropore AXF-Mini at 30 mL/min.*** *This figure displays the hydrodynamic size of SM-102:DSPC:Chol:DMG-PEG2000 (50:10:38.5:1.5) poly A containing - LNPs and PDI of particle population prior to and succeeding spin column purification at 4°C. The particle sizes and PDI were measured by DLS using a Malvern zeta-sizer ultra-series utilising a 632.8 nm 10 mW He-Ne laser with a detection angle set at 173°. LNPs were measured using a 1.47 refractive index and a 1.28 cP viscosity with the dispersant set at citrate buffer prior to purification and LNPs were then measured using a 1.34 refractive index and a 1.02 cP viscosity with the dispersant set at PBS after purification. Zeta potential (mV) was additionally measured succeeding LNP purification and is displayed above bar chart measurements. Zetasizer Software v.7.11 (Malvern Instruments Ltd.) was used for the acquisition of data. Statistical analysis of data was undertaken through a one or two- way ANOVA with a Tukey's post ad-hoc on GraphPad Prism 10 software, shown in Appendix 7Q.*

Table 17: Ribogreen analysis of SM-102 LNPs synthesised at 30 mL/min and purified through varying dilution volumes

| *Sample* | | *Encapsulation Efficiency (%) – PolyA* | *Nucleic acid recovery (%) – PolyA* |
|---|---|---|---|
| **SM-102 dialysis** | **Day 1** | 100 ± 1 | 88 ± 0 |
| | **Day 2** | 100 ± 0 | 84 ± 0 |
| | **Day 3** | 100 ± 1 | 71 ± 2 |
| **SM-102 10x dilution** | **Day 1** | 100 ± 3 | 107 ± 3 |
| | **Day 2** | 100 ± 0 | 106 ± 0 |
| | **Day 3** | 100 ± 0 | 101 ± 0 |
| **SM-102 20x dilution** | **Day 1** | 99 ± 0 | 103 ± 1 |
| | **Day 2** | 100 ± 0 | 108 ± 0 |
| | **Day 3** | 99 ± 1 | 104 ± 4 |
| **SM-102 40x dilution** | **Day 1** | 100 ± 0 | 100 ± 1 |
| | **Day 2** | 99 ± 1 | 102 ± 1 |
| | **Day 3** | 99 ± 0 | 102 ± 0 |

***Table 17: Ribogreen analysis of SM-102 LNPs.*** *This figure displays the calculated encapsulation efficiency and nucleic acid recovery (Mass Balance) of SM-102 LNPs utilising both 1000 ng/mL and 200 ng/mL poly A standard curves. Encapsulation efficiency was calculated by the difference in fluorescent emission in triton-X treated samples, causing lysis, against the untreated samples. Mass balance recovery of poly A cargo in LNP samples were then calculated using both standard curves and percentage recovery was calculated against a theoretical 100% yield of 750 ng/mL of poly A. The samples were analysed at 475 - 525 nm excitation/emission on GloMax Explorer.*

3.13: Evaluation of LNP concentration scaling methods.

Following establishment of the effect of external buffer volume on SM-102 LNP CQAs, concentration scaling methods were examined. SM-102 LNPs were synthesised at 0.02 mg/mL, 0.05 mg/mL and 0.1 mg/mL poly A concentrations at a TFR30 mL/min (*Figure 23A*). Comparatively, SM-102 LNPs were manufactured at 0.02mg/mL and concentrated through spin column purification techniques to a poly A final concentration of 0.06 mg/mL, 0.1 mg/mL and 0.14 mg/mL (*Figure 23B*). As seen in *Figure 23A*, SM-102 LNPs manufactured at a poly A concentration of 0.02 mg/mL presented a reproducible particle population prior to purification of 85 nm ± 2 nm and PDI <0.2 (0.12 ± 0.01). Succeeding dialysis purification, LNPs displayed a particle size of 83 nm ± 1 nm and PDI <0.2 (0.14 ± 0.02). The zeta potential of the particle population additionally stayed within a neutral range of -1.3 mV ± 0.7. SM-102 LNPs manufactured at a poly A concentration of 0.05mg/mL presented a reproducible particle population prior to purification of 100 nm ± 6 nm and PDI <0.2 (0.14 ± 0.01). Succeeding dialysis purification, LNPs displayed a particle size of 98 nm ± 7 nm and PDI <0.2 (0.12 ± 0.01). The zeta potential of the particle population additionally stayed within a neutral range of 1.4 mV ± 1.1. LNPs manufactured at a poly A concentration of 0.1 mg/mL presented a reproducible particle population prior to purification of 118 nm ± 4 nm and PDI <0.2 (0.14 ± 0.01). Succeeding dialysis purification, LNPs displayed a particle size of 116 nm ± 7 nm and PDI <0.2 (0.13 ± 0.03). The zeta potential of the particle population additionally stayed within a neutral range of 5.6 mV ± 1.7.

Following spin column purification and concentration, SM-102 LNPs purified through spin column presented an average particle size of 98 nm ± 3 nm and PDI <0.2 (0.08 SD ± 0.02). The zeta potential of the particle population additionally stayed within a neutral range of -3.4 mV SD ± 0.7. LNPs concentrated to a final poly A concentration of 0.06mg/mL presented an average particle size of 97 nm ± 5 nm and PDI <0.2 (0.09 ± 0.02). The zeta potential of the particle population remained within a neutral range of -1.5 mV ± 1. LNPs concentrated to a final poly A concentration of 0.14 mg/mL presented an average particle size of 97 nm ± 4 nm and PDI <0.2 (0.12 ± 0.01). The zeta potential of the particle population remained within a neutral range of 1.4 mV ± 0.4 (*Figure 23B*). Following initial LNP characterisation, samples were diluted to a nucleic acid concentration of 3 µg/mL and assessed for encapsulation efficiency and poly A recovery through a ribogreen assay. All SM-102 LNP samples tested,

presented >99 % encapsulation efficiency when fluorescence difference was measure between triton-X treated vs non-triton-X treated samples. An average Poly A recovery of 82 % was observed in samples manufactured at a poly A concentration of 0.02 mg/mL, SM-102 LNPs manufactured at 0.05 mg/mL and 0.1 mg/mL presented an average poly A recovery of 98 % and 99 % respectively. An average Poly A recovery of 100 % was observed in samples manufactured at a poly A concentration of 0.02 mg/mL, SM-102 LNPs concentrated to a poly A end concentration of 0.06 mg/mL, 0.1 mg/mL and 0.14 mg/mL presented an average poly A recovery of 94 %, 92 % and 84 % respectively (*Table 18*).

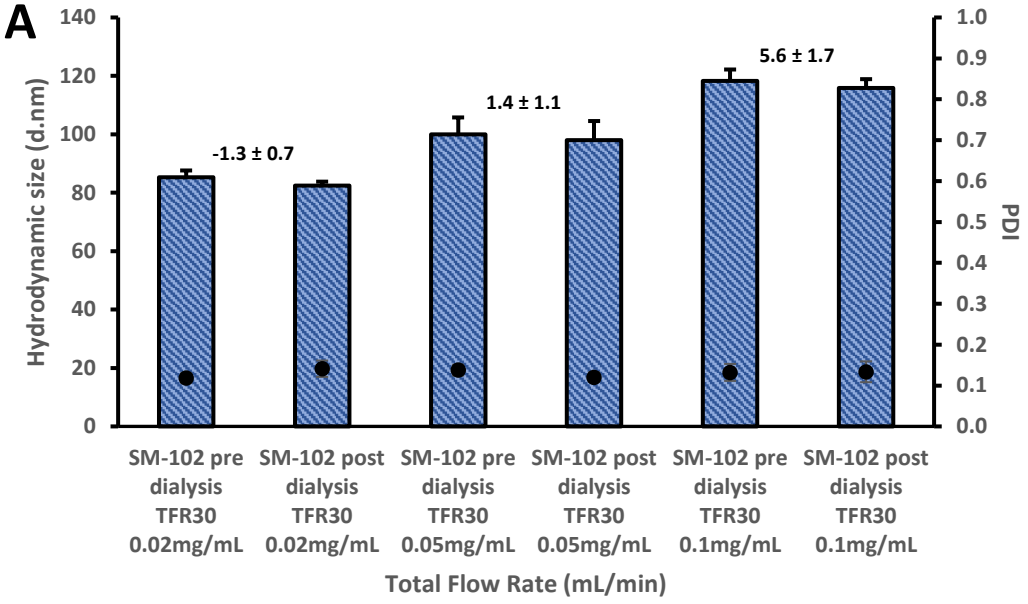


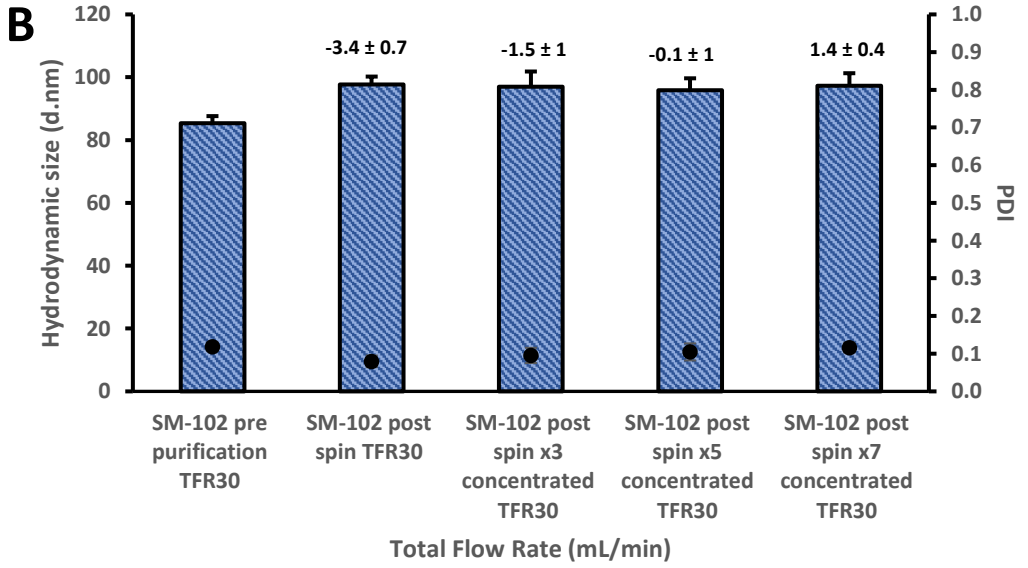

***Figure 23: Particle diameter and PDI before and after purification of SM-102 LNP samples synthesised on the Micropore AXF-Mini at 30 mL/min. (A) Particle size and PDI of SM-102 LNPs manufactured at 0.02 mg/mL, 0.05 mg/mL and 0.1 mg/mL poly A concentration. (B) Particle size and PDI of SM-102 LNPs manufactured at 0.02 mg/mL poly A and concentrated to 0.06 mg/mL, 0.1 mg/mL and 0.14 mg/mL through spin column centrifugation.*** *This figure displays the hydrodynamic size of SM-102:DSPC:Chol:DMG-PEG2000 (50:10:38.5:1.5) poly A containing - LNPs and PDI of particle population prior to and succeeding purification at 4°C. The particle sizes and PDI were measured by DLS using a Malvern zeta-sizer ultra-series utilising a 632.8 nm 10 mW He-Ne laser with a detection angle set at 173°. LNPs were measured using a 1.47 refractive index and a 1.28 cP viscosity with the dispersant set at citrate buffer prior to purification and LNPs were then measured using a 1.34 refractive index and a 1.02 cP viscosity with the dispersant set at PBS after purification. Zeta potential (mV) was additionally measured succeeding LNP purification and is displayed above bar chart measurements. Zetasizer Software v.7.11 (Malvern Instruments Ltd.) was used for the acquisition of data. Statistical analysis of data was undertaken through a one or two- way ANOVA with a Tukey's post ad-hoc on GraphPad Prism 10 software, shown in Appendix 7R and 7T.*

Table 18: Ribogreen analysis of SM-102 LNPs synthesised and concentrated at varying poly A end concentrations, manufactured at 30 mL/min

| ***Sample*** | | ***Encapsulation Efficiency (%) – PolyA*** | ***Nucleic acid recovery (%) – PolyA*** |
|---|---|---|---|
| **SM-102 dialysis 0.02mg/mL** | **Day 1** | 100 ± 0 | 78 ± 0 |
| | **Day 2** | 100 ± 0 | 78 ± 0 |
| | **Day 3** | 100 ± 0 | 89 ± 2 |
| **SM-102 dialysis 0.05mg/mL** | **Day 1** | 100 ± 0 | 102 ± 2 |
| | **Day 2** | 100 ± 1 | 93 ± 5 |
| | **Day 3** | 100 ± 1 | 100 ± 1 |
| **SM-102 dialysis 0.1mg/mL** | **Day 1** | 100 ± 2 | 105 ± 0 |
| | **Day 2** | 100 ± 0 | 100 ± 1 |
| | **Day 3** | 100 ± 1 | 93 ± 6 |
| **SM-102 spin 0.02mg/mL** | **Day 1** | 100 ± 0 | 100 ± 1 |
| | **Day 2** | 99 ± 1 | 102 ± 1 |
| | **Day 3** | 99 ± 0 | 102 ± 0 |
| **SM-102 x3 concentrated (0.06mg/mL)** | **Day 1** | 99 ± 0 | 94 ± 0 |
| | **Day 2** | 100 ± 1 | 87 ± 0 |
| | **Day 3** | 100 ± 2 | 100 ± 4 |
| **SM-102 x5 concentrated (0.1mg/mL)** | **Day 1** | 100 ± 0 | 89 ± 0 |
| | **Day 2** | 100 ± 0 | 79 ± 0 |
| | **Day 3** | 100 ± 1 | 107 ± 2 |
| **SM-102 x7 concentrated (0.14mg/mL)** | **Day 1** | 100 ± 3 | 81 ± 2 |
| | **Day 2** | 100 ± 1 | 65 ± 1 |
| | **Day 3** | 99 ± 1 | 105 ± 4 |

***Table 18: Ribogreen analysis of SM-102 LNPs.*** *This figure displays the calculated encapsulation efficiency and nucleic acid recovery (Mass Balance) of SM-102 LNPs utilising 1000 ng/mL and 200 ng/mL poly A standard curves. Encapsulation efficiency was calculated by the difference in fluorescent emission in triton-X treated samples, causing lysis, against the untreated samples. Mass balance recovery of poly A cargo in LNP samples were then calculated using both standard curves and percentage recovery was calculated against a theoretical 100 % yield of 750 ng/mL of poly A. The samples were analysed at 475 - 525 nm excitation/emission on GloMax Explorer. Statistical analysis of data was undertaken through a one or two- way ANOVA with a Tukey's post ad-hoc on GraphPad Prism 10 software, shown in Appendix 7S and 7U.*

# Chapter 4: Discussion

## 4. Discussion

Following investigation into the effect of mixing speed on LNP CQA, shown in *Figure 2 and 3*, LNPs presented a stable reproducible inter-day particle size that significantly reduced (Two-way ANOVA, *P< 0.001*) as the TFR of mixing was increased. LNPs manufactured at a TFR10, 20 and 30mL/min produced particles at 125 nm ± 7 nm, 104 nm ± 4 nm and 92 nm ± 3 nm respectively *(Figure 2)* (Two-way ANOVA *P< 0.001*). Despite varying mixing speeds all particle PDIs presented a value of <0.2 (0.17 ± 0.03, 0.16 ± 0.03 and 0.15 ± 0.03) which in turn was consistent following dialysis purification. Particles presented a near neutral average zeta potential ranging from 4 – 7.8 mV. Further analysis of DOTAP LNPs manufactured at a TFR of 40, 50 and 60 mL/min produced particles at 108 nm ± 7 nm, 103 nm ± 4 nm and 100 nm ± 3 nm respectively. Once more, despite varying mixing speeds all particle PDIs presented a value of <0.2 (0.16 ± 0.03, 0.17 ± 0.03 and 0.19 SD ± 0.03) which in turn was consistent following dialysis purification. In addition, Particles presented a near neutral average zeta potential ranging from 2.2-5.9 mV.

Following initial analysis of DOTAP LNPs, a significant (Two-way ANOVA*, P< 0.001*) notable size increase was observed in particle diameter between LNPs synthesised at mixing speeds of 30 mL/min and 40 mL/min as seen in *Figure 2*. Due to inconsistency with previous findings, mixing speeds 30-60 mL/min was reassessed as shown in *Figure 3*. LNPs manufactured at a TFR30, 40, 50 and 60 mL/min produced particles at 106 nm ± 2 nm, 102 nm ± 4 nm, 100 nm ± 9 nm and 95 nm ± 4 nm respectively (Two-way ANOVA, *P< 0.05*). Despite varying mixing speeds all particle PDIs presented a value of <0.2 (0.15 ± 0.03, 0.15 ± 0.01, 0.14 ± 0.02 and 0.16 ± 0.02) which in turn was consistent following dialysis purification. Particles presented a near neutral average zeta potential ranging from 1.4 – -2.2 mV. This observation additionally coincides with the observation and hypotheses proposed by C. Roces, J.S. Shepard (C. B. Roces *et al*., 2020; Shepherd *et al*., 2021) that T-junction based microfluidic systems require higher mixing speeds, in comparison to other microfluidic architectures, to create a more turbulent mixing environment conducive to smaller LNP particle formation.

Following reassessment of DOTAP LNP's, samples were retested to evaluate the encapsulation efficiency and poly A recovery through a ribogreen assay. All samples presented >99 % encapsulation efficiency when fluorescence difference was measure between triton-X treated vs non-triton-X treated samples. Additionally,

DOTAP LNPs had a poly A retention ranging 53- 69 % across LNPs manufactured at all speeds tested. This poly A retention can be due to the fact that the primary cationic lipid component, DOTAP, of this formulation is cationic at physiological pH and consists of unsaturated oleic acid hydrocarbon chains. As such, this owes to reduced inter-alkyl interactions and a less compact membrane structure (Swetha *et al*., 2023). As this should not be the case for ionizable SM-102 formulations, following a reduced poly A recovery, shown in *Table 4,* lipid concentration was assessed through the lipophilic tracing dye, $DilC_{18.}$

Following the reduced poly A recovery of previous SM-102 formulations, $DilC_{18.}$ fluorescence was assessed before and after dialysis purification of DOTAP- $DilC_{18.}$ LNPs. As seen in *Table 5,* $DilC_{18}$ fluorescence analysis of DOTAP LNP's presented a decrease in emission signal ranging from 7-18 % compared to that of pre-dialysed samples. This reduction was then accounted for in the ribogreen assay and further LNP characterisation of samples through ribogreen analysis was tested. All DOTAP presented >99% encapsulation efficiency when fluorescence difference was measure between triton-X treated vs non-triton-X treated samples. Additionally, DOTAP LNPs had a poly A retention ranging 88 – 100 % across all speeds tested, as shown in *Table 6*. Despite this increase in poly A recovery, it was determined that to ensure a FRR of 3:1 was being achieved under current manufacturing parameters on the Micropore AXF-Mini, $DilC_{18}$ fluorescence needed to be monitored at each stage of the manufacturing process and quantified utilising a standard curve.

As seen in *Figure 6*, analysis of DOTAP- $DilC_{18}$ lipid phase dilution series ranging 2400 – 0 µg/mL did not display the linear regression criteria necessary for lipid quantification ($R^2$= >0.98) of DOTAP LNPs. It was hypothesised that oversaturation of the Omega POLARstar fluorescence spectrophotometer, exhibited at the higher concentrations of the dilution series, resulted in a fluorescence plateau presented from the 1000 µg/mL dilution point. Consequently, as shown in *Figure 7*, the molar ratio of $DilC_{18}$ utilised within the lipid formulation was reduced from 1 % to 0.25 %. Once adjusted DOTAP- $DilC_{18}$ lipid phase dilution series presented the linear regression criteria necessary for lipid quantification ($R^2$= >0.98) and as such was utilised in subsequent experiments for validation lipid content through synthesis and purification procedures. $DilC_{18}$-containing DOTAP LNPs synthesized at TFR's of 60 mL/min presented a stable reproducible particle size 97 nm $\pm$ 6 nm and a PDI < 0.2 (0.191 $\pm$ 0.03) with near neutral zeta potentials of -3.3 mV (*Figure 8*).

Subsequent assessment of lipid content, based of $DilC_{18}$ fluorescence, presented a markedly higher lipid concentration in LNPs than the desired theoretical concentration of 461 µg/mL (*Table 7*). It was theorised that if this was a true reflection of lipid concentration, greater deviation would be observed in previous assessed LNP CQAs (particle diameter, PDI and zeta potential). Reinforced by previous findings that increases in LNP FRR results in significant alteration in nanoparticle structure (Anderluzzi & Perrie, 2020; Kimura *et al*., 2018; C. B. Roces *et al*., 2020). Further examination showed that $DilC_{18}$, belonging to the carbocyanine group, produces a higher fluorescence intensity when incorporated into a lipid membrane than in aqueous solution. This comes as a result of a polarity shift associated with membrane incorporation and reduction of dye solvation leading to a shift in fluorescence excitation and emission spectra observed by Honig, revised by Poulain in 2010 and Ptaszek in 2013 (Heilemann *et al*., 2005; Honig & Hume, 1989; Poulain *et al*., 2010; Ptaszek, 2013). Consequently, it was determined that to appropriately quantify LNP lipid concentration throughout the manufacturing and purification process, both and DOTAP- $DilC_{18}$ lipid phase dilution series and a LNP dilution series would be required.

To achieve this, a post microfluidic LNP curve starting at 1000 µg/mL was synthesized using the PNI Nanoassemblr. DOTAP-$DilC_{18}$ LNPs were manufactured utilising the same organic and aqueous phase on the Micropore AXF-Mini and PNI Nanoassemblr to ensure that differing particle size did not compromise $DilC_{18}$ fluorescence representation and that these two factors were irrespective of one another. LNPs presented a stable reproducible particle size 101 nm $\pm$ 7 nm and a PDI < 0.2 (0.177 $\pm$ 0.03) on the Micropore AXF-Mini and 60 nm $\pm$ 2 nm and a PDI >0.2 (0.214 $\pm$ 0.03) on the PNI Nanoassemblr. Particles presented a near neutral average zeta potential (-5.5 $\pm$ 4.4 & -2.3 $\pm$ 3.1) as seen in *Figure 10*. LNPs presented ~40nm difference in particle diameter (Two-way ANOVA, *P< 0.001*) highlighting the effect of microfluidic architecture on particle structure. This was observed in data generated by D. Jurgens and reiterated by findings from Maeki and Ripoll (Jürgens *et al*., 2023; Maeki *et al*., 2017; Ripoll *et al*., 2022). Authors found that T-junction based microfluidic mixing led to larger LNP particle production due to the slow passing of critical ethanol concentration required for LNP formation and consequently higher TFR's would be required for optimal turbulent mixing (Evers *et al*., 2018; Jürgens *et al*., 2023; Maeki *et al*., 2017; Ripoll *et al*., 2022).

Following quantification of lipid concentration utilising lipid phase and LNP standard curves shown *Figure 11*, both Micropore AXF -Mini and Nanoassemblr-synthesized DOTAP- $DilC_{18}$ aliquots presented comparable lipid concentration to theoretical concentrations prior to microfluidics and post microfluidics. However, post purification aliquots presented >10 % deviation from desired theoretical values. As seen in *Table 9*, DOTAP LNPs exhibited ~20 % reduction in lipid concentration however, having coincided with the addition of ~20 % volume occurring during LNP purification, this was attributed to a dilution occurring during the buffer exchange process. As such, it was determined no lipid loss was observed during the manufacturing process of DOTAP LNPs on the Micropore AXF-Mini. To ensure suitable alignment with theoretical lipid concentration values and calculations required for downstream LNP processing, dilution factors during purification should be considered. Ribogreen assessment of samples tested, presented 100 % encapsulation efficiency when fluorescence difference was measure between triton-X treated vs non-triton treated samples. Poly A recovery was comparable to previous findings providing a mass balance of ~69 % and ~81 % for Micropore AXF-Mini and PNI Nanoassemblr-synthesised samples respectively, as shown in *Table 10*.

Following establishment of desired lipid recovery from AXF-Mini mediated crossflow mixing, the effect of vary TFR's on ionizable LNP formation was reviewed. LNPs presented a stable reproducible particle size that reduced as the TFR of mixing was increased. This observation additionally coincides with the observation and hypothesis' proposed by C. Roces, D. Jurgens and N. Kimura (Jürgens *et al*., 2023; Kimura *et al*., 2018; C. B. Roces *et al*., 2020) LNPs manufactured at a TFR10, 30 and 60 mL/min produced particles at 134 nm SD $\pm$ 7 nm, 106 nm SD $\pm$ 4 nm and 89 nm $\pm$ 3 nm respectively (Two-way ANOVA, $P< 0.001$). Despite varying mixing speeds all particle PDIs presented a value of > 0.2 (0.133 $\pm$ 0.03, 0.13 $\pm$ 0.03 and 0.14 $\pm$ 0.03) which in turn improved to > 0.1 following spin column purification. Particles presented a near neutral average zeta potential (-5 $\pm$ 0.6). Furthermore, following spin column purification the particle diameter increased, with the greatest difference observed in the smallest particles (TFR10: ~4 nm, TFR30: ~11 nm, TFR60: ~16 nm) ($P< 0.001$). This change in particle diameter could be a result of LNP aggregation during centrifugal force or impediment of the membrane filter however it is unclear whether this is finding is of significance and for definitive causation to be determined, further experiments would need to be undertaken.

Ribogreen assay assessment of all samples presented >98 % encapsulation efficiency when fluorescence difference was measure between triton-X treated vs non-triton-X treated samples. Poly A cargo of SM-102 LNPs had a markedly increased retention than that of alternative DOTAP LNPs, presenting poly A recovery of >84 % across LNPs manufactured at all speeds tested. This improved poly A recovery could be attributed to many physiological differences between SM-102 and DOTAP lipid components. SM-102's pH-mediated protonation could result in less arduous dissociation of nucleic acid cargo during triton-X lysis of LNPs given this occurrence is at a physiological pH, in turn freeing poly A anionic residues for ribogreen dye intercalation. This, as well as the saturated nature of SM-102s hydrocarbon chains, encourages inter-alkyl interaction between lipids within the bilayer owing to a more compact membrane organization (Swetha *et al*., 2023).

Progression into automation of AL-1000 and AL-1010 syringe drivers through PPL mediated command scripts led to the establishment of organic and aqueous pathlengths and validatory experiments to discover initial optimal start waste. Furthermore, this experiment would help elucidate the behaviour of LNPs over a 5 mL production volume collected in 1 mL aliquots and gain a better understanding if priming the Mini-AXF tubing would affect LNP production. Displayed in *Figure 13, 14* and *15* DOTAP LNPs presented particle diameters ranging from 88 – 99 nm and PDIs < 0.2 regardless of whether the AXF-Mini had been primed or non-primed with aqueous and organic phase. Samples showed minimal deviation through dialysis purification and all particles presented a near neutral average zeta potential ranging from 0 – 1.8 mV meeting the suitable criteria for *in vivo* efficacy. The only noteworthy distinction exhibited between the two data sets showed that the initial start wastage when the AXF-Mini PFA tubing had been primed, presented a larger variation between inter-day replicates. This larger particle size could be attributed to variable internal pathlengths of organic and aqueous phase within the AXF-Mini resulting in an improper 3:1 FRR distribution that is later normalised during sample collection, however further experiments and breakdowns of internal vessel geometries would need to be undertaken to definitively determine causation.

Concordant with previous theories and observations, all DOTAP LNPs presented an encapsulation efficiency of 100 % and Poly A recovery 65-71 %, demonstrating a slightly less efficient poly A retention compared to SM-102 ionizable alternatives. This was also reiterated in *Table 13*, which showed, once validated (shown in *Figure 16*),

all inter-day replicates of SM-102 formulations tested presented a 100 % encapsulation efficiency and poly A recovery ranging 73-79 %.

Following evaluation and exploration of PPL mediated automation of syringe drivers, further investigation to assess the effect of changing AXF-Mini 9.9 mm low volume insert with a 9.9 mm UltraLow Volume (ULV) insert on DOTAP LNPs synthesised under mixing speeds of 30 mL/min was undertaken. As shown in *Figure 18*, LNPs synthesised under the same TFR conditions with the low volume insert exhibited a particle diameter reduction of approximately 20 nm (*P< 0.001*) with minimal deviation observed in particle PDI, zeta potential and improved poly A recovery ranging 77 – 88 % (*Table 14*). This noteworthy particle size reduction could be the consequence of an increase in internal AXF-Mini vessel pressure accompanied by a reduced fluid path diameter and hold up volume (~500 µL). This theory is supported by the observations Dutta and Mavrogiannis (Dutta *et al*., 2006; Mavrogiannis *et al*., 2016) that changing device geometry can result in a change in total flow rate velocity, however further experimental work would need to be undertaken to definitively determine causation.

After preliminary validation of the ULV insert with cationic lipid formulations (DOTAP), performance of the AXF-Mini/ULV insert was further explored, employing three ionizable formulations previously described: SM-102; ALC-0315 and C-12 200. All formulations presented suitable CQAs following manufacture at a mixing speed of 30 mL/min. SM-102 and ALC-0315, formulations implemented in the SARS-CoV2 response, showed robust reproducibility producing particles with an average diameter of 98 nm and 95 nm respectively (Two-way ANOVA *,* ns). C-12 200 LNPs presented a markedly reduced size, comparative to that of alternative ionizable formulations, with LNPs presenting an average particle size of 73 nm (Two-way ANOVA, *P< 0.001*). This notable size difference could be attributed to lipid structure. Differing from SM-102 and ALC-0315, C-12 200 is a multi-tailed ionizable lipid with five tails, which said to aid in its enhanced endosome disruption capabilities (Han *et al*., 2021; Tang *et al*., 2023). Additionally, this could be attributed to both a higher poly A concentration and a reduced ionizable component within the molar ratio, owing to a more compact membrane structure. This supports the previous findings of C. Roces *et al* (C. B. Roces *et al*., 2020) that increasing cholesterol content and simultaneously decreasing the ionizable cationic lipid component resulted in a reduced particle size and PDI. Ribogreen analysis of LNP formulations showed very similar encapsulation efficiencies and poly A recovery across all formulation triplicates, presenting an

encapsulation efficiency >92 % and poly A recovery of >82 % (Two-way ANOVA *, P< 0.05*). Subsequently, SM-102 was down selected to evaluate *in vitro* performance, this decision was made after demonstration of suitable SM-102 LNPs with desired CQAs, were produced by the AXF-Mini and was further supported by the findings of Zhang *et al.* (2023) who reported SM-102 out-performed ALC-0315 in mRNA delivery (Zhang *et al*., 2023).

Succeeding evaluation of the ULV 9.9 mm insert on LNP CQAs, this new insert was then utilised to synthesise SM-102-Fluc mRNA LNPs at a concentration of 0.021 mg/mL. SM-102-Fluc mRNA LNPs exhibited a particle diameter of 71 nm $\pm$ 2 nm and PDI <0.2 (0.17 $\pm$ 0.03). Additionally, the zeta potential of the particle population additionally stayed within a neutral range of -0.9 mV $\pm$ 8, shown in *Figure 18.* Following dialysis purification, both poly A and Fluc mRNA formulated LNPs increased particle diameter to 80 and 82 nm respectively (Two-way ANOVA *,* ns), with minimal deviation to the PDI of each particle population. Following initial LNP characterisation, samples were diluted to a nucleic acid concentration of 3 µg/mL and assessed for encapsulation efficiency and nucleic acid recovery through a ribogreen assay. All samples tested, presented >97 % encapsulation efficiency when fluorescence difference was measure between triton-X treated vs non- triton-X treated samples. A Poly A recovery ranging 78 – 100 % was observed across triplicate samples whilst a Fluc mRNA recovery ranging 77 – 88 % was seen across triplicate samples (*Table 15*) (Two-way ANOVA*,* ns). After LNP characterisation, SM-102 LNPs were dosed at a mRNA concentration range of 2, 1, 0.5 and 0.25 µg/mL. SM-102 LNPs presented minimal detriment to HEK293 cell viability, displaying both a dose dependant uptake through $DiIC_{18}$ fluorescence and Fluc bioluminescence (*P< 0.001*), indicating successful delivery of mRNA cargo. In addition to this, analysis of sample mRNA through gel electrophoresis visualisation showed SM-102 formulations were effective at limiting mRNA degradation from endogenous endonuclease activity.

After demonstration of effective vaccine manufacture on the AXF-Mini, validated through *in vitro* investigation, methods exploring the scale up of LNP dosage concentration whilst maintaining LNP CQAs were studied. The aim was to ensure a 0.1 mg/mL mRNA dosage concentration was able to be achieved whilst ensuring LNPs presented a particle diameter <100 nm, PDI <0.2, neutral zeta potential ranging -10 mV/+10 mV, Encapsulation efficiency > 90 % and nucleic acid recovery >80 %. This criterion was established through previous lab group and literature-based

evidence (Anderluzzi *et al*., 2022; Lou *et al*., 2020; Ripoll *et al*., 2022; Samaridou *et al*., 2020). A reduced particle size proves particularly important in avoidance of the RES system and improved LNP circulation. Due to the natural hepatic uptake of LNPs through *ApoE* mediated delivery, particle size is particularly pertinent given the enhanced fenestrated nature of liver tissue (Blanco *et al*., 2015; Kiaie *et al*., 2022). Highlighted by Hassett *et al.* (2021) (Hassett *et al*., 2021), authors found that murine models presented a decreased antibody titre when LNPs exceeded 100nm. Authors suggested that this could be attributed to anatomical difference in lymphatic vessels resulting in a heightened sensitivity to particle size over primate models. With these considerations in mind, maintaining a PDI <0.2 creates a narrower size distribution, in-turn leading to a greater portion of the particle population avoiding RES clearance and a reduced variation in dosage/response. Further affirming the importance of encapsulation efficiency and nucleic acid recovery when evaluating process parameters. A 0.1 mg/mL nucleic acid dosage target was established from previous findings of Y. Perrie group (Anderluzzi *et al*., 2022; Jung *et al*., 2022; Lou *et al*., 2020) and reiterated by El-Mayta *et al*. (2023) (El-Mayta *et al*., 2023) who demonstrated that this dosage concentration avoided oversaturation of bioluminescent signals allowing for effective potency comparisons across formulations whilst simultaneously avoiding upregulation of serum alanine transaminase, aspartate transaminase and alkaline phosphatase associated with liver damage.

With determined criterion, initial experiments explored the effect of dilution volume used in spin column purification on SM-102 LNP CQAs. As seen in *Figure 22* and *Table 17,* despite varying dilution volumes SM-102 CQAs were sustained with the most significant difference being observed in the 40x dilution sample set (Two-way ANOVA, $P< 0.001$). SM-102 LNPs presented a 15 nm increase in diameter following spin column purification whilst 10x and 20x dilution sample sets presented an approximate 7 nm increase in size (Two-way ANOVA, $P< 0.05$). Despite this larger increase in particle size, it was determined that a 40X dilution volume was suitable for maintaining LNP CQAs and would be employed in spin column-based purification and concentration methods. This was to ensure following purification methods, the ethanol content within LNP samples remained below 1 %. This follows the findings of Cheng *et al*. (2023) (Cheng *et al*., 2023), residual ethanol, due to its low polarity and small molecular structure, can permeate the lipid membrane displacing water molecules on the LNP surface and inducing morphological changes in the lipid membrane. As a

result, lipids become more susceptible to membrane fusion, consequently resulting in nucleic acid leakage.

After elucidation of the dilution effect on SM-102 LNPs, concentrations scaling methods were investigated. As seen in *Figure 23A*, SM-102 LNPs manufactured at a poly A concentration of 0.02 mg/mL, 0.05 mg/mL and 0.1 mg/mL poly A concentration displayed post purification particle diameters of 83 nm, 98 nm and 116 nm respectively. This showed that increasing both lipid and poly A concentration at the manufacturing stage resulted in a direct influence on SM-102 LNP particle size ($P< 0.001$). This could be attributed to a combination of increased free lipid availability and the fixed nature of AXF-Mini organic phase compartmentalisation, however further investigation would need to be undertaken to definitively determine causation. Regardless of microfluidic architecture, this observation mirrors the findings of Matsuura-Sawada *et al*. (2022) (Matsuura-Sawada *et al*., 2022) when synthesising ionizable LNPs showed increasing lipid concentration resulted in marked increase in LNP particle size, with a 10-fold increase resulting in LNPs ranging 130-140 nm, regardless of TFR (Ickenstein & Garidel, 2019; Osouli-Bostanabad *et al*., 2022; Roberts *et al*., 2018; Tenchov *et al*., 2021; Zhang *et al*., 2020). Despite all other LNP CQAs meeting suitable *in vivo* criteria, it was determined that increasing concentration at the manufacturing phase of production resulted in loss of LNP size modulation and was more costly due to an increased nucleic acid wastage.

Furthermore, exploration of concentrating LNP samples through spin column centrifugation was undertaken. As shown in *Figure 23B*, SM-102 LNPs concentrated to a poly A end concentration of 0.06 mg/mL, 0.1 mg/mL and 0.14 mg/mL showed minimal variation in LNP CQA assessment (ns). Regardless of poly A concentration, SM-102 LNPs remained below <100 nm with minimal fluctuation between samples. Additionally, all SM-102 LNP samples tested, presented >99 % encapsulation efficiency when fluorescence difference was measured between triton-X treated vs non-triton-X treated samples. An average Poly A recovery of 100 % was observed in samples manufactured at a poly A concentration of 0.02 mg/mL, SM-102 LNPs concentrated to a poly A end concentration of 0.06 mg/mL, 0.1 mg/mL and 0.14mg/mL presented an average poly A recovery of 94 %, 92 % and 84 % respectively (*Table 18*) (Two-way ANOVA, ns). These results show at the highest concentration of 0.14 mg/mL poly A, SM-102 LNP CQAs were able to be maintained.

# Chapter 5: Conclusions

## 5. Conclusions

In conclusion as mixing speed of aqueous and organic phases was increased, particle diameter decreased amongst both DOTAP and SM-102 formulations. Moreover, both dialysis and spin column purification can affect LNP particle size, PDI and zeta potential differently and should be considered when evaluating downstream applications. Analysis of DOTAP- $DilC_{18}$ formulated LNPs presented a desired 3:1 FRR indicating accurate crossflow mixing was achieved. Furthermore, SM-102 LNPs presented a higher poly A recovery than that of alternative cationic DOTAP formulations, demonstrating the different pH-mediated binding capabilities of ionizable lipids. Additionally, automation of syringe drivers and establishment of waste volumes required for robust reproducible LNPs was achieved. Reducing hold up volume through utilisation of a ULV insert reduced LNP particle diameter across both DOTAP and SM-102 formulations. Following manufacturing process optimisation, robust demonstration of LNP synthesis utilising varying ionizable formulations inclusive of Moderna, Pfizer-BioNTech and C-12 200, was achieved, highlighting effectiveness of Micropore's AXF crossflow technology irrespective of formulation composition. Downstream selection and further elucidation of SM-102 LNP performance *in vitro* demonstrated manufactured LNPs showed minimal cytotoxicity, dose dependant uptake, and delivery of translational competent Fluc mRNA. This was further supported by the visualisation of mRNA integrity through gel electrophoresis following LNP encapsulation. Moreover, exploration and display of effective methods scaling dosage concentration whilst retaining optimal LNP CQAs was achieved. These findings and the demonstration of continuous flow manufacturing shown in *Figure 15*, prove to be a progressive step in producing LNPs capable of effective mRNA payload delivery and bypassing the scalability bottlenecks of conventional microfluidic manufacture(Carla B. Roces *et al*., 2020; Shepherd *et al*., 2021). In conclusion, a culmination of research findings further elucidated the process parameters and fluid mixing dynamics within Micropore's crossflow technology to support the fast and easy scale-up of LNP production processes. Continual investigation into different LNP formulations *in vivo* performance such as dissemination, potency and stability could provide a valuable insight into the robustness of AXF-crossflow technology and further solidify this novel platform's utility within the vaccine manufacturing landscape.

# Chapter 6: References

## 6. References


1. Ali, M. S., Hooshmand, N., El-Sayed, M., & Labouta, H. I. (2021). Microfluidics for Development of Lipid Nanoparticles: Paving the Way for Nucleic Acids to the Clinic. *ACS Applied Bio Materials*. https://doi.org/10.1021/acsabm.1c00732
2. Anderluzzi, G., Lou, G., Woods, S., Schmidt, S. T., Gallorini, S., Brazzoli, M., Johnson, R., Roberts, C. W., O'Hagan, D. T., Baudner, B. C., & Perrie, Y. (2022). The role of nanoparticle format and route of administration on self-amplifying mRNA vaccine potency. *Journal of Controlled Release*, *342*, 388-399. https://doi.org/10.1016/j.jconrel.2021.12.008
3. Anderluzzi, G., & Perrie, Y. (2020). Microfluidic Manufacture of Solid Lipid Nanoparticles: A Case Study on Tristearin-Based Systems. *Drug Delivery Letters*, *10*(3), 197-208. https://doi.org/http://dx.doi.org/10.2174/2210303109666190807104437
4. Barenholz, Y. (2012). Doxil®--the first FDA-approved nano-drug: lessons learned. *J Control Release*, *160*(2), 117-134. https://doi.org/10.1016/j.jconrel.2012.03.020
5. Blanco, E., Shen, H., & Ferrari, M. (2015). Principles of nanoparticle design for overcoming biological barriers to drug delivery. *Nature Biotechnology*, *33*(9), 941-951. https://doi.org/10.1038/nbt.3330
6. Chaudhary, N., Weissman, D., & Whitehead, K. A. (2021). mRNA vaccines for infectious diseases: principles, delivery and clinical translation. *Nature Reviews Drug Discovery*, *20*(11), 817-838. https://doi.org/10.1038/s41573-021-00283-5
7. Cheng, F., Wang, Y., Bai, Y., Liang, Z., Mao, Q., Liu, D., Wu, X., & Xu, M. (2023). Research Advances on the Stability of mRNA Vaccines. *Viruses*, *15*(3), 668. https://doi.org/10.3390/v15030668
8. Dutta, D., Ramachandran, A., & Leighton, D. T. (2006). Effect of channel geometry on solute dispersion in pressure-driven microfluidic systems. *Microfluidics and Nanofluidics*, *2*(4), 275-290. https://doi.org/10.1007/s10404-005-0070-7
9. El-Mayta, R., Padilla, M. S., Billingsley, M. M., Han, X., & Mitchell, M. J. (2023). Testing the <em>In Vitro</em> and <em>In Vivo</em> Efficiency of mRNA-Lipid Nanoparticles Formulated by Microfluidic Mixing. *Journal of Visualized Experiments*(191). https://doi.org/10.3791/64810

10. Evers, M. J. W., Kulkarni, J. A., Van Der Meel, R., Cullis, P. R., Vader, P., & Schiffelers, R. M. (2018). State-of-the-Art Design and Rapid-Mixing Production Techniques of Lipid Nanoparticles for Nucleic Acid Delivery. *Small Methods*, *2*(9), 1700375. https://doi.org/10.1002/smtd.201700375
11. Forbes, N., Hussain, M. T., Briuglia, M. L., Edwards, D. P., Horst, J. H. T., Szita, N., & Perrie, Y. (2019). Rapid and scale-independent microfluidic manufacture of liposomes entrapping protein incorporating in-line purification and at-line size monitoring. *International Journal of Pharmaceutics*, *556*, 68-81. https://doi.org/10.1016/j.ijpharm.2018.11.060
12. Gregoriadis, G. (2016). Liposomes in Drug Delivery: How It All Happened. *Pharmaceutics*, *8*(2), 19. https://doi.org/10.3390/pharmaceutics8020019
13. Han, X., Zhang, H., Butowska, K., Swingle, K. L., Alameh, M.-G., Weissman, D., & Mitchell, M. J. (2021). An ionizable lipid toolbox for RNA delivery. *Nature Communications*, *12*(1). https://doi.org/10.1038/s41467-021-27493-0
14. Hassett, K. J., Higgins, J., Woods, A., Levy, B., Xia, Y., Hsiao, C. J., Acosta, E., Almarsson, Ö., Moore, M. J., & Brito, L. A. (2021). Impact of lipid nanoparticle size on mRNA vaccine immunogenicity. *Journal of Controlled Release*, *335*, 237-246. https://doi.org/10.1016/j.jconrel.2021.05.021
15. Heilemann, M., Margeat, E., Kasper, R., Sauer, M., & Tinnefeld, P. (2005). Carbocyanine Dyes as Efficient Reversible Single-Molecule Optical Switch. *Journal of the American Chemical Society*, *127*(11), 3801-3806. https://doi.org/10.1021/ja044686x
16. Honig, M. G., & Hume, R. I. (1989). Dil and DiO: versatile fluorescent dyes for neuronal labelling and pathway tracing. *Trends in Neurosciences*, *12*(9), 333-341. https://doi.org/https://doi.org/10.1016/0166-2236(89)90040-4
17. Hou, X., Zaks, T., Langer, R., & Dong, Y. (2021). Lipid nanoparticles for mRNA delivery. *Nature Reviews Materials*, *6*(12), 1078-1094. https://doi.org/10.1038/s41578-021-00358-0
18. Hu, Y. B., Dammer, E. B., Ren, R. J., & Wang, G. (2015). The endosomal-lysosomal system: from acidification and cargo sorting to neurodegeneration. *Transl Neurodegener*, *4*, 18. https://doi.org/10.1186/s40035-015-0041-1
19. Ickenstein, L. M., & Garidel, P. (2019). Lipid-based nanoparticle formulations for small molecules and RNA drugs. *Expert Opinion on Drug Delivery*, *16*(11), 1205-1226. https://doi.org/10.1080/17425247.2019.1669558

20. Jung, H. N., Lee, S.-Y., Lee, S., Youn, H., & Im, H.-J. (2022). Lipid nanoparticles for delivery of RNA therapeutics: Current status and the role of in vivo imaging. *Theranostics*, *12*(17), 7509-7531. https://doi.org/10.7150/thno.77259
21. Jürgens, D. C., Deßloch, L., Porras-Gonzalez, D., Winkeljann, J., Zielinski, S., Munschauer, M., Hörner, A. L., Burgstaller, G., Winkeljann, B., & Merkel, O. M. (2023). Lab-scale siRNA and mRNA LNP manufacturing by various microfluidic mixing techniques – an evaluation of particle properties and efficiency. *OpenNano*, *12*, 100161. https://doi.org/https://doi.org/10.1016/j.onano.2023.100161
22. Kiaie, S. H., Majidi Zolbanin, N., Ahmadi, A., Bagherifar, R., Valizadeh, H., Kashanchi, F., & Jafari, R. (2022). Recent advances in mRNA-LNP therapeutics: immunological and pharmacological aspects. *Journal of Nanobiotechnology*, *20*(1). https://doi.org/10.1186/s12951-022-01478-7
23. Kimura, N., Maeki, M., Sato, Y., Note, Y., Ishida, A., Tani, H., Harashima, H., & Tokeshi, M. (2018). Development of the iLiNP Device: Fine Tuning the Lipid Nanoparticle Size within 10 nm for Drug Delivery. *ACS Omega*, *3*(5), 5044-5051. https://doi.org/10.1021/acsomega.8b00341
24. Lou, G., Anderluzzi, G., Schmidt, S. T., Woods, S., Gallorini, S., Brazzoli, M., Giusti, F., Ferlenghi, I., Johnson, R. N., Roberts, C. W., O'Hagan, D. T., Baudner, B. C., & Perrie, Y. (2020). Delivery of self-amplifying mRNA vaccines by cationic lipid nanoparticles: The impact of cationic lipid selection. *Journal of Controlled Release*, *325*, 370-379. https://doi.org/10.1016/j.jconrel.2020.06.027
25. Maeki, M., Fujishima, Y., Sato, Y., Yasui, T., Kaji, N., Ishida, A., Tani, H., Baba, Y., Harashima, H., & Tokeshi, M. (2017). Understanding the formation mechanism of lipid nanoparticles in microfluidic devices with chaotic micromixers. *PLOS ONE*, *12*(11), e0187962. https://doi.org/10.1371/journal.pone.0187962
26. Maeki, M., Uno, S., Niwa, A., Okada, Y., & Tokeshi, M. (2022). Microfluidic technologies and devices for lipid nanoparticle-based RNA delivery. *J Control Release*, *344*, 80-96. https://doi.org/10.1016/j.jconrel.2022.02.017
27. Matsuura-Sawada, Y., Maeki, M., Nishioka, T., Niwa, A., Yamauchi, J., Mizoguchi, M., Wada, K., & Tokeshi, M. (2022). Microfluidic Device-Enabled Mass Production of Lipid-Based Nanoparticles for Applications in

Nanomedicine and Cosmetics. *ACS Applied Nano Materials*, *5*(6), 7867-7876. https://doi.org/10.1021/acsanm.2c00886

28. Mavrogiannis, N., Ibo, M., Fu, X., Crivellari, F., & Gagnon, Z. (2016). Microfluidics made easy: A robust low-cost constant pressure flow controller for engineers and cell biologists. *Biomicrofluidics*, *10*(3), 034107. https://doi.org/10.1063/1.4950753
29. Namiot, E. D., Sokolov, A. V., Chubarev, V. N., Tarasov, V. V., & Schiöth, H. B. (2023). Nanoparticles in Clinical Trials: Analysis of Clinical Trials, FDA Approvals and Use for COVID-19 Vaccines. *International Journal of Molecular Sciences*, *24*(1), 787. https://doi.org/10.3390/ijms24010787
30. Osouli-Bostanabad, K., Puliga, S., Serrano, D. R., Bucchi, A., Halbert, G., & Lalatsa, A. (2022). Microfluidic Manufacture of Lipid-Based Nanomedicines. *Pharmaceutics*, *14*(9), 1940. https://doi.org/10.3390/pharmaceutics14091940
31. Poulain, F. E., Gaynes, J. A., Hörndli, C. S., Law, M.-Y., & Chien, C.-B. (2010). Chapter 1 - Analyzing Retinal Axon Guidance in Zebrafish. In H. W. Detrich, M. Westerfield, & L. I. Zon (Eds.), *Methods in Cell Biology* (Vol. 100, pp. 2-26). Academic Press. https://doi.org/https://doi.org/10.1016/B978-0-12-384892-5.00001-3
32. Ptaszek, M. (2013). Chapter Three - Rational Design of Fluorophores for In Vivo Applications. In M. C. Morris (Ed.), *Progress in Molecular Biology and Translational Science* (Vol. 113, pp. 59-108). Academic Press. https://doi.org/https://doi.org/10.1016/B978-0-12-386932-6.00003-X
33. Ripoll, M., Martin, E., Enot, M., Robbe, O., Rapisarda, C., Nicolai, M.-C., Deliot, A., Tabeling, P., Authelin, J.-R., Nakach, M., & Wils, P. (2022). Optimal self-assembly of lipid nanoparticles (LNP) in a ring micromixer. *Scientific Reports*, *12*(1). https://doi.org/10.1038/s41598-022-13112-5
34. Roberts, S. A., Parikh, N., Blower, R. J., & Agrawal, N. (2018). SPIN: rapid synthesis, purification, and concentration of small drug-loaded liposomes. *Journal of Liposome Research*, *28*(4), 331-340. https://doi.org/10.1080/08982104.2017.1381115
35. Roces, C. B., Khadke, S., Christensen, D., & Perrie, Y. (2019). Scale-Independent Microfluidic Production of Cationic Liposomal Adjuvants and Development of Enhanced Lymphatic Targeting Strategies. *Molecular Pharmaceutics*, *16*(10), 4372-4386. https://doi.org/10.1021/acs.molpharmaceut.9b00730

36. Roces, C. B., Lou, G., Jain, N., Abraham, S., Thomas, A., Halbert, G. W., & Perrie, Y. (2020). Manufacturing Considerations for the Development of Lipid Nanoparticles Using Microfluidics. *Pharmaceutics*, *12*(11). https://doi.org/10.3390/pharmaceutics12111095
37. Roces, C. B., Port, E. C., Daskalakis, N. N., Watts, J. A., Aylott, J. W., Halbert, G. W., & Perrie, Y. (2020). Rapid scale-up and production of active-loaded PEGylated liposomes. *International Journal of Pharmaceutics*, *586*, 119566. https://doi.org/10.1016/j.ijpharm.2020.119566
38. Samaridou, E., Heyes, J., & Lutwyche, P. (2020). Lipid nanoparticles for nucleic acid delivery: Current perspectives. *Advanced Drug Delivery Reviews*, *154-155*, 37-63. https://doi.org/10.1016/j.addr.2020.06.002
39. Schlake, T., Thess, A., Fotin-Mleczek, M., & Kallen, K. J. (2012). Developing mRNA-vaccine technologies. *RNA Biol*, *9*(11), 1319-1330. https://doi.org/10.4161/rna.22269
40. Shah, S., Dhawan, V., Holm, R., Nagarsenker, M. S., & Perrie, Y. (2020). Liposomes: Advancements and innovation in the manufacturing process. *Advanced Drug Delivery Reviews*, *154-155*, 102-122. https://doi.org/10.1016/j.addr.2020.07.002
41. Shepherd, S. J., Warzecha, C. C., Yadavali, S., El-Mayta, R., Alameh, M.-G., Wang, L., Weissman, D., Wilson, J. M., Issadore, D., & Mitchell, M. J. (2021). Scalable mRNA and siRNA Lipid Nanoparticle Production Using a Parallelized Microfluidic Device. *Nano Letters*, *21*(13), 5671-5680. https://doi.org/10.1021/acs.nanolett.1c01353
42. Swetha, K., Kotla, N. G., Tunki, L., Jayaraj, A., Bhargava, S. K., Hu, H., Bonam, S. R., & Kurapati, R. (2023). Recent Advances in the Lipid Nanoparticle-Mediated Delivery of mRNA Vaccines. *Vaccines (Basel)*, *11*(3). https://doi.org/10.3390/vaccines11030658
43. Tang, X., Zhang, Y., & Han, X. (2023). Ionizable Lipid Nanoparticles for mRNA Delivery. *Advanced NanoBiomed Research*, *3*(8). https://doi.org/10.1002/anbr.202300006
44. Tenchov, R., Bird, R., Curtze, A. E., & Zhou, Q. (2021). Lipid Nanoparticles─From Liposomes to mRNA Vaccine Delivery, a Landscape of Research Diversity and Advancement. *ACS Nano*, *15*(11), 16982-17015. https://doi.org/10.1021/acsnano.1c04996

45. Thi, T. T. H., Suys, E. J. A., Lee, J. S., Nguyen, D. H., Park, K. D., & Truong, N. P. (2021). Lipid-Based Nanoparticles in the Clinic and Clinical Trials: From Cancer Nanomedicine to COVID-19 Vaccines. *Vaccines*, *9*(4), 359. https://doi.org/10.3390/vaccines9040359
46. Verma, M., Imran Ozer, Wen Xie, Ryan Gallagher, Alexandra Teixeira, and Michael Choy. . (2023). The Landscape for Lipid-nanoparticle-based Genomic Medicines. *Nature Reviews*, *22*(5), 349-350. https://doi.org/10.1038/d41573-023-00002-2
47. Wagner, A., & Vorauer-Uhl, K. (2011). Liposome Technology for Industrial Purposes. *Journal of Drug Delivery*, *2011*, 1-9. https://doi.org/10.1155/2011/591325
48. Webb, C., Forbes, N., Roces, C. B., Anderluzzi, G., Lou, G., Abraham, S., Ingalls, L., Marshall, K., Leaver, T. J., Watts, J. A., Aylott, J. W., & Perrie, Y. (2020). Using microfluidics for scalable manufacturing of nanomedicines from bench to GMP: A case study using protein-loaded liposomes. *Int J Pharm*, *582*, 119266. https://doi.org/10.1016/j.ijpharm.2020.119266
49. Yung, B. C., Li, J., Zhang, M., Cheng, X., Li, H., Yung, E. M., Kang, C., Cosby, L. E., Liu, Y., Teng, L., & Lee, R. J. (2016). Lipid Nanoparticles Composed of Quaternary Amine–Tertiary Amine Cationic Lipid Combination (QTsome) for Therapeutic Delivery of AntimiR-21 for Lung Cancer. *Molecular Pharmaceutics*, *13*(2), 653-662. https://doi.org/10.1021/acs.molpharmaceut.5b00878
50. Zhang, L., More, K. R., Ojha, A., Jackson, C. B., Quinlan, B. D., Li, H., He, W., Farzan, M., Pardi, N., & Choe, H. (2023). Effect of mRNA-LNP components of two globally-marketed COVID-19 vaccines on efficacy and stability. *npj Vaccines*, *8*(1). https://doi.org/10.1038/s41541-023-00751-6
51. Zhang, X., Goel, V., & Robbie, G. J. (2020). Pharmacokinetics of Patisiran, the First Approved RNA Interference Therapy in Patients With Hereditary Transthyretin-Mediated Amyloidosis. *The Journal of Clinical Pharmacology*, *60*(5), 573-585. https://doi.org/10.1002/jcph.1553

# Chapter 7: Appendix

## 7. Appendix

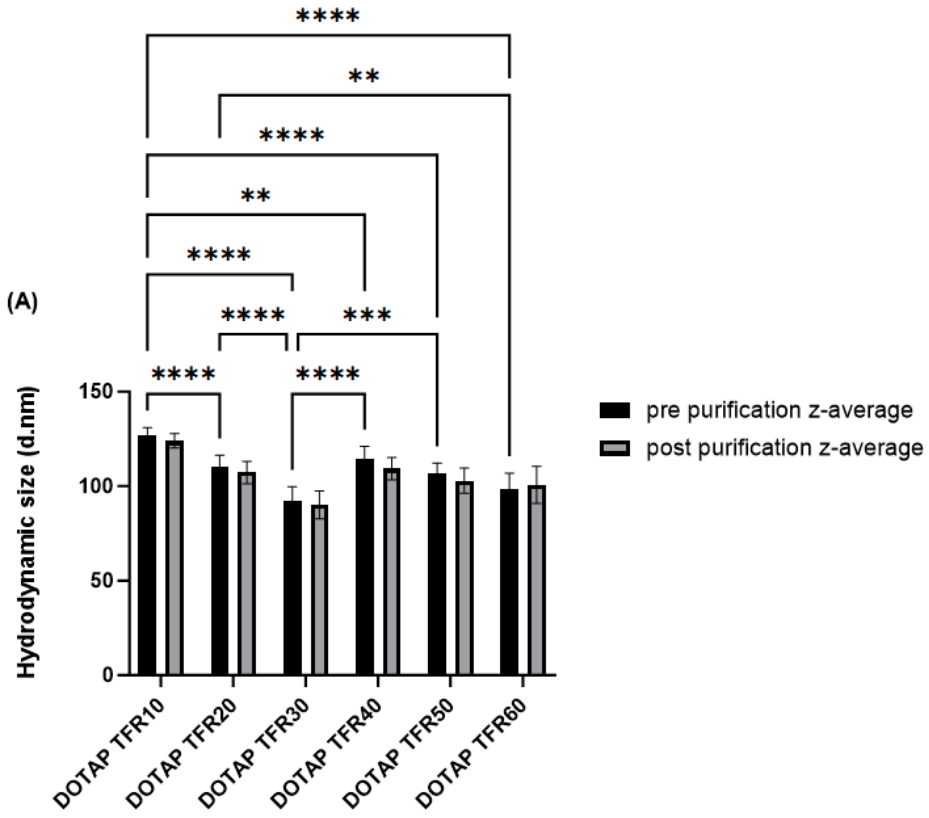


***Appendix 7A: Statistical analysis of DOTAP LNPs particle diameter and PDI before and after dialysis purification.*** *The particle sizes and PDI were measured by DLS using a Malvern zeta-sizer ultra-series utilising a 632.8 nm 10 mW He-Ne laser with a detection angle set at 173°. LNPs were measured using a 1.47 refractive index and a 1.28 cP viscosity with the dispersant set at citrate buffer prior to dialysis and LNPs were then measured using a 1.34 refractive index and a 1.02 cP viscosity with the dispersant set at PBS after dialysis. Statistical analysis of data was undertaken through a two- way ANOVA with a Tukey's post ad-hoc on GraphPad Prism 10 software. Results represent mean ± SD. n = 3.*

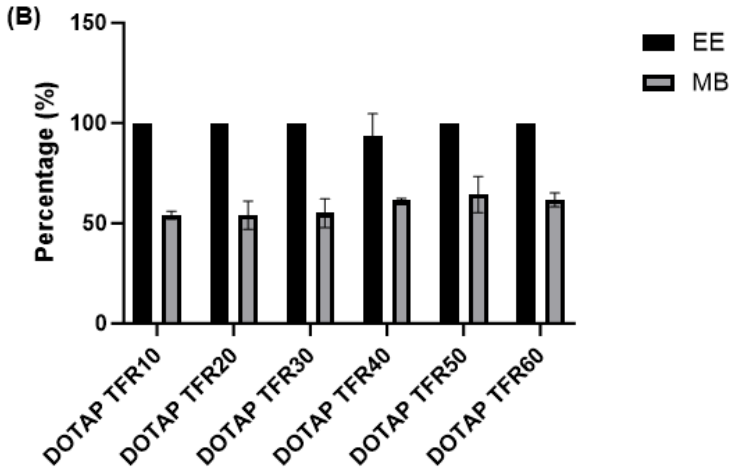


***Appendix 7B: Statistical analysis of encapsulation efficiency and nucleic acid loading of DOTAP LNPs.*** *This figure displays the calculated statistical significance of encapsulation efficiency and nucleic acid recovery (Mass Balance) of DOTAP LNPs utilising 1000 ng/mL and 200 ng/mL poly A standard curves. Encapsulation efficiency was calculated by the difference in fluorescent emission in triton-X treated samples, causing lysis, against the untreated samples. Mass balance recovery of poly A cargo in LNP samples were then calculated using the 1000 ng/mL poly A standard curve and percentage recovery was calculated against a theoretical 100 % yield of 750 ng/mL of polyA. The samples were analysed at 475 - 525 nm excitation/emission on GloMax Explorer. Statistical analysis of data was undertaken through a two- way ANOVA with a Tukey's post ad-hoc on GraphPad Prism 10 software.*

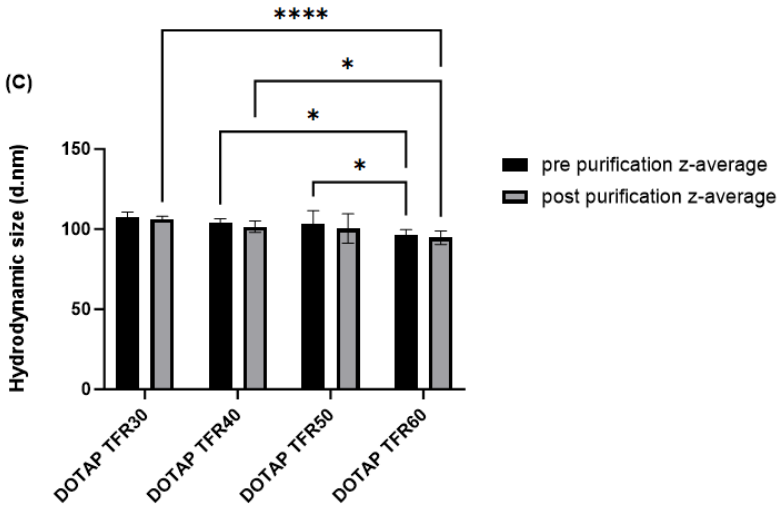


***Appendix 7C: Statistical analysis of DOTAP LNPs particle diameter and PDI before and after dialysis purification.*** *The particle sizes and PDI were measured by DLS using a Malvern zeta-sizer ultra-series utilising a 632.8 nm 10 mW He-Ne laser with a detection angle set at 173°. LNPs were measured using a 1.47 refractive index and a 1.28 cP viscosity with the dispersant set at citrate buffer prior to dialysis and LNPs were then measured using a 1.34 refractive index and a 1.02 cP viscosity with the dispersant set at PBS after dialysis. Statistical analysis of data was undertaken through a two- way ANOVA with a Tukey's post ad-hoc on GraphPad Prism 10 software. Results represent mean ± SD. n = 3.*

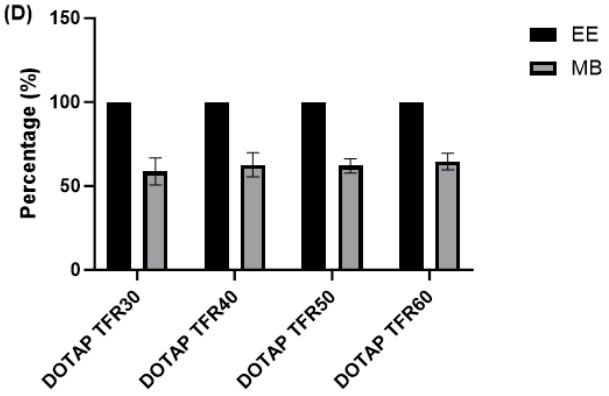


***Appendix 7D: Statistical analysis of encapsulation efficiency and nucleic acid loading of DOTAP LNPs.*** *This figure displays the calculated statistical significance of encapsulation efficiency and nucleic acid recovery (Mass Balance) of DOTAP LNPs utilising 1000 ng/mL and 200 ng/mL poly A standard curves. Encapsulation efficiency was calculated by the difference in fluorescent emission in triton-X treated samples, causing lysis, against the untreated samples. Mass balance recovery of poly A cargo in LNP samples were then calculated using the 1000 ng/mL poly A standard curve and percentage recovery was calculated against a theoretical 100 % yield of 750 ng/mL of polyA. The samples were analysed at 475 - 525 nm excitation/emission on GloMax Explorer. Statistical analysis of data was undertaken through a two- way ANOVA with a Tukey's post ad-hoc on GraphPad Prism 10 software.*

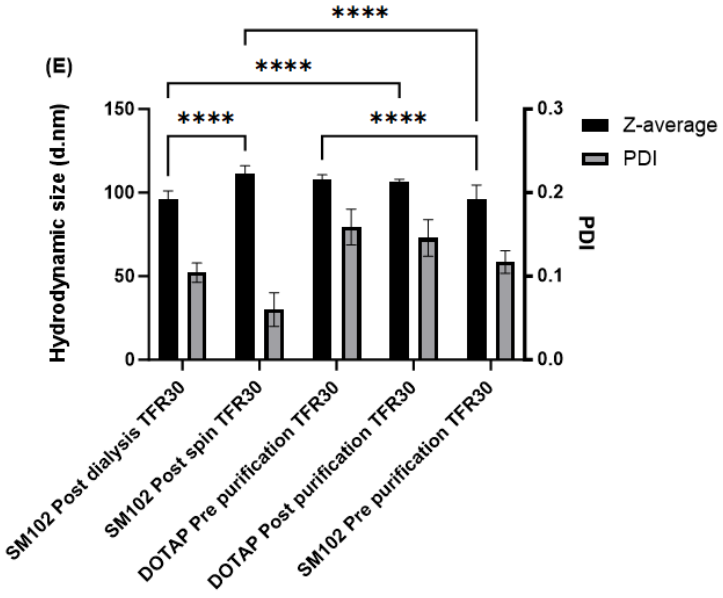

***Appendix 7E: Statistical analysis of DOTAP and SM-102 LNPs particle diameter and PDI before and after dialysis purification.*** *The particle sizes and PDI were measured by DLS using a Malvern zeta-sizer ultra-series utilising a 632.8 nm 10 mW He-Ne laser with a detection angle set at 173°. LNPs were measured using a 1.47 refractive index and a 1.28 cP viscosity with the dispersant set at citrate buffer prior to dialysis and LNPs were then measured using a 1.34 refractive index and a 1.02 cP viscosity with the dispersant set at PBS after dialysis. Statistical analysis of data was undertaken through a two- way ANOVA with a Tukey's post ad-hoc on GraphPad Prism 10 software. Results represent mean ± SD. n = 3.*

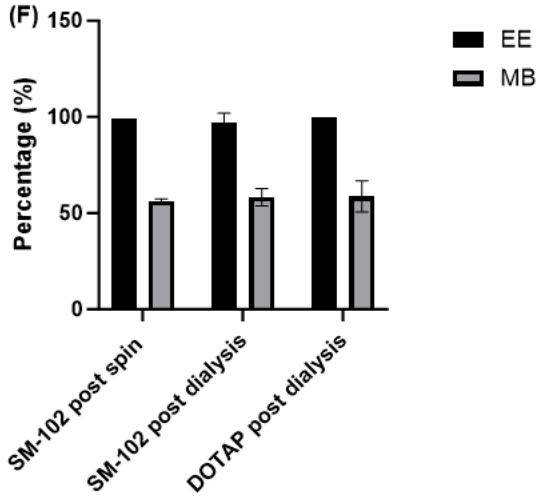


***Appendix 7F: Statistical analysis of encapsulation efficiency and nucleic acid loading of DOTAP LNPs.*** *This figure displays the calculated statistical significance of encapsulation efficiency and nucleic acid recovery (Mass Balance) of SM-102 and DOTAP LNPs utilising 1000 ng/mL and 200 ng/mL poly A standard curves. Encapsulation efficiency was calculated by the difference in fluorescent emission in triton-X treated samples, causing lysis, against the untreated samples. Mass balance recovery of poly A cargo in LNP samples were then calculated using the 1000 ng/mL poly A standard curve and percentage recovery was calculated against a theoretical 100 % yield of 750 ng/mL of polyA. The samples were analysed at 475 - 525 nm excitation/emission on GloMax Explorer. Statistical analysis of data was undertaken through a two- way ANOVA with a Tukey's post ad-hoc on GraphPad Prism 10 software.*

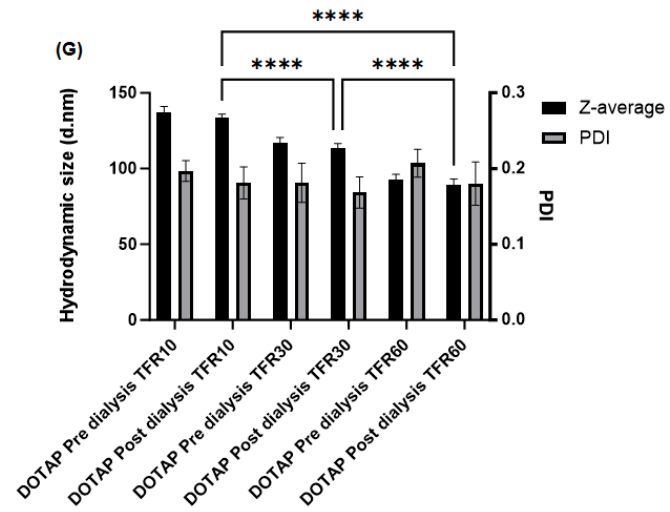


***Appendix 7G: Statistical analysis of DOTAP LNPs particle diameter and PDI before and after dialysis purification.*** *The particle sizes and PDI were measured by DLS using a Malvern zeta-sizer ultra-series utilising a 632.8 nm 10 mW He-Ne laser with a detection angle set at 173°. LNPs were measured using a 1.47 refractive index and a 1.28 cP viscosity with the dispersant set at citrate buffer prior to dialysis and LNPs were then measured using a 1.34 refractive index and a 1.02 cP viscosity with the dispersant set at PBS after dialysis. Statistical analysis of data was undertaken through a two- way ANOVA with a Tukey's post ad-hoc on GraphPad Prism 10 software. Results represent mean ± SD. n = 3.*

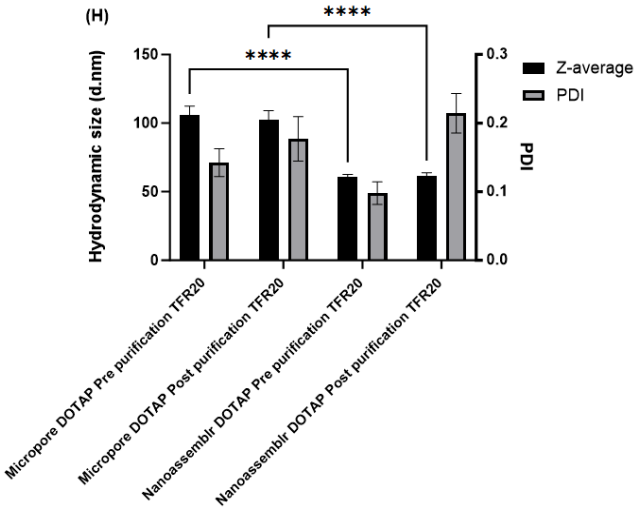


***Appendix 7H: Statistical analysis of DOTAP LNPs particle diameter and PDI before and after dialysis purification.*** *The particle sizes and PDI were measured by DLS using a Malvern zeta-sizer ultra-series utilising a 632.8 nm 10 mW He-Ne laser with a detection angle set at 173°. LNPs were measured using a 1.47 refractive index and a 1.28 cP viscosity with the dispersant set at citrate buffer prior to dialysis and LNPs were then measured using a 1.34 refractive index and a 1.02 cP viscosity with the dispersant set at PBS after dialysis. Statistical analysis of data was undertaken through a one way ANOVA with a Tukey's post ad-hoc on GraphPad Prism 10 software. Results represent mean ± SD. n = 3.*

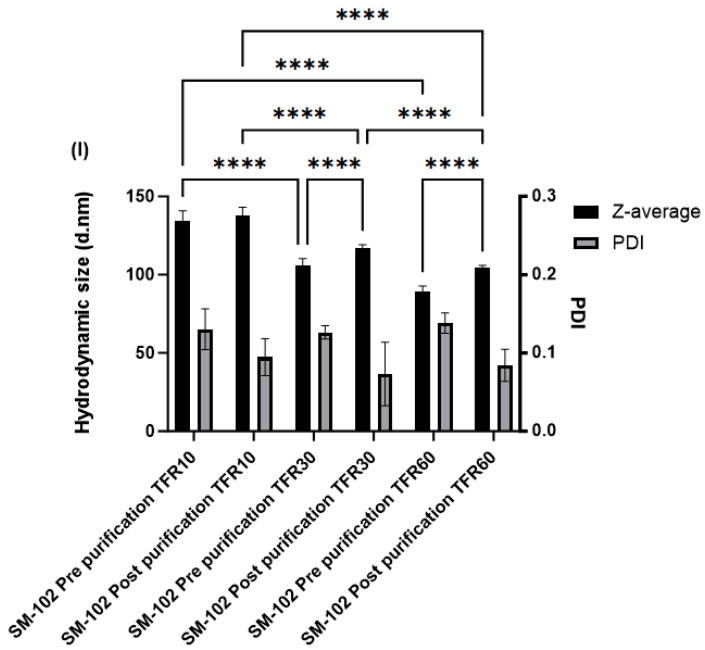


***Appendix 7I: Statistical analysis of SM-102 LNPs particle diameter and PDI before and after dialysis purification.*** *The particle sizes and PDI were measured by DLS using a Malvern zeta-sizer ultra-series utilising a 632.8 nm 10 mW He-Ne laser with a detection angle set at 173°. LNPs were measured using a 1.47 refractive index and a 1.28 cP viscosity with the dispersant set at citrate buffer prior to dialysis and LNPs were then measured using a 1.34 refractive index and a 1.02 cP viscosity with the dispersant set at PBS after dialysis. Statistical analysis of data was undertaken through a two- way ANOVA with a Tukey's post ad-hoc on GraphPad Prism 10 software. Results represent mean ± SD. n = 3.*

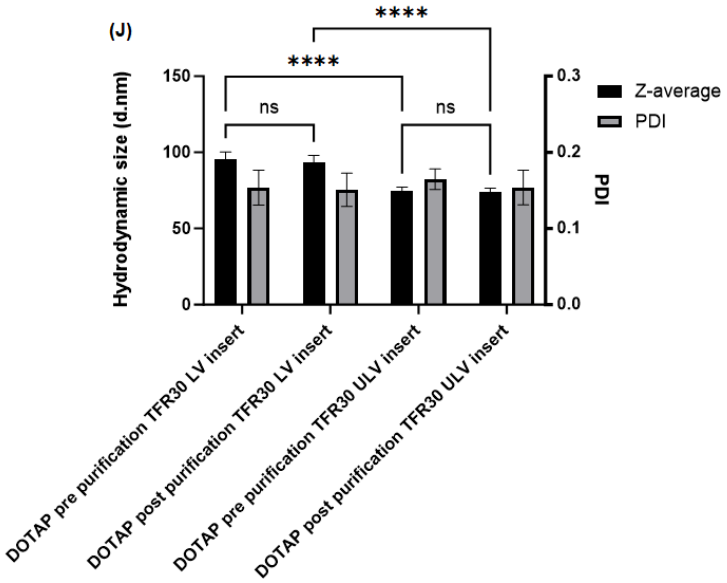

***Appendix 7J: Statistical analysis of DOTAP and LNPs particle diameter and PDI before and after dialysis purification.*** *The particle sizes and PDI were measured by DLS using a Malvern zeta-sizer ultra-series utilising a 632.8 nm 10 mW He-Ne laser with a detection angle set at 173°. LNPs were measured using a 1.47 refractive index and a 1.28 cP viscosity with the dispersant set at citrate buffer prior to dialysis and LNPs were then measured using a 1.34 refractive index and a 1.02 cP viscosity with the dispersant set at PBS after dialysis. Statistical analysis of data was undertaken through a one way ANOVA with a Tukey's post ad-hoc on GraphPad Prism 10 software. Results represent mean ± SD. n = 3.*

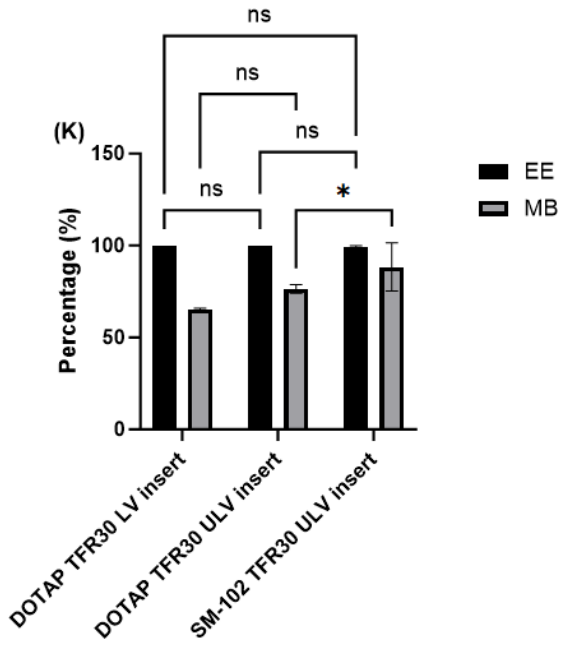


***Appendix 7K: Statistical analysis of Ribogreen assay of DOTAP LNPs manufactured using LV insert and new ULV insert.*** *This table displays the calculated encapsulation efficiency and nucleic acid recovery (Mass Balance) of DOTAP LNPs utilising 1000 ng/mL and 200 ng/mL poly A standard curves. Encapsulation efficiency was calculated by the difference in fluorescent emission in triton-X treated samples, causing lysis, against the untreated samples. Mass balance recovery of poly A cargo in LNP samples were then calculated using the 1000 ng/mL poly A standard curve and percentage recovery was calculated against a theoretical 100 % yield of 750 ng/mL of poly A. The samples were analysed at 475 - 525 nm excitation/emission on GloMax Explorer. Statistical analysis of data was undertaken through a one way ANOVA with a Tukey's post ad-hoc on GraphPad Prism 10 software.*

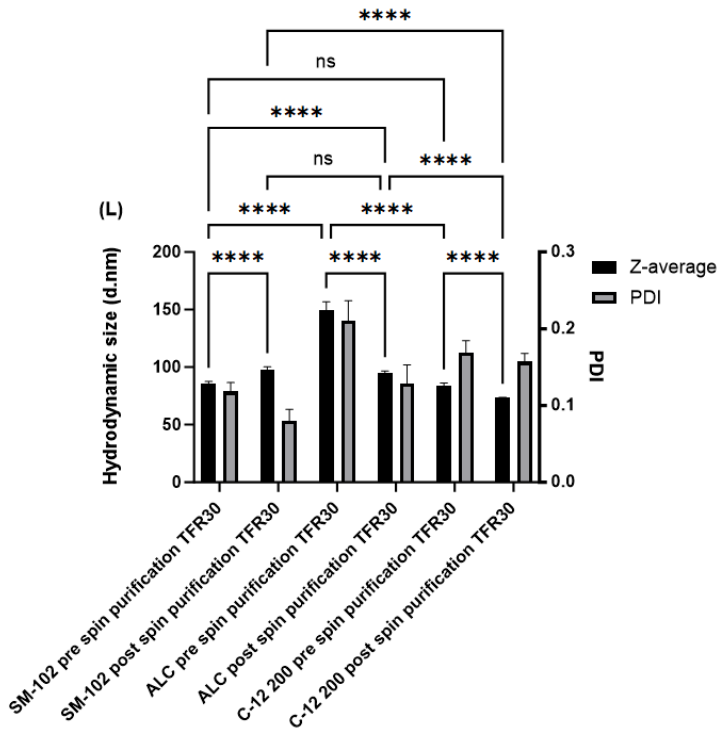


***Appendix 7L: Statistical analysis of SM-102, ALC and C-12 200 LNPs particle diameter and PDI before and after dialysis purification.*** *The particle sizes and PDI were measured by DLS using a Malvern zeta-sizer ultra-series utilising a 632.8 nm 10 mW He-Ne laser with a detection angle set at 173°. LNPs were measured using a 1.47 refractive index and a 1.28 cP viscosity with the dispersant set at citrate buffer prior to dialysis and LNPs were then measured using a 1.34 refractive index and a 1.02 cP viscosity with the dispersant set at PBS after dialysis. Statistical analysis of data was undertaken through a two- way ANOVA with a Tukey's post ad-hoc on GraphPad Prism 10 software. Results represent mean ± SD, n = 3.*

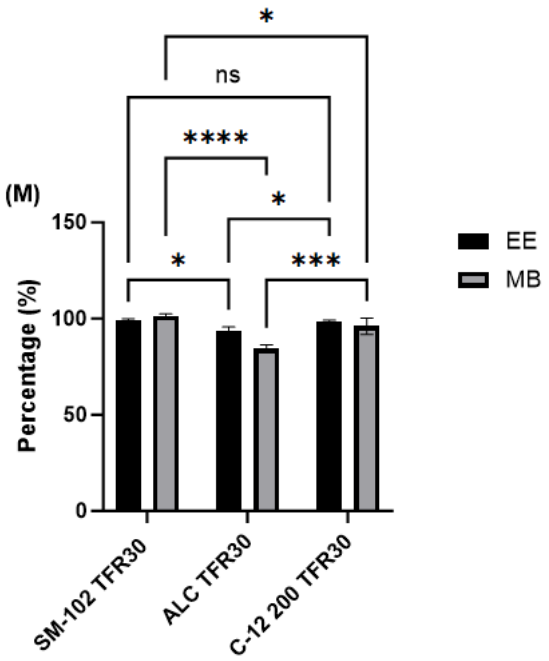


***Appendix 7M: Statistical analysis of encapsulation efficiency and mass balance of SM-102, ALC and C-12 200 LNPs manufactured using ULV insert.*** *This table displays the calculated encapsulation efficiency and nucleic acid recovery (Mass Balance) of ionisable LNPs utilising 1000 ng/mL and 200 ng/mL poly A standard curves. Encapsulation efficiency was calculated by the difference in fluorescent emission in triton-X treated samples, causing lysis, against the untreated samples. Mass balance recovery of poly A cargo in LNP samples were then calculated using the 1000 ng/mL poly A standard curve and percentage recovery was calculated against a theoretical 100 % yield of 750 ng/mL of poly A. The samples were analysed at 475 - 525 nm excitation/emission on GloMax Explorer. Statistical analysis of data was undertaken through a two- way ANOVA with a Tukey's post ad-hoc on GraphPad Prism 10 software.*

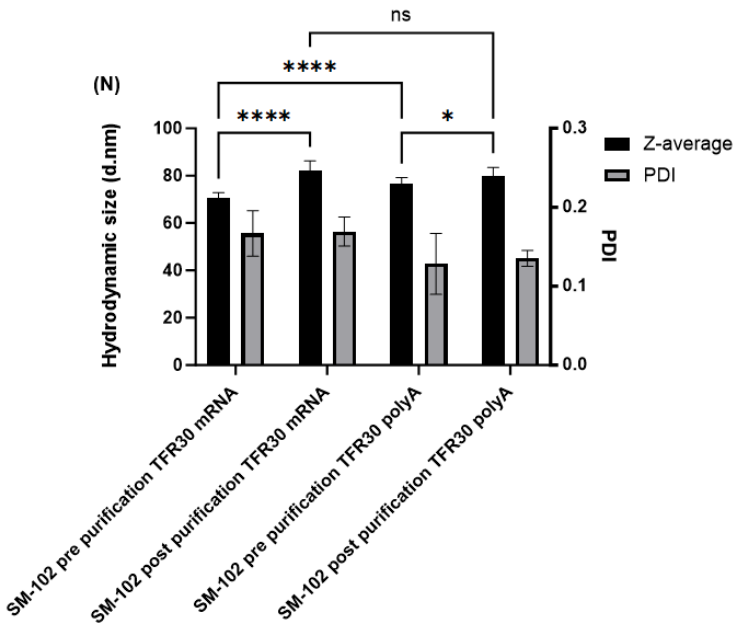

***Appendix 7N: Statistical analysis of SM-102 LNPs particle diameter and PDI before and after dialysis purification.*** *The particle sizes and PDI were measured by DLS using a Malvern zeta-sizer ultra-series utilising a 632.8 nm 10 mW He-Ne laser with a detection angle set at 173°. LNPs were measured using a 1.47 refractive index and a 1.28 cP viscosity with the dispersant set at citrate buffer prior to dialysis and LNPs were then measured using a 1.34 refractive index and a 1.02 cP viscosity with the dispersant set at PBS after dialysis. Statistical analysis of data was undertaken through a two- way ANOVA with a Tukey's post ad-hoc on GraphPad Prism 10 software. Results represent mean ± SD, n = 3.*

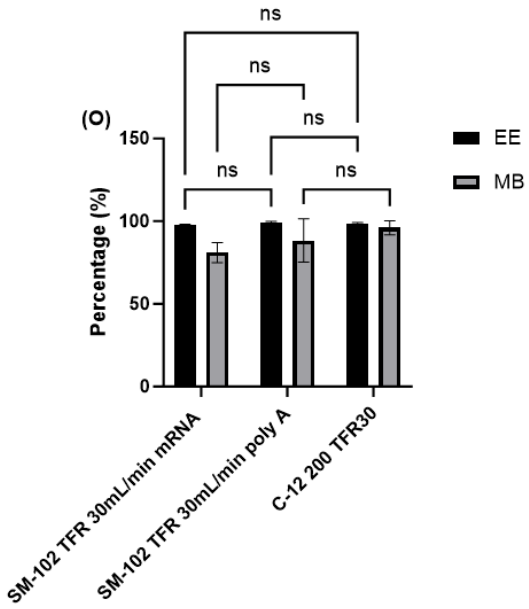


***Appendix 7O: Statistical analysis of encapsulation efficiency and mass balance of SM-102 LNPs manufactured using ULV insert.*** *This table displays the calculated encapsulation efficiency and nucleic acid recovery (Mass Balance) of SM-102 LNPs utilising 1000 ng/mL and 200 ng/mL poly A standard curves. Encapsulation efficiency was calculated by the difference in fluorescent emission in triton-X treated samples, causing lysis, against the untreated samples. Mass balance recovery of poly A cargo in LNP samples were then calculated using the 1000 ng/mL poly A standard curve and percentage recovery was calculated against a theoretical 100 % yield of 750 ng/mL of poly A. The samples were analysed at 475 - 525 nm excitation/emission on GloMax Explorer. Statistical analysis of data was undertaken through a two- way ANOVA with a Tukey's post ad-hoc on GraphPad Prism 10 software. Results represent mean ± SD, n = 3.*

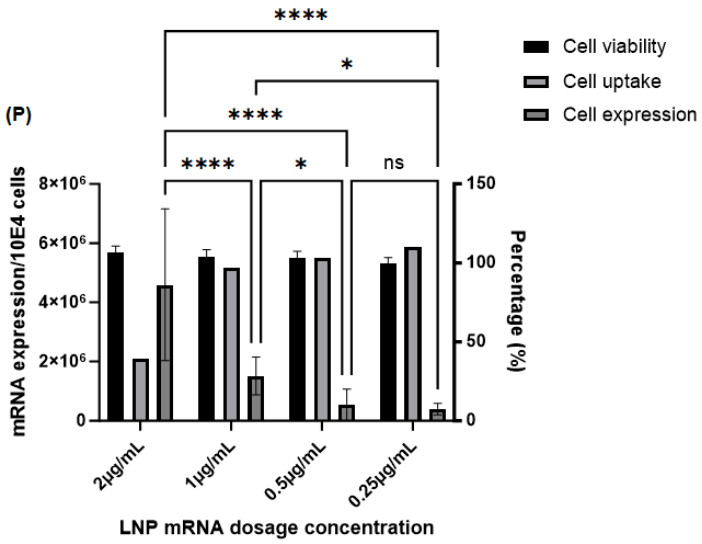


***Appendix 7P: Statistical analysis of In vitro efficacy of SM-102 LNPs in HEK293 cell lines.****. Fluorescence emission of HEK293 cells treated at varying SM-102 concentrations and incubated or 24 hrs. Dye metabolism was measured relative to untreated HEK293 cells and cell viability was measured (Ex/Em 520 nm/580/640 nm). Measurement of SM-102 LNP uptake into HEK293 cells through $DilC_{18}$ fluorescence. Cells were treated with varying concentrations of LNPs and $DilC_{18}$ fluorescence was measured at time of dosage and at a 24 hr time point at which point cell culture media was removed and cells were treated with 1 % triton-X PBS. Fluorescence measurements were undertaken, and uptake was calculated relative to initial dosage readings (Ex/Em 52 0nm/580/640 nm). Evaluation of Fluc mRNA expression succeeding SM-102 LNP treatment and 24 hr incubation. Cells were treated with varying LNP concentrations and incubated for 24 hrs. Succeeding incubation, wells were supplemented with luciferin substrate and bioluminescence was measured. Investigation of mRNA integrity following LNP synthesis and cell treatments. A denaturing gel electrophoresis was undertaken to evaluate the stability of Fluc mRNA following LNP synthesis on the micropore AXF-Mini. Gel electrophoresis was undertaken on 1 % agarose containing 5 µL of SYBR Green II dye and submerged in 1x MOPS Buffer. The gel was run for 1 hr at 90 V, and isolate band sizes were calculated using the corresponding RNA Millenium Marker Hyperladder (9 kb). H: RNA Millenium Marker Hyperladder, n1-3: sample, Pos: Positive Fluc mRNA control, NTC: No template control. Statistical analysis of data was undertaken through a two- way ANOVA with a Tukey's post ad-hoc on GraphPad Prism 10 software. Results represent mean ± SD, n = 3.*

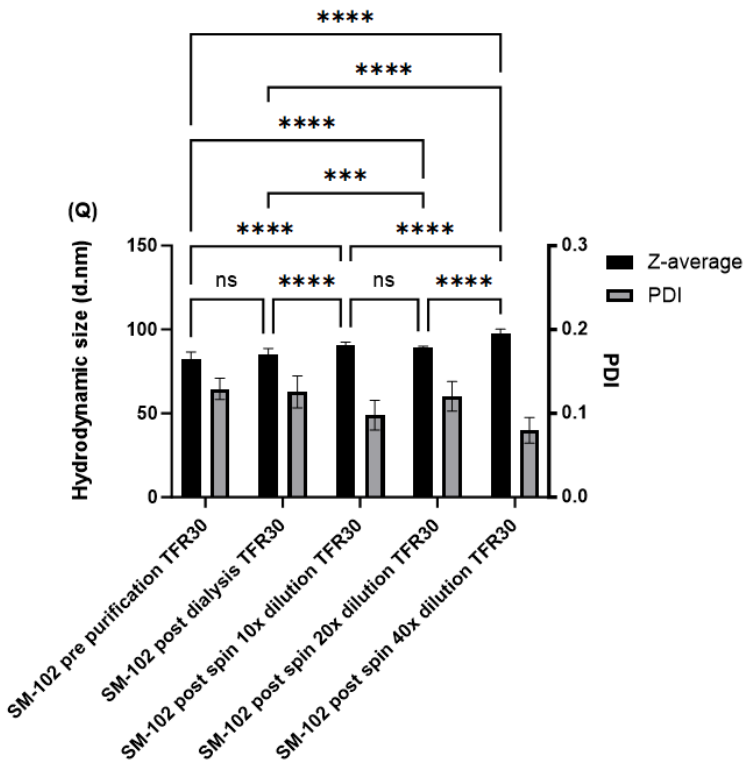


***Appendix 7Q: Particle diameter and PDI before and after spin column purification, utilising varying dilution volumes, of SM-102 LNP samples synthesised on the Micropore AXF-Mini at 30 mL/min.*** *This figure displays the hydrodynamic size of SM-102:DSPC:Chol:DMG-PEG2000 (50:10:38.5:1.5) poly A containing - LNPs and PDI of particle population prior to and succeeding spin column purification at 4°C. The particle sizes and PDI were measured by DLS using a Malvern zeta-sizer ultra-series utilising a 632.8 nm 10 mW He-Ne laser with a detection angle set at 173°. LNPs were measured using a 1.47 refractive index and a 1.28 cP viscosity with the dispersant set at citrate buffer prior to purification and LNPs were then measured using a 1.34 refractive index and a 1.02 cP viscosity with the dispersant set at PBS after purification. Zeta potential (mV) was additionally measured succeeding LNP purification and is displayed above bar chart measurements. Zetasizer Software v.7.11 (Malvern Instruments Ltd.) was used for the acquisition of data. Statistical analysis of data was undertaken through a two- way ANOVA with a Tukey's post ad-hoc on GraphPad Prism 10 software. Results represent mean ± SD, n = 3.*

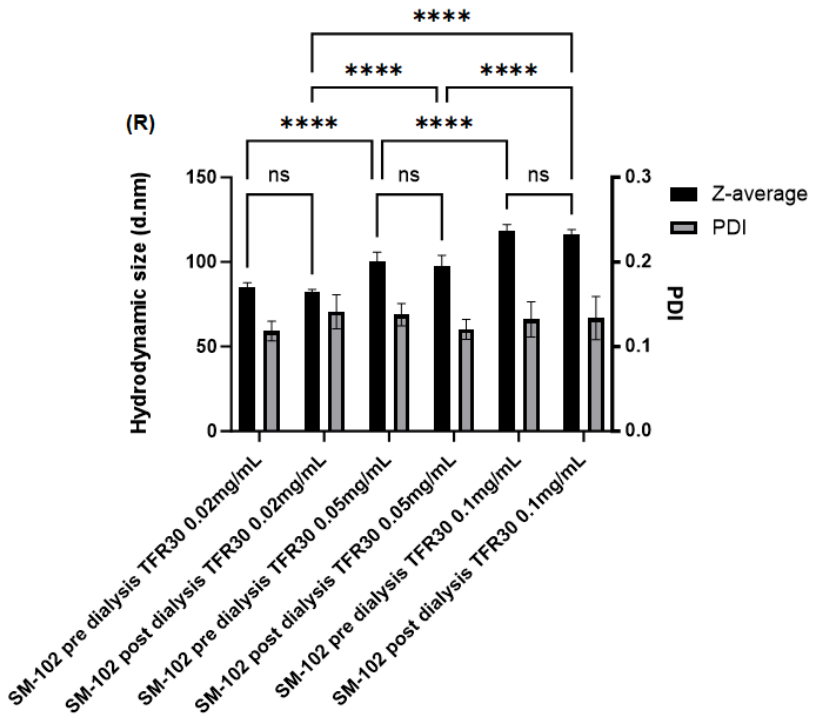


***Appendix 7R: Particle diameter and PDI before and after purification of SM-102 LNP samples synthesised on the Micropore AXF-Mini at 30 mL/min. Particle size and PDI of SM-102 LNPs manufactured at 0.02 mg/mL, 0.05 mg/mL and 0.1 mg/mL poly A concentration.*** *This figure displays the hydrodynamic size of SM-102:DSPC:Chol:DMG-PEG2000 (50:10:38.5:1.5) poly A containing - LNPs and PDI of particle population prior to and succeeding purification at 4°C. The particle sizes and PDI were measured by DLS using a Malvern zeta-sizer ultra-series utilising a 632.8 nm 10 mW He-Ne laser with a detection angle set at 173°. LNPs were measured using a 1.47 refractive index and a 1.28 cP viscosity with the dispersant set at citrate buffer prior to purification and LNPs were then measured using a 1.34 refractive index and a 1.02 cP viscosity with the dispersant set at PBS after purification. Zeta potential (mV) was additionally measured succeeding LNP purification and is displayed above bar chart measurements. Zetasizer Software v.7.11 (Malvern Instruments Ltd.) was used for the acquisition of data. Statistical analysis of data was undertaken through a two- way ANOVA with a Tukey's post ad-hoc on GraphPad Prism 10 software. Results represent mean ± SD, n = 3.*

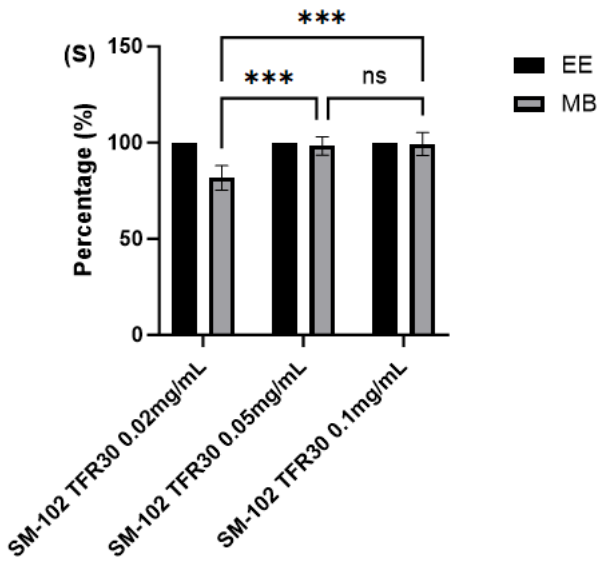


***Appendix 7S: Statistical analysis of encapsulation efficiency and mass balance of SM-102 LNPs.*** *This figure displays the calculated encapsulation efficiency and nucleic acid recovery (Mass Balance) of SM-102 LNPs utilising 1000 ng/mL and 200 ng/mL poly A standard curves. Encapsulation efficiency was calculated by the difference in fluorescent emission in triton-X treated samples, causing lysis, against the untreated samples. Mass balance recovery of poly A cargo in LNP samples were then calculated using both standard curves and percentage recovery was calculated against a theoretical 100 % yield of 750 ng/mL of poly A. The samples were analysed at 475 - 525 nm excitation/emission on GloMax Explorer. Statistical analysis of data was undertaken through a two- way ANOVA with a Tukey's post ad-hoc on GraphPad Prism 10 software. Results represent mean ± SD, n = 3.*

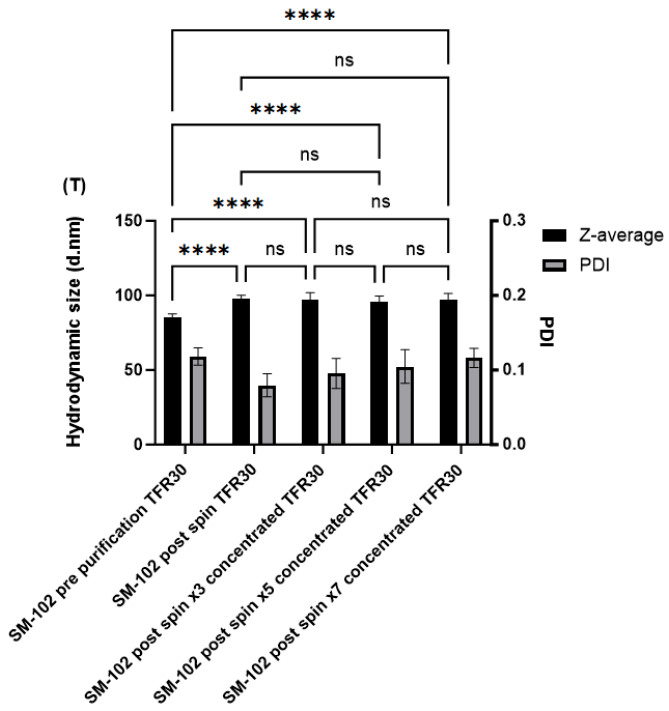

***Appendix 7T: Statistical analysis of particle diameter and PDI before and after purification of SM-102 LNP samples synthesised on the Micropore AXF-Mini at 30 mL/min. Particle size and PDI of SM-102 LNPs manufactured at 0.02 mg/mL poly A and concentrated to 0.06 mg/mL, 0.1 mg/mL and 0.14 mg/mL through spin column centrifugation.*** *This figure displays the hydrodynamic size of SM-102:DSPC:Chol:DMG-PEG2000 (50:10:38.5:1.5) poly A containing - LNPs and PDI of particle population prior to and succeeding purification at 4°C. The particle sizes and PDI were measured by DLS using a Malvern zeta-sizer ultra-series utilising a 632.8 nm 10 mW He-Ne laser with a detection angle set at 173°. LNPs were measured using a 1.47 refractive index and a 1.28 cP viscosity with the dispersant set at citrate buffer prior to purification and LNPs were then measured using a 1.34 refractive index and a 1.02 cP viscosity with the dispersant set at PBS after purification. Zeta potential (mV) was additionally measured succeeding LNP purification and is displayed above bar chart measurements. Zetasizer Software v.7.11 (Malvern Instruments Ltd.) was used for the acquisition of data. Statistical analysis of data was undertaken through a two- way ANOVA with a Tukey's post ad-hoc on GraphPad Prism 10 software. Results represent mean ± SD, n = 3.*

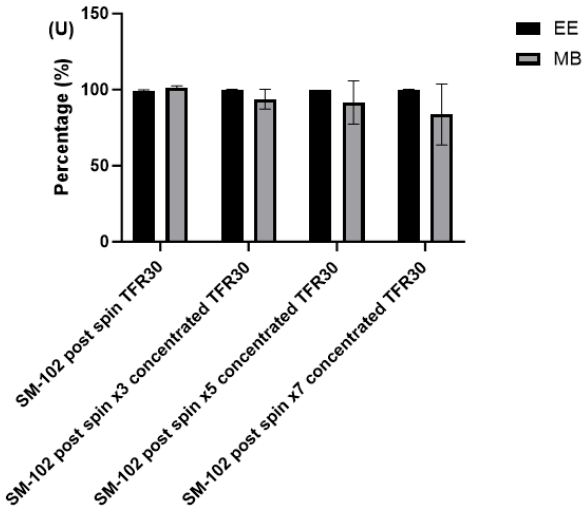


***Appendix 7U: Statistical analysis of encapsulation efficiency and mass balance of SM-102 LNPs.*** *This figure displays the calculated encapsulation efficiency and nucleic acid recovery (Mass Balance) of SM-102 LNPs utilising 1000 ng/mL and 200 ng/mL poly A standard curves. Encapsulation efficiency was calculated by the difference in fluorescent emission in triton-X treated samples, causing lysis, against the untreated samples. Mass balance recovery of poly A cargo in LNP samples were then calculated using both standard curves and percentage recovery was calculated against a theoretical 100 % yield of 750 ng/mL of poly A. The samples were analysed at 475 - 525 nm excitation/emission on GloMax Explorer. Statistical analysis of data was undertaken through a two- way ANOVA with a Tukey's post ad-hoc on GraphPad Prism 10 software. Results represent mean ± SD, n = 3.*